NATIONAL ADVISORY COMMITTEE FOR AERONAUTICS

TECHNICAL NOTE 2482

STABILITY AND CONTROL CHARACTERISTICS OF A COMPLETE AIRPLANE MODEL HAVING A WING WITH QUARTER-CHORD LINE SWEPT BACK 40°, ASPECT RATIO 2.50, AND TAPER RATIO 0.42

By Marvin Schuldenfrei, Paul Comisarow, and Kenneth W. Goodson

Langley Aeronautical Laboratory
Langley Field, Va.

Washington
December 1951

NATIONAL ADVISORY COMMITTEE FOR AERONAUTICS

TECHNICAL NOTE 2482

STABILITY AND CONTROL CHARACTERISTICS OF A COMPLETE AIRPLANE MODEL HAVING A WING WITH QUARTER-CHORD LINE SWEPT BACK 40°, ASPECT RATIO 2.50, AND TAPER RATIO 0.42[1]

By Marvin Schuldenfrei, Paul Comisarow, and Kenneth W. Goodson

SUMMARY

An investigation has been made of an airplane model having a wing with quarter-chord line swept back 40°, aspect ratio 2.50, and taper ratio 0.42 and a horizontal tail with quarter-chord line swept back 40°, aspect ratio 3.87, and taper ratio 0.49 to determine its low-speed stability and control characteristics. The test Reynolds number was 2.87×10^6, based on a mean aerodynamic chord of 2.47 feet, except for some of the aileron tests which were made at a Reynolds number of 2.05×10^6.

With the horizontal tail located near the fuselage juncture on the vertical tail, model results indicated static longitudinal instability above a lift coefficient that was 0.15 below the lift coefficient at which stall occurred. Static longitudinal stability, however, was manifested throughout the lift range with the horizontal tail located near the top of the vertical tail. The use of 10° negative dihedral on the wing had little effect on the static longitudinal stability characteristics.

Preliminary tests of the complete model revealed an undesirable flat spot in the yawing-moment curves at low angles of attack, the directional stability being neutral for yaw angles of ±2°. This undesirable characteristic was improved by replacing the thick original vertical tail with a thin vertical tail and by flattening the top of the dorsal fairing.

---

[1]Supersedes the recently declassified NACA RM L7B25, "Stability and Control Characteristics of an Airplane Model Having a 45.1° Swept-Back Wing with Aspect Ratio 2.50 and Taper Ratio 0.42 and a 42.8° Swept-Back Horizontal Tail with Aspect Ratio 3.87 and Taper Ratio 0.49" by Marvin Schuldenfrei, Paul Comisarow, and Kenneth W. Goodson, 1947.

The effective dihedral was reduced and the directional stability was increased either by incorporating negative geometric dihedral in the wing or by adding end plates under the wing tips.

The ailerons exhibited a very large increase in upfloating tendency for angles of attack greater than 14°. With flaps down, the ailerons could not trim the model in roll for sideslip angles greater than about 10°.

INTRODUCTION

The present paper contains the results of a stability and control investigation of an unpowered airplane model having a 40° sweptback wing with aspect ratio 2.50 and taper ratio 0.42 and a 40° sweptback horizontal tail with aspect ratio 3.87 and taper ratio 0.49. The investigation was undertaken primarily to obtain stability and control data on a basic design configuration. The test program was curtailed when the model was revised for use in another project. The results are believed to be of interest, however, inasmuch as they reflect the typical low-speed stability problems encountered with contemporary high-speed airplane designs.

For the evaluation of longitudinal stability characteristics, the investigation included stabilizer and tail-off tests with different wing dihedral angles ($\Gamma = 0^\circ$ and $\Gamma = -10^\circ$) over an angle-of-attack range for the cruising and landing configurations and tests with a high horizontal-tail location ($\Gamma = -10^\circ$) for the cruising configuration. Tests were also made of the wing alone and to determine the effect of wing end plates in pitch. All tail-on tests were made with the elevator at 0°.

An investigation was also made with a $\frac{5}{16}$-inch flat-plate vertical tail and with several dorsal modifications to determine the best configuration for directional stability. Lateral stability characteristics were determined for the airplane with different geometric wing dihedrals and with end plates. Tests were made with ailerons and spoilers to determine control characteristics.

COEFFICIENTS AND SYMBOLS

The results of the tests are presented as standard NACA coefficients of forces and moments. Pitching-moment, rolling-moment, and yawing-moment coefficients are referred to the test center of gravity

shown in figure 1 (35.9 percent mean aerodynamic chord). The data are referred to the stability axes, which are a system of axes having their origin at the center of gravity and in which the Z-axis is in the plane of symmetry and perpendicular to the relative wind, the X-axis is in the plane of symmetry and perpendicular to the Z-axis, and the Y-axis is perpendicular to the plane of symmetry. The positive directions of the stability axes, of angular displacements of the airplane and control surface, and of hinge moments are shown in figure 2.

The coefficients and symbols are defined as follows:

C_L	lift coefficient (Lift/qS)
C_X	longitudinal-force coefficient (X/qS)
C_m	pitching-moment coefficient (M/qSc')
C_Y	side-force coefficient (Y/qS)
C_l	rolling-moment coefficient (L/qSb)
C_n	yawing-moment coefficient (N/qSb)
C_h	hinge-moment coefficient ($H/qb'\overline{c}^2$)

Lift = -Z

Drag = -X (only at $\Psi = 0^\circ$)

X,Y,Z	forces along axes, pounds
L,M,N	moments about axes, foot-pounds
H	hinge moment of control surface, foot-pounds
q	free-stream dynamic pressure, pounds per square foot ($\rho V^2/2$)
q_t	effective dynamic pressure at tail, pounds per square foot
S	wing area, square feet (13.64)
c'	wing mean aerodynamic chord (M.A.C.), feet (2.47)
$\overline{c}$	root-mean-square chord of aileron control surface back of hinge line, feet (0.35)
c	chord measured perpendicular to 25-percent-chord line

b	wing span, feet (5.83)
b'	single aileron control-surface span along hinge line, feet (1.58)
V	air velocity, feet per second
V_s	sinking speed, feet per minute
ρ	mass density of air, slugs per cubic foot
α	angle of attack of wing chord line, degrees
ψ	angle of yaw, degrees
ϵ	angle of downwash, degrees
i_t	angle of stabilizer with respect to wing chord line; positive when trailing edge is down
δ	control-surface deflection, degrees
Γ	geometric dihedral angle, degrees
n_p	neutral-point location, percent M.A.C. (center-of-gravity location for neutral stability in trimmed flight)
A	aspect ratio (b^2/S)
M_o	free-stream Mach number in tunnel
W	weight, pounds
γ	glide-path angle, degrees

Subscripts:

a	aileron (a_R and a_L, right and left aileron, respectively)
f	flap
w	wing

max maximum

meas measured

α or ψ partial derivatives of a coefficient with respect to angle of attack or angle of yaw $\left(\text{example, } C_{l_\psi} = \frac{\partial C_l}{\partial \psi}\right)$

MODEL AND APPARATUS

The model is shown mounted for testing in the Langley 300 MPH 7- by 10-foot tunnel in figure 3, and a three-view drawing of the model as tested is presented as figure 4.

The elevator, rudder, ailerons, and wing flap were 20-percent plain flaps and were flat-sided from the hinge line to the trailing edge, except for the wing flap which was a continuation of the airfoil section. The regular and high locations of the horizontal tail as tested are given in figure 5.

Several modifications were made on the dorsal fairing and on the vertical tail (figs. 6 to 8). The vertical tail was replaced by a $\frac{5}{16}$-inch steel plate of the same plan form as the original tail. A ventral fin with the dimensions shown for configuration E of figure 7 was also added below the vertical tail (under the fuselage).

A special wing of all-wood construction with the same airfoil sections and plan form as the original wing was constructed for the purpose of obtaining data for a geometric dihedral angle of -10°. (See fig. 9.)

A strain gage for measuring aileron hinge moments was installed in the model.

TESTS AND RESULTS

Test Conditions

Tests were made at a dynamic pressure of 40.0 pounds per square foot ($M_o = 0.16$) for all configurations, except for several aileron tests for which the dynamic pressure was reduced to 20.1 pounds per square foot ($M_o = 0.12$) in order to obtain hinge moments. The

corresponding Reynolds numbers (based on the M.A.C. of 2.47 ft) are 2.87×10^6 and 2.05×10^6, respectively. The Reynolds numbers were computed by use of a turbulence factor of unity. The degree of turbulence of the tunnel is not known quantitatively but is believed to be small because of the high contraction ratio (14:1).

Corrections

All data have been corrected for tares caused by the model support struts. Jet-boundary corrections, which are approximate for a swept-back wing, were computed as follows (reference 1):

$$\alpha = \alpha_{meas} + 1.45C_{L_{meas}}$$

$$C_X = C_{X_{meas}} - 0.0218C_{L_{meas}}^2$$

$$C_m = C_{m_{meas}} + 0.015C_{L_{meas}} \text{ (for tail on)}$$

All force and moment coefficients were corrected for blocking by the method of reference 2. An increment in longitudinal-force coefficient of 0.00148 has been applied to take into account the horizontal buoyancy effected by the longitudinal static-pressure gradient in the tunnel for all tests.

Presentation of Results

The following table outlines the figures in which the results of the present tests are given:

	Figure
Longitudinal stability:	
Wing-alone tests	10
Stabilizer tests (c.g. at 35.9 percent M.A.C.)	
For $\Gamma = 0^\circ$	11 to 12
For $\Gamma = -10^\circ$	13 to 15
Stabilizer tests (c.g. at 23.0 percent M.A.C.)	
For $\Gamma = 0^\circ$	16
For $\Gamma = -10^\circ$	17
Sinking speed and glide-path angle	18
Neutral points	19
Downwash and dynamic-pressure ratio at tail	20
End-plate tests	21
Contribution of various components to longitudinal stability; $\Gamma = 0^\circ$	22

DISCUSSION

Longitudinal Stability

The data in the present paper are believed to reflect the aerodynamic characteristics of the airplane at low Mach numbers.

Lift characteristics.- The lift characteristics are presented in figures 10 to 17. For the complete model the lift characteristics are summarized as follows:

	$\Gamma = 0^\circ$ (original wing, plain flap)		$\Gamma = -10^\circ$ (dihedral wing, split flap)	
	$\delta_f = 0^\circ$	$\delta_f = 50^\circ$	$\delta_f = 0^\circ$	$\delta_f = 50^\circ$
$C_{L_{max}}$ (trimmed; c.g. at 23.0 percent M.A.C.)	0.94	1.02	0.93	1.02
ΔC_L (due to flaps)				
At $C_{L_{max}}$ (trimmed)	----	.08	----	.09
At untrimmed $\alpha = 0^\circ$	----	.24	----	.23

For the wing alone ($\Gamma = 0^\circ$) with flaps undeflected, the slope $C_{L_\alpha} = 0.047$ (fig. 10).

If the wing had been unswept, it would have had an estimated value of C_{L_α} of 0.065, which when multiplied by the cosine of the leading-edge sweepback angle would have given a value of C_{L_α} of 0.050 for the sweptback wing as compared with a test value of 0.047. The calculated induced drag $\frac{C_L^2}{\pi A}$ is plotted in figure 10 along with the test data. The curve is fairly similar at low lift coefficients and diverges at a value of C_L above 0.5.

Sinking speed.- The low values of lift-drag ratio at landing lift coefficients for swept wings with low aspect ratio are associated with high sinking speeds and limit the pilot's ability to make a successful landing flare and to make contact at a desired point. The effect of landing-aid devices on sinking speed was therefore estimated for a full-scale airplane model with W/S assumed to be 30.5 pounds per square foot at sea level. The effect of flap deflection on the estimated sinking speed of a full-scale model is presented in figure 18. With flaps retracted ($\delta_f = 0^\circ$), the sinking speed is appreciably lower than with flaps deflected ($\delta_f = 50^\circ$). The flaps increase the glide-path angle γ and $C_{L_{max}}$ only slightly and thus appear to be quite ineffective as landing-aid devices. The effect of full-scale Reynolds number on sinking-speed characteristics is not known. The sinking speeds shown in figure 18 indicate either that the airplane cannot be flown into ground contact but will have to be flared to reduce the landing-gear loads at contact or that power will be required to land. For a more heavily loaded airplane, the sinking speed and the velocities shown in figure 18 increase as the square root of the weight ratio, and landing without power will be almost precluded.

Static longitudinal stability.- The stick-fixed neutral points for both the high-speed and the landing configurations were computed from the data of figures 16 and 17 (c.g. at 23.0 percent M.A.C.) by using a method described in reference 3 and are presented in figure 19. The average static margins at values of C_L below 0.8 are presented in the following table:

Γ (deg)	Static margin (percent M.A.C.)	
	$\delta_f = 0^\circ$	$\delta_f = 50^\circ$
0	9	10
-10	10	11
-10 (with high horizontal tail)	16	--

On the basis of low-speed wind-tunnel tests, the static longitudinal stability appears inadequate above a lift coefficient which is 0.15 below that at which stall occurs except with the high horizontal-tail location.

Downwash and dynamic-pressure ratio at tail.- The average downwash angles and dynamic-pressure ratios at the horizontal tail have been determined from the stabilizer tests (figs. 16 and 17 - c.g. at 23.0 percent M.A.C.) and are presented in figure 20 for flap deflections of 0° and 50°. The values of the slope $\partial\epsilon/\partial\alpha$ in the linear range are summarized in the following table:

Γ (deg)	$\partial\epsilon/\partial\alpha$	
	$\delta_f = 0^\circ$	$\delta_f = 50^\circ$
0	0.47	0.66
-10	.38	.63
-10 (wing with high horizontal tail)	.12	----

Brief tuft studies indicated that the initial stall occurred slightly inboard of the wing tips at $C_L \approx 0.7$ and spread rapidly to envelop the tip and toward the center section. The increased relative loading on the unstalled inboard section of the wing is thought to account for the large increase in downwash observed at the tail beyond $C_L = 0.7$ with flaps up. Also at high lift coefficients the tail is close to the wake and the profile-drag coefficient for the wing is high, which results in a further increase in the downwash at the tail.

Changing the dihedral angle to -10° had a slight stabilizing effect on the downwash angles for both flap configurations, which is as expected because of the lowering of the wing-tip vortices with respect to the horizontal tail. Changing the horizontal tail to the high location shown in figure 5 had a marked stabilizing effect on the downwash angles for the flaps-retracted configuration, especially at high lift coefficients (fig. 20(b)). The very large reduction in downwash at the high tail location causes the model with the high tail to be stable at the stall, whereas the original model was unstable at the stall (fig. 17).

Wing end plates.- The effect of end plates on the wing is presented in figure 21 (c.g. at 35.9 percent M.A.C.) for the landing configuration. The pitching moment indicates a slight increase in stability for

the model with end plates on. With the addition of end plates, the slope C_{L_α} shows an increase to 0.060 as compared with a value of 0.050 without end plates ($\Gamma = 0^\circ$).

Contribution of various components to longitudinal stability.- The contribution of the various components to longitudinal stability is presented in figure 22 (c.g. at 23.0 percent M.A.C.). These pitching-moment slopes were obtained from the data for the complete model ($i_t = -3^\circ$), the fuselage-wing combination, and the wing. The difference between the pitching-moment slopes for the complete model and for the wing-fuselage combination is the contribution of the tail, and the fuselage pitching-moment slope was obtained from the difference of the fuselage-wing combination and the wing. The curve for the complete model shows that the model has a stable pitching-moment slope which rapidly becomes unstable at lift coefficients above 0.7. The most important contribution to the instability of the complete model at the high values of lift coefficient is due to the tail which is in a region of high downwash at large values of C_L. A higher location of the horizontal tail tends to alleviate this condition.

The fuselage has an unstable pitching-moment variation, which shifts the neutral point forward 4 percent at low angles of attack and increases with higher angles of attack. As a check, the pitching moment of the fuselage was also computed (reference 4) and was found to account for a 6-percent change in neutral point.

Lateral Stability and Control

Initial tests of the original complete model revealed an undesirable flat spot in the yawing-moment curves at low angles of attack, the stability being almost neutral for about $\pm 2^\circ$ yaw. Since this condition could lead to a constant and annoying Dutch roll type of oscillation in flight, a fairly extensive investigation of the cause of the reduction in stability was made. The investigation indicated that the cause of the low directional stability at small angles of yaw was separation of the air flow at the rear part of the fuselage. This separation was caused by the combination of a large boundary layer built up along the fuselage and an adverse pressure gradient at the tail end of the fuselage because of the expansion between the fuselage and the horizontal tail on the vertical tail. Tuft observation confirmed a tendency toward separation on both the tail end of the fuselage and on the vertical tail below the horizontal tail for small yaw angles.

A number of modifications as shown in figure 7 were made in an attempt to correct the flat spot in the yawing-moment curve. The aerodynamic data for these configurations are given in figure 23. Removal

of any of the dorsal fairing arrangements shown (fig. 7) results in an increase in the directional stability C_{n_ψ} of about -0.0004 to -0.0009 and has the further effect of maintaining the restoring force at large angles of yaw. (Compare configurations E and F and configurations H and I of fig. 7.) This action of the dorsal fairings is opposite to that of dorsal fins on conventional airplanes probably because so much of the dorsal area is ahead of the design center of gravity for this type of model. It is desirable then to keep the dorsal fairing area ahead of the center of gravity to a minimum. As shown by the modification data, it is also desirable to keep the top of the dorsal fairing (ahead of the center of gravity) rounded rather than ridged as for the original dorsal. Configuration I was selected as the optimum configuration from these modifications because it improved the stability through the small yaw-angle range to a point at which it was considered satisfactory and also because it provided space in the dorsal fairing for the necessary pressure tubes and control leads. The optimum configuration (fig. 7, configuration I) consists of a $\frac{5}{16}$-inch sheet-steel vertical tail of the original plan form, with a rounded nose and sharpened trailing edge, and a modified dorsal having a flat top instead of the original ridged top. The rest of the tests were made with the configuration described (configuration I).

General stability characteristics.- Stability parameters C_{n_ψ}, C_{l_ψ}, and C_{Y_ψ} are given in figures 24 and 27 for the revised model configuration previously described with the original wing replaced by the similar wing of all-wood construction. This wing had provisions for changing the dihedral angle. The stability parameters were computed from tests made through the angle-of-attack range at $\pm 5^\circ$ of yaw. Flap-down tests were made by using split flaps of the same chord and span (0.20 chord, 1/2 semispan per flap) as the original plain flaps.

The wing-fuselage combination tends to become more stable directionally with increasing values of C_L up to 0.8; this effect is associated with the stability of the wing itself rather than with any wing-fuselage interference since the wing-alone values taken from figure 26 show the same tendency. The effect is probably the result of increasing drag difference at higher values of C_L between the two wing panels for a given change in angle of yaw. When the tips stall, the effect is reversed, and increasing C_L decreases the directional stability. The dihedral effect C_{l_ψ} drops sharply when the tips stall. The data of figure 24 indicate directional instability at the stall for both the flaps-neutral and the flaps-deflected configurations. The tail-on directional stability (for $\Gamma = 0^\circ$) as determined from tests (fig. 24) at small angles of yaw ($\pm 5^\circ$) usually is about -0.0008 larger than values determined from corresponding yaw tests (fig. 25). This

discrepancy in values is a result of the degree of accuracy of the two methods used to determine the slopes. The values of the parameters C_{l_ψ} and C_{Y_ψ} (figs. 24 and 25) obtained by the two test methods compare favorably.

The contribution of the vertical tail to the directional stability $\left(\partial C_n/\partial\psi\right)_v$ has a fairly constant value of -0.0035 with undeflected flaps, which is found to be somewhat greater (about 30 percent) than elementary considerations of effective vertical-tail area, lift-curve slope, and tail length would indicate. Several investigations (for example, see references 5 and 6) indicate that the sidewash angle produced at the vertical tail for midwing arrangements is in the stabilizing direction and may contribute increases in the vertical-tail effectiveness of the order found. It may also be noted that with flaps deflected the directional stability is greater than with flaps neutral, which is attributed to favorable wing-fuselage interference effect with flaps deflected on the stability contribution of the vertical tail as is shown in reference 6.

The increments in C_{n_ψ}, C_{l_ψ}, and C_{Y_ψ} caused by the addition of the vertical tail indicate that the center of pressure of the vertical-tail load is somewhat lower and farther forward than might be expected. The vertical tail appears to alter the pressure distribution over the fuselage in such a way as to decrease the instability of the fuselage. The mutual effect is mentioned in reference 6 but no data are available. Tests of an isolated vertical tail in the presence of the fuselage would be required to obtain such data.

Effect of geometric dihedral.- The data of figure 24 indicate that the effective dihedral was excessive. The geometric dihedral angle of the wing was therefore changed from 0° to -10° in an effort to decrease the effective dihedral. The change in geometric dihedral extended from the wing tip to the fuselage intersection.

The lateral-stability parameters (for $\Gamma = -10^\circ$) of figure 28 compare favorably with the parameters obtained in tests made at ±5° yaw (fig. 27); however, alteration of the dihedral angle to -10° (fig. 27) increased the tail-on directional stability C_{n_ψ} slightly at a given value of $-C_L$ and decreased the effective dihedral C_{l_ψ} by about 0.0010, or about 0.0001 per degree dihedral change. Directional instability, however, still occurred at the stall for the flaps-neutral configuration (fig. 27(a)). The values of C_{l_ψ} for -10° dihedral were considered to be satisfactory insofar as their effect on the lateral flying qualities was concerned.

The data for the configurations with 0° and -10° dihedral presented in figures 24 and 27 are given about the test center of gravity. The design center of gravity of the model is higher (vertically) than that used in the presentation of the data. The vertical transfer of the data from the test center of gravity to the design center of gravity would decrease C_{l_ψ} by about $0.04C_{Y_\psi}$, which amounts to a correction ΔC_{l_ψ} of about -0.0004 for the 0° dihedral wing and -0.0005 for the dropped wing (-10° dihedral). It should also be noted that forward movement of the center of gravity from the test location (0.36 M.A.C.) to the design location (0.23 M.A.C.) increases the directional stability by about $-0.045C_{Y_\psi}$ or by about the same numerical magnitude as the effective dihedral was increased by the vertical transfer of the center of gravity.

Effect of end plates.- Two sizes of rectangular wing-tip end plates (tip fins) having total areas (for both wing panels) of 10 percent and 20 percent of the wing area were tested. The configurations and data are given in figure 29. The following table gives the values of slopes measured from figure 29:

Fins	C_{l_ψ}	C_{n_ψ}	C_{Y_ψ}
$\alpha = 5.4°$; $\delta_f = 0°$; $C_L = 0.26$			
Off	0.0024	-0.0018	0.010
Small	.0016	-.0023	.014
Large	.0002	-.0035	.018
$\alpha = 11.2°$; $\delta_f = 50°$; $C_L = 0.82$			
Off	0.0041	-0.0031	0.012
Small	.0026	-.0037	.016
Large	.0019	-.0042	.021

For the high-speed conditions, the effective dihedral is reduced to about 0° with large tip fins, and an appreciable increase in directional stability occurs. The small tip fins also have a large effect. With flaps down a large decrease in effective dihedral also occurs with final values of C_{l_ψ} in the normal range for unswept wings (about -0.0010 to -0.0020).

Part of the increment in C_{l_ψ} caused by tip fins may be attributed to the side force acting on the end plates below the center of gravity. This effect was checked by approximate calculation of the side force on the end plates with the end plates considered as low-aspect-ratio wings with the wing itself acting as an end plate for the tip fins. The side force on the plates also accounts directly for the increased directional stability caused by the addition of the tip fins.

Figure 29(b) also shows that the rolling moment remains essentially constant for yaw angles between 5° and 20° with the large end plates.

Aileron characteristics.- Aileron effectiveness was measured through the angle-of-attack range with flaps up and with flaps down and the data are presented in figure 30. The effectiveness of the aileron in yaw is shown in figure 31. Aileron hinge-moment data were also obtained as shown in these figures.

For angles of attack greater than about 14°, the ailerons exhibit a very large increase in upfloating tendency (fig. 30) coincident with the point at which the lift curve begins to round off as the wing tips begin to stall. The stalling was observed in tuft studies to occur at angles of attack of about 14°. The aileron effectiveness in the region beyond 14° with flaps up, however, remains relatively unaffected except at the large aileron angles. With flaps down (fig. 30(b)), there is a marked decrease in aileron effectiveness beyond the angle of initial tip stalling (very near $C_{L_{max}}$; see fig. 12).

Since most tests were made with only the left aileron deflected, a single test was made (fig. 31) to determine whether the effects of deflecting two ailerons simultaneously are approximately additive. The curves indicate that the effects are additive, within the experimental accuracy, and that the total rolling moment for two ailerons deflected equally and oppositely is almost constant with angle of yaw.

Based upon untrimmed data (for $\alpha = 11.2°$), the ailerons are not capable of trimming out sideslip angles greater than about 10°, with flaps down, because of the large value of the effective dihedral C_{l_ψ}.

SUMMARY OF RESULTS

The following conclusions are based on tests of an airplane model having a wing with quarter-chord line swept back 40°, aspect ratio 2.50 and taper ratio 0.42 and a horizontal tail with quarter-chord line swept back 40°, aspect ratio 3.87, and taper ratio 0.49 to determine its low-speed stability and control characteristics:

1. The longitudinal stability becomes inadequate above a lift coefficient which is 0.15 below the stall for the horizontal tail located near the fuselage juncture on the vertical tail. The model shows instability at the stall, which is probably promoted by wing-tip stalling.

2. Changing the wing dihedral from 0° to -10° or adding end plates extending down from the tips had little effect on the longitudinal stability characteristics.

3. Location of the horizontal tail near the top of the vertical tail resulted in satisfactory longitudinal stability throughout the lift range because the tail was in a region of more favorable downwash.

4. The directional stability at small yaw angles was improved by replacing the original vertical tail with a steel flat plate to improve the tail-fuselage intersection and by flattening the top of the dorsal.

5. Removal of any of the dorsal fairing arrangements increased the directional stability an increment of about -0.0004 to -0.0009 and had the effect of maintaining the restoring force at high yaw angles. The dorsal action was opposite to that of conventional airplanes probably because of the large area forward of the center of gravity.

6. The wing-fuselage combination tends to become more stable directionally with increasing values of lift coefficient up to 0.8, which was a result of the wing itself rather than fuselage interference since the wing-alone values show the same tendency.

7. The directional stability was greater with flaps deflected than with flaps neutral.

8. The tail-on directional stability was increased and the effective dihedral was decreased (by about 0.0001 per degree dihedral change) when the geometric dihedral angle was changed from 0° to -10°.

9. End plates greatly reduced the effective dihedral and increased the directional stability for the high-speed condition.

10. The ailerons show a very large increase in upfloating tendency for angles of attack greater than 14°. The aileron effectiveness was relatively unaffected where the stall occurred (14°) with flaps neutral; however, with flaps deflected there was a decrease in aileron

effectiveness. The ailerons (for $\alpha = 11.2^{\circ}$) for the untrimmed condition cannot hold a sideslip angle greater than about 10° for the flaps-down configuration.

Langley Aeronautical Laboratory
National Advisory Committee for Aeronautics
Langley Field, Va., March 6, 1947

REFERENCES

1. Gillis, Clarence L., Polhamus, Edward C., and Gray, Joseph L., Jr.: Charts for Determining Jet-Boundary Corrections for Complete Models in 7- by 10-Foot Closed Rectangular Wind Tunnels. NACA ARR L5G31, 1945.

2. Thom, A.: Blockage Corrections in a Closed High-Speed Tunnel. R. & M. No. 2033, British A.R.C., 1943.

3. Schuldenfrei, Marvin: Some Notes on the Determination of the Stick-Fixed Neutral Point from Wind-Tunnel Data. NACA RB 3I20, 1943.

4. Multhopp, H.: Aerodynamics of the Fuselage. NACA TM 1036, 1942.

5. Recant, Isidore G., and Wallace, Arthur R.: Wind-Tunnel Investigation of the Effect of Vertical Position of the Wing on the Side Flow in the Region of the Vertical Tail. NACA TN 804, 1941.

6. Recant, Isidore G., and Wallace, Arthur R.: Wind-Tunnel Investigation of Effect of Yaw on Lateral-Stability Characteristics. III - Symmetrically Tapered Wing at Various Positions on Circular Fuselage with and without a Vertical Tail. NACA TN 825, 1941.

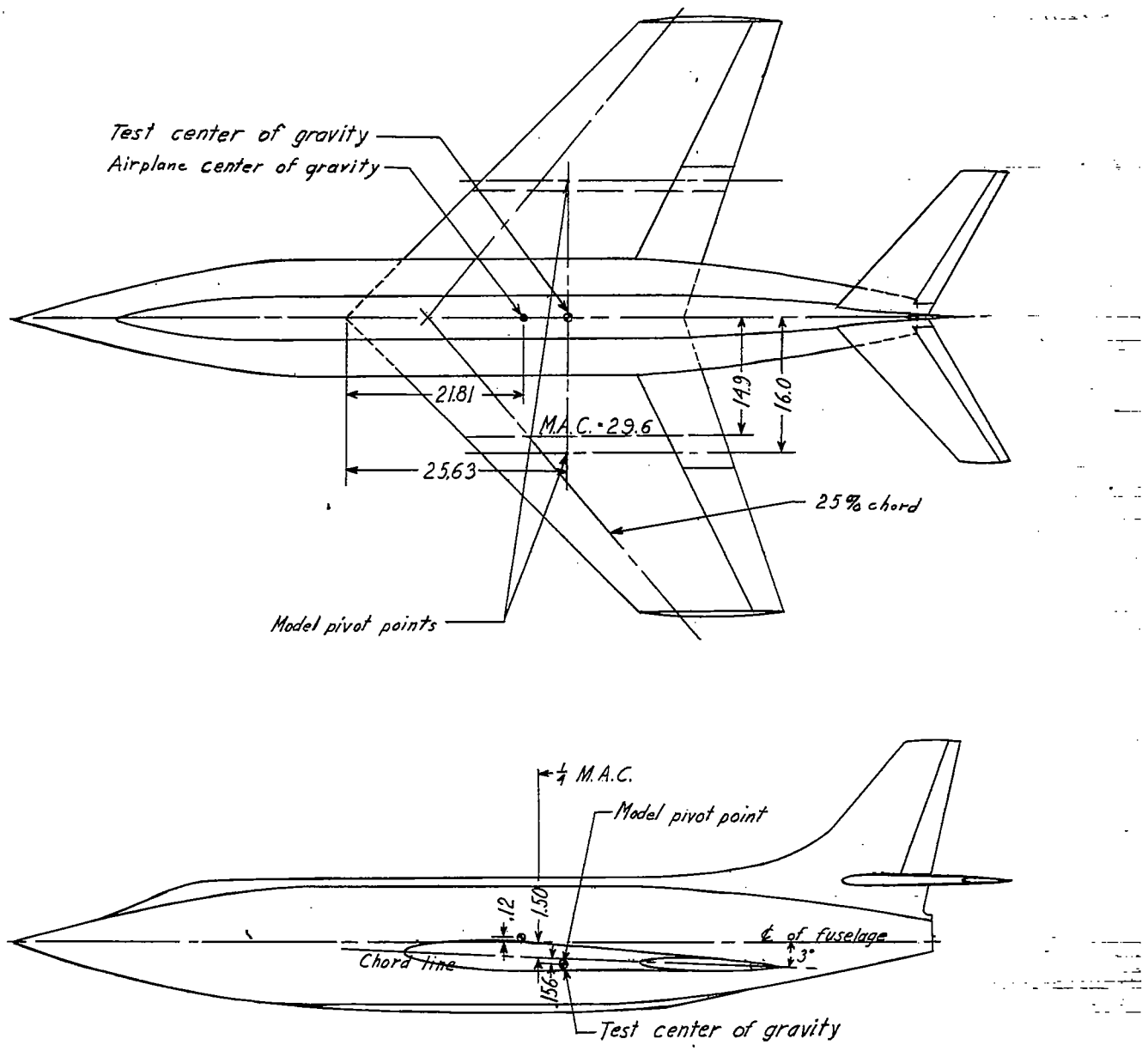

Figure 1.- Location of test center of gravity and airplane center of gravity of model having a 40° sweptback wing with aspect ratio 2.50 and taper ratio 0.42. All dimensions are in inches.

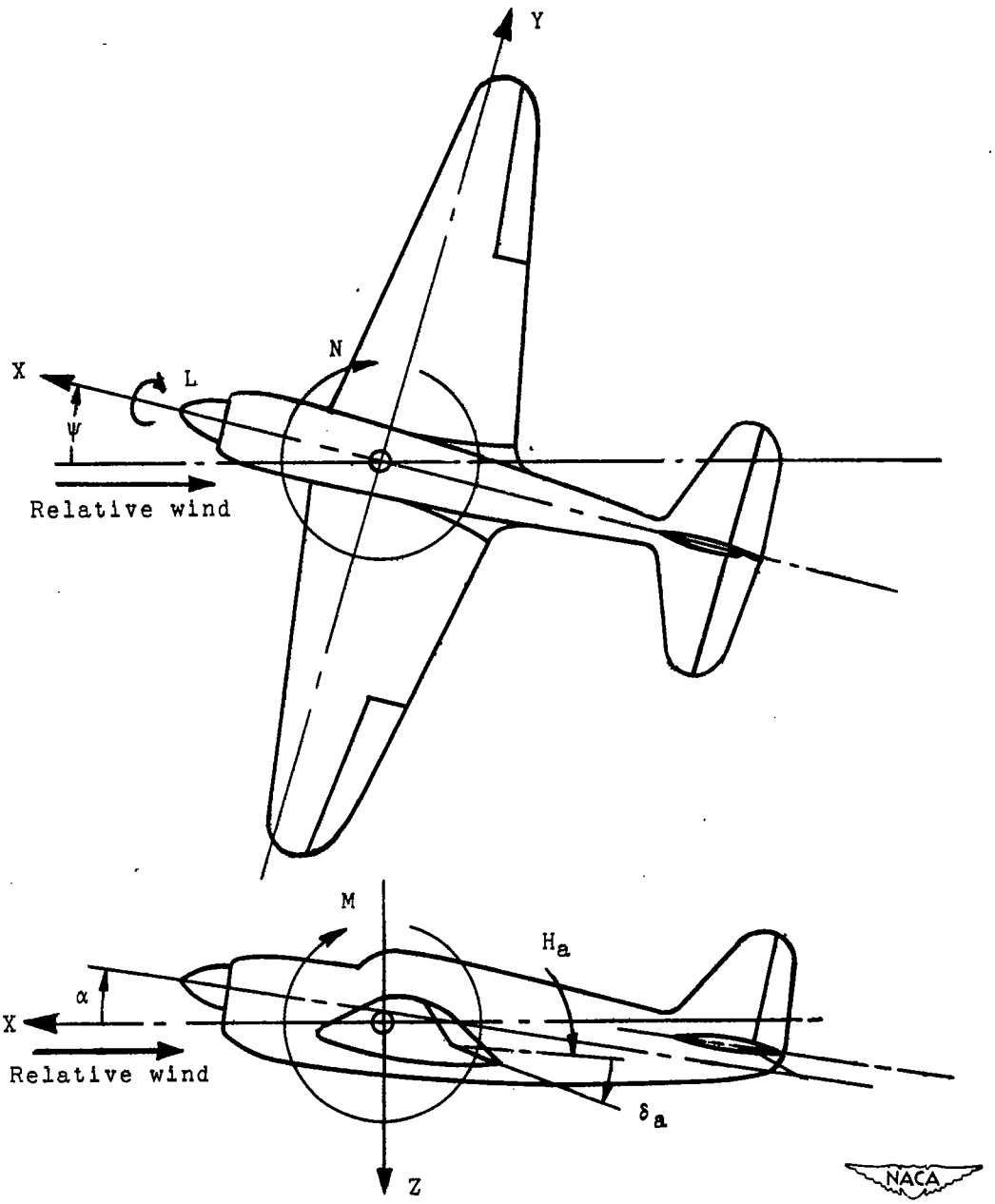

Figure 2.- System of axes and control-surface hinge moments and deflections. Positive values of forces, moments, and angles are indicated by arrows. Positive values of tab hinge moments and deflections are in the same directions as the positive values for the control surfaces to which the tabs are attached.

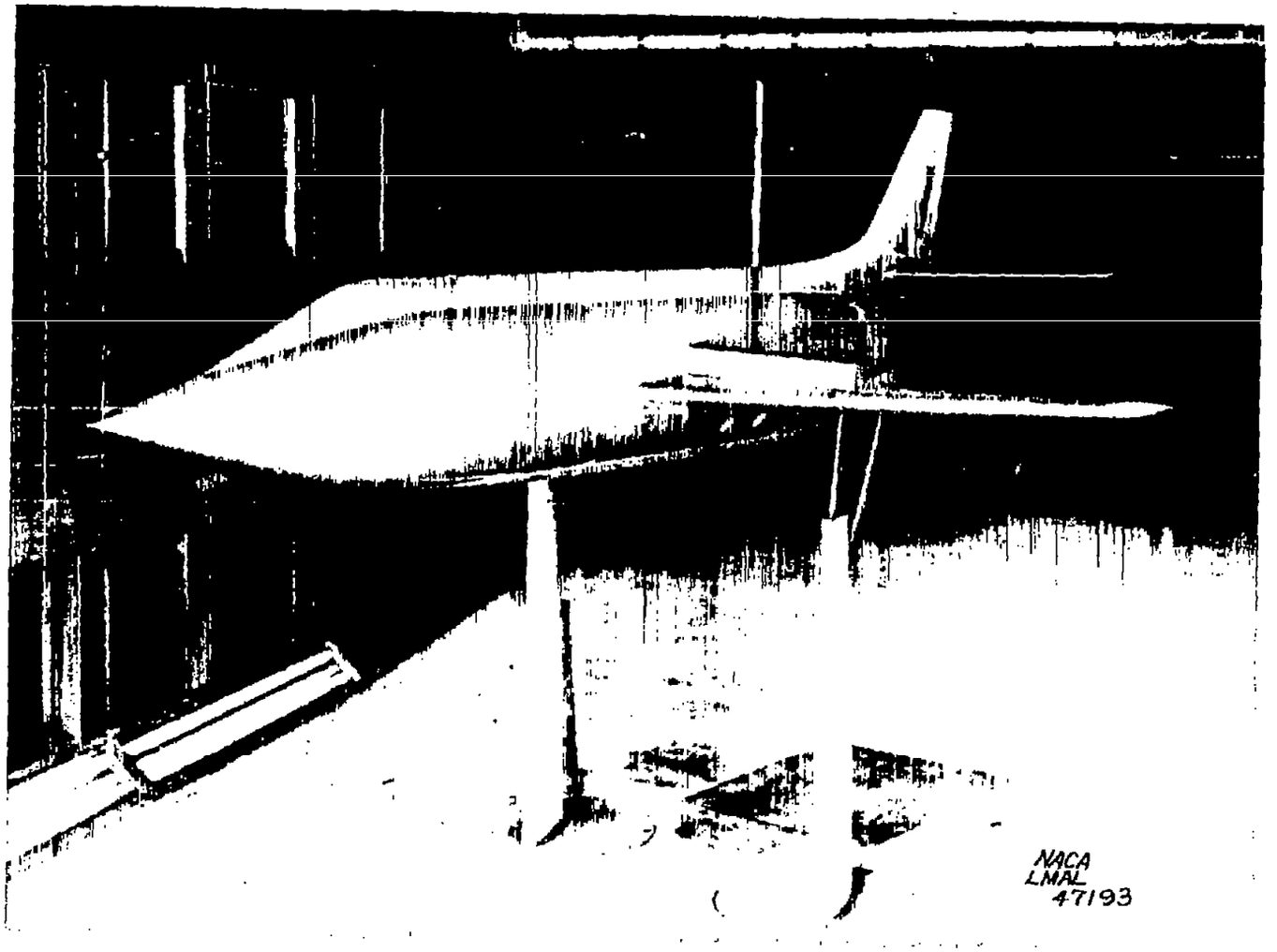

(a) Three-quarter front view.

Figure 3.- Model used in investigation mounted in the Langley 300 MPH 7- by 10-foot tunnel. $\delta_f = 0^\circ$; $\Gamma = 0^\circ$.

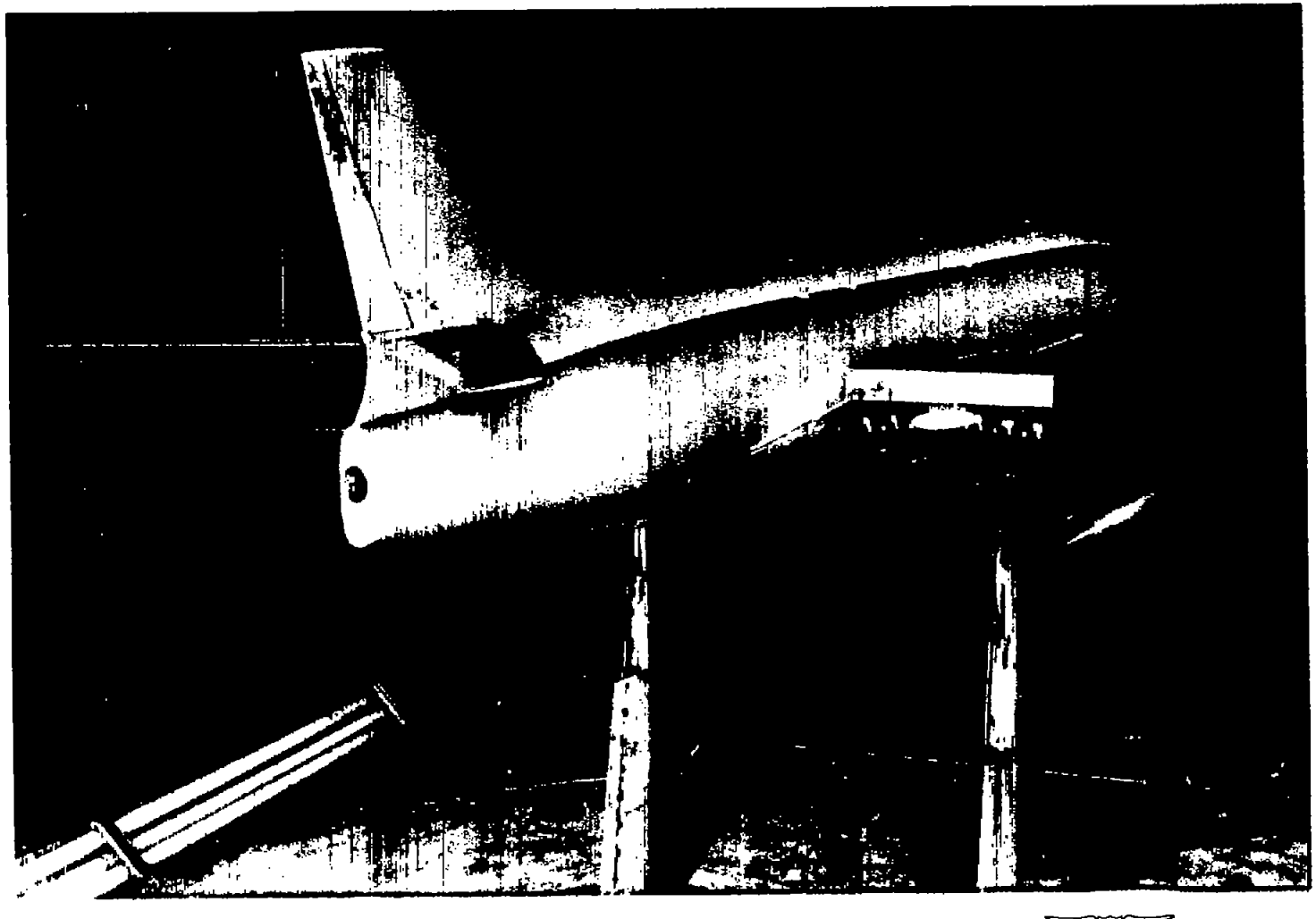

(b) Three-quarter rear view.

Figure 3.- Concluded.

AREAS (sq ft)

Wing area (including ailerons, flaps, fuselage). . . 13.64

Control-surface areas:

Wing flaps	0.95
Ailerons (total behind hinge line)	1.08
Horizontal tail (total)	2.06
Stabilizer	1.66
Elevator (behind hinge line)	0.40
Vertical tail (total)	1.67
Fin (excluding dorsal)	1.43
Rudder (behind hinge line)	0.24

AIRFOIL SECTION

Root and tip (measured perpendicular to 0.25c line) . . . . . NACA 65-110 (a = 1)

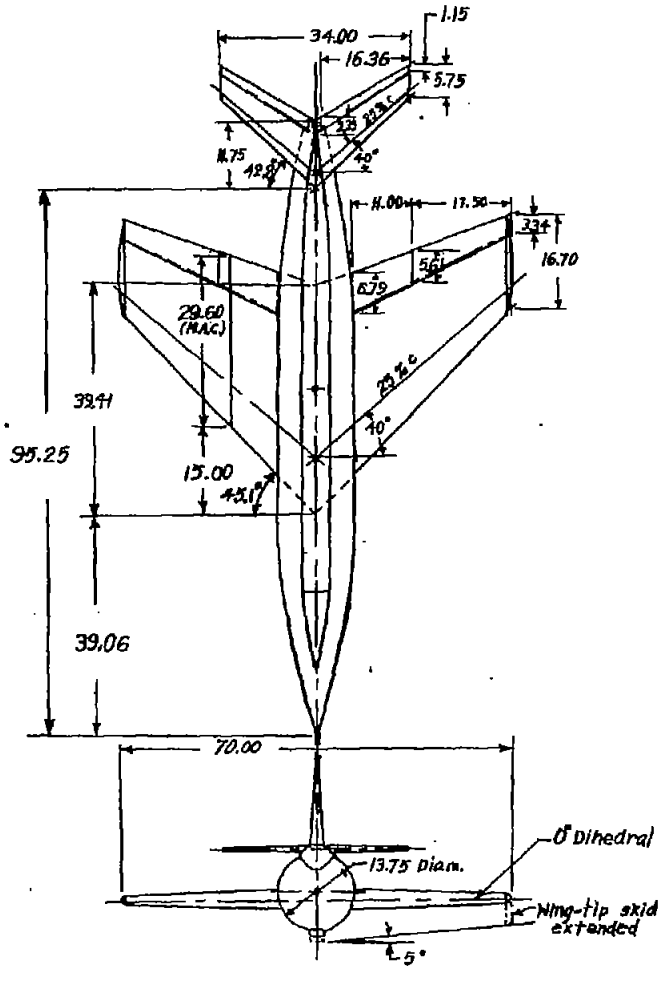

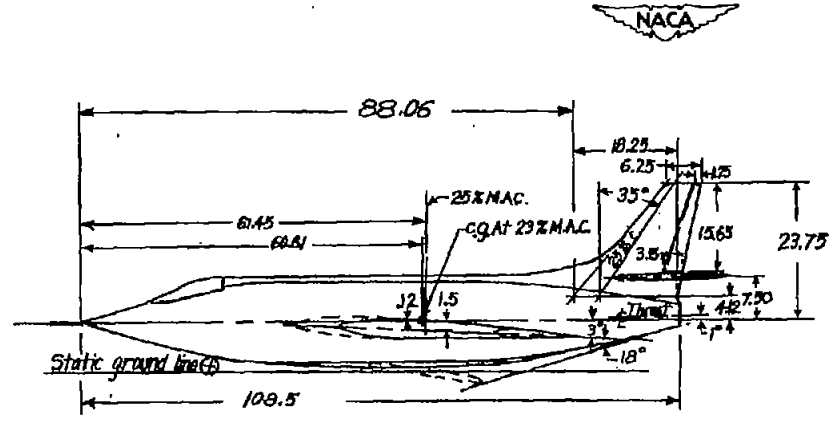

Figure 4.- Three-view drawing of test model. All dimensions are in inches.

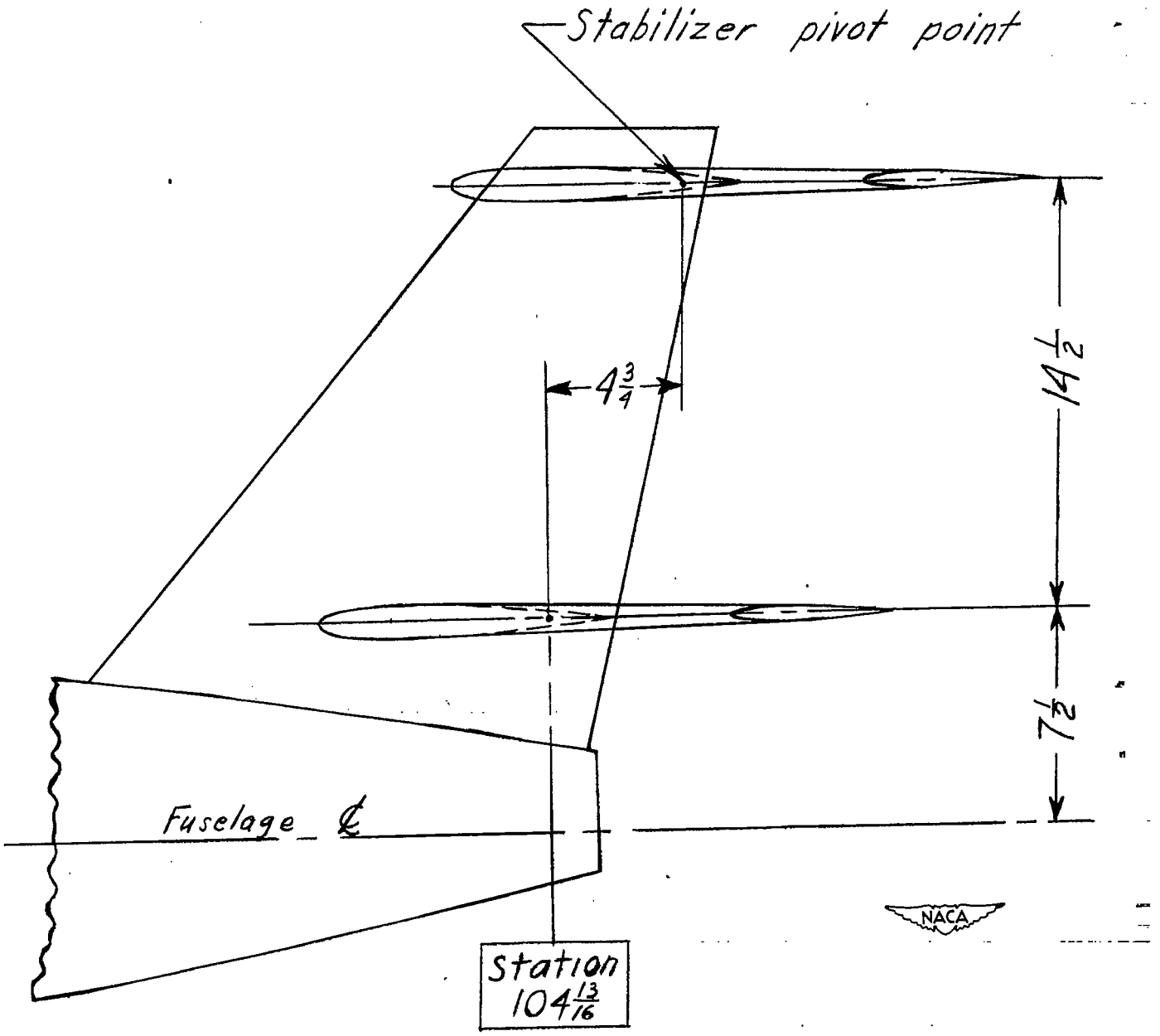

Figure 5.- Horizontal-tail locations of model. All dimensions are in inches.

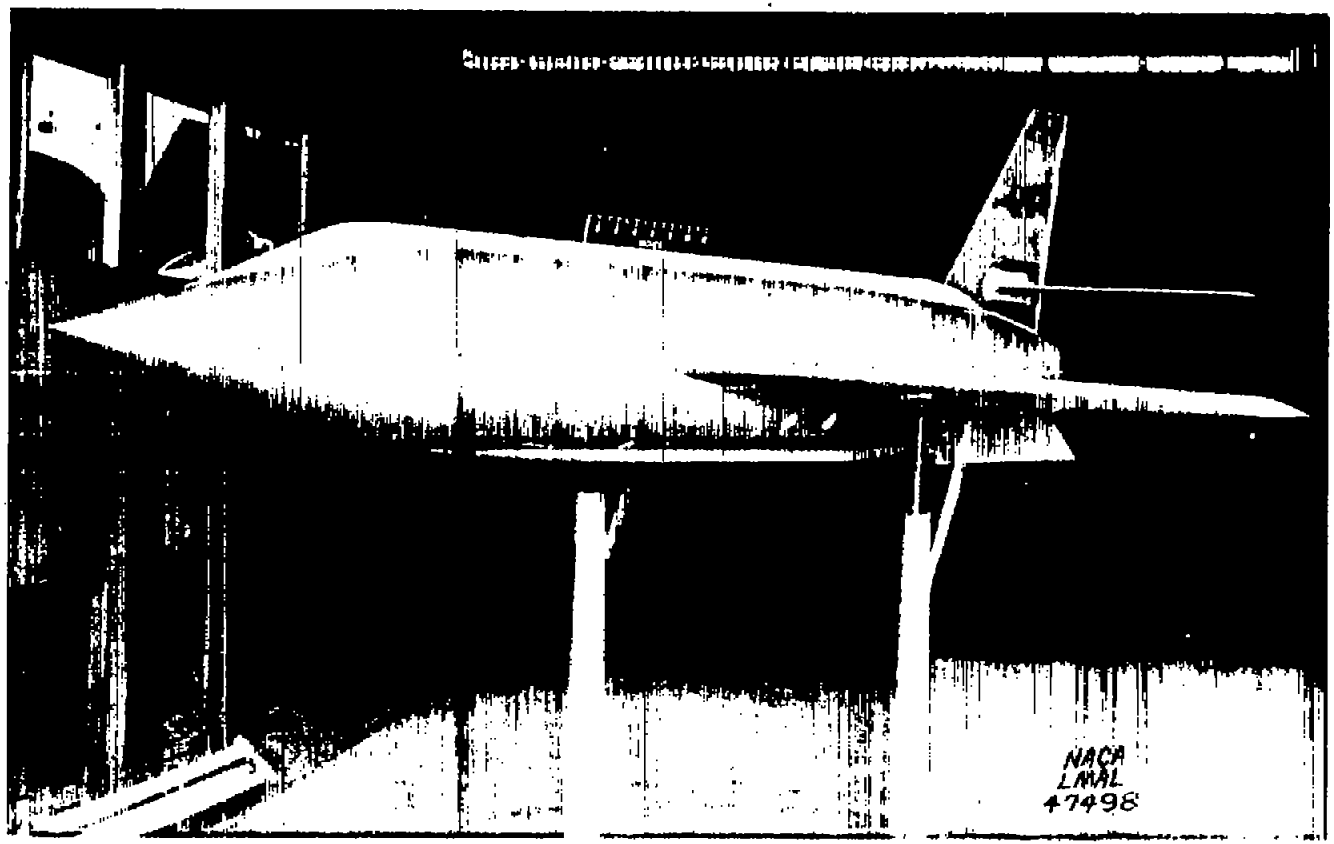

(a) Three-quarter front view.

Figure 6.- Test model with revised vertical tail and dorsal mounted in the Langley 300 MPH 7- by 10-foot tunnel. $\delta_f = 50^\circ$ (split flaps); $\Gamma = 0^\circ$.

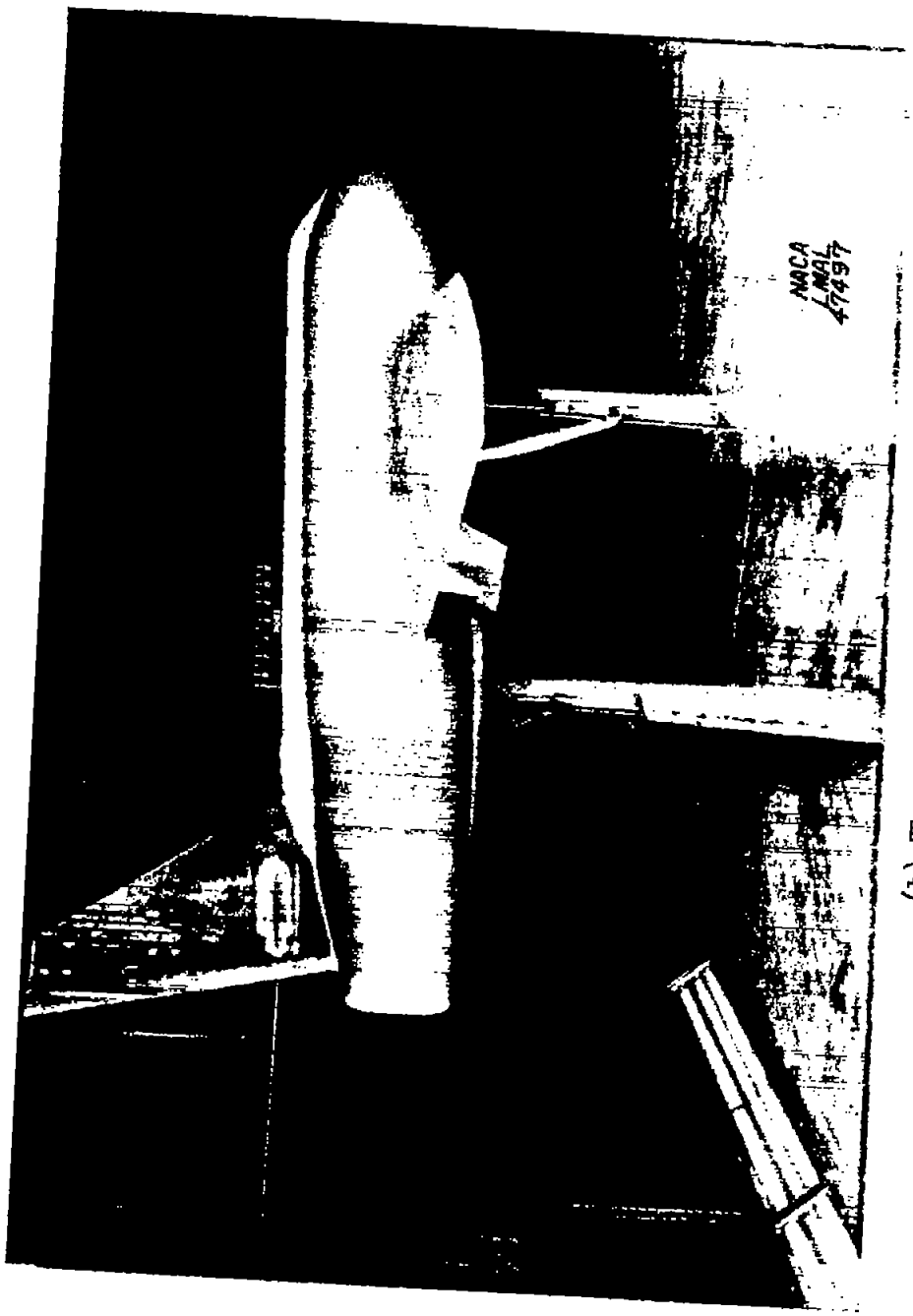

(b) Three-quarter rear view.

Figure 6.- Concluded.

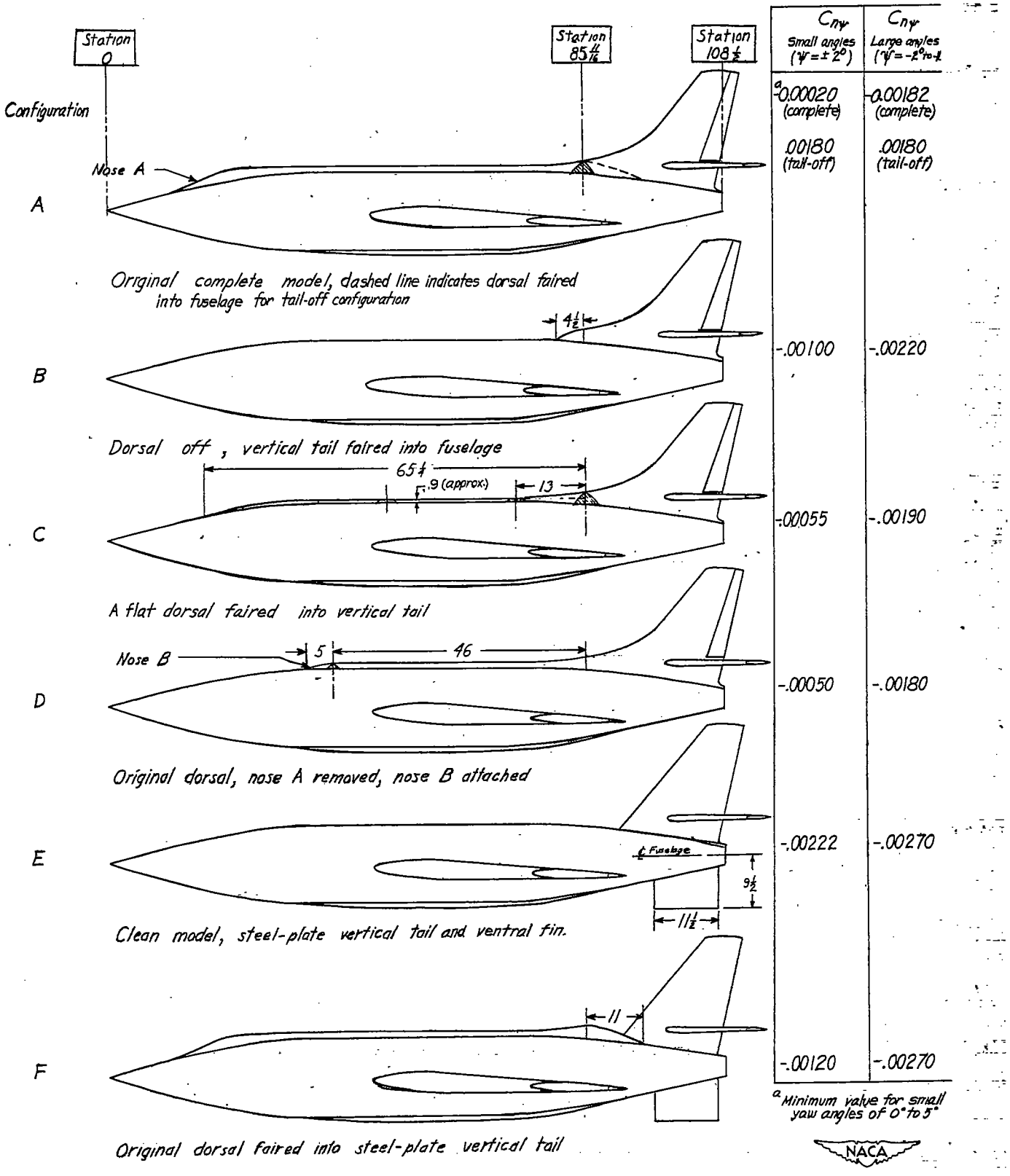

Figure 7.- Effect of dorsal and vertical-tail modifications on the directional stability of test model.

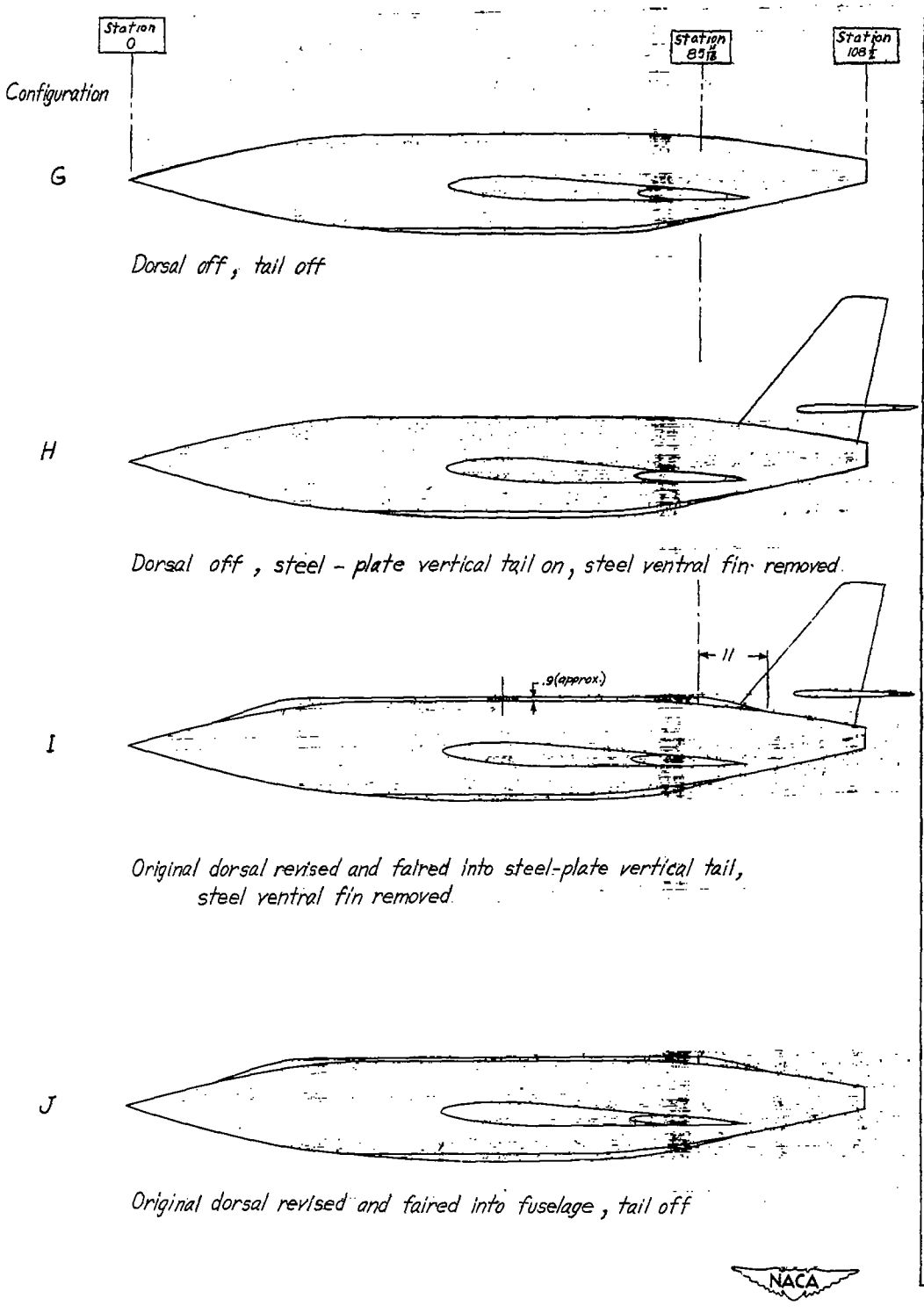

Configuration	C_{n_ψ} Small angles ($\psi = \pm 2°$)	C_{n_ψ} Large angles ($\psi = -2°$ to $-10°$)
G	0.00230	0.00180
H	-.00165	-.00250
I	-.00130	-.00200
J	.00250	.00200

Figure 7.- Concluded.

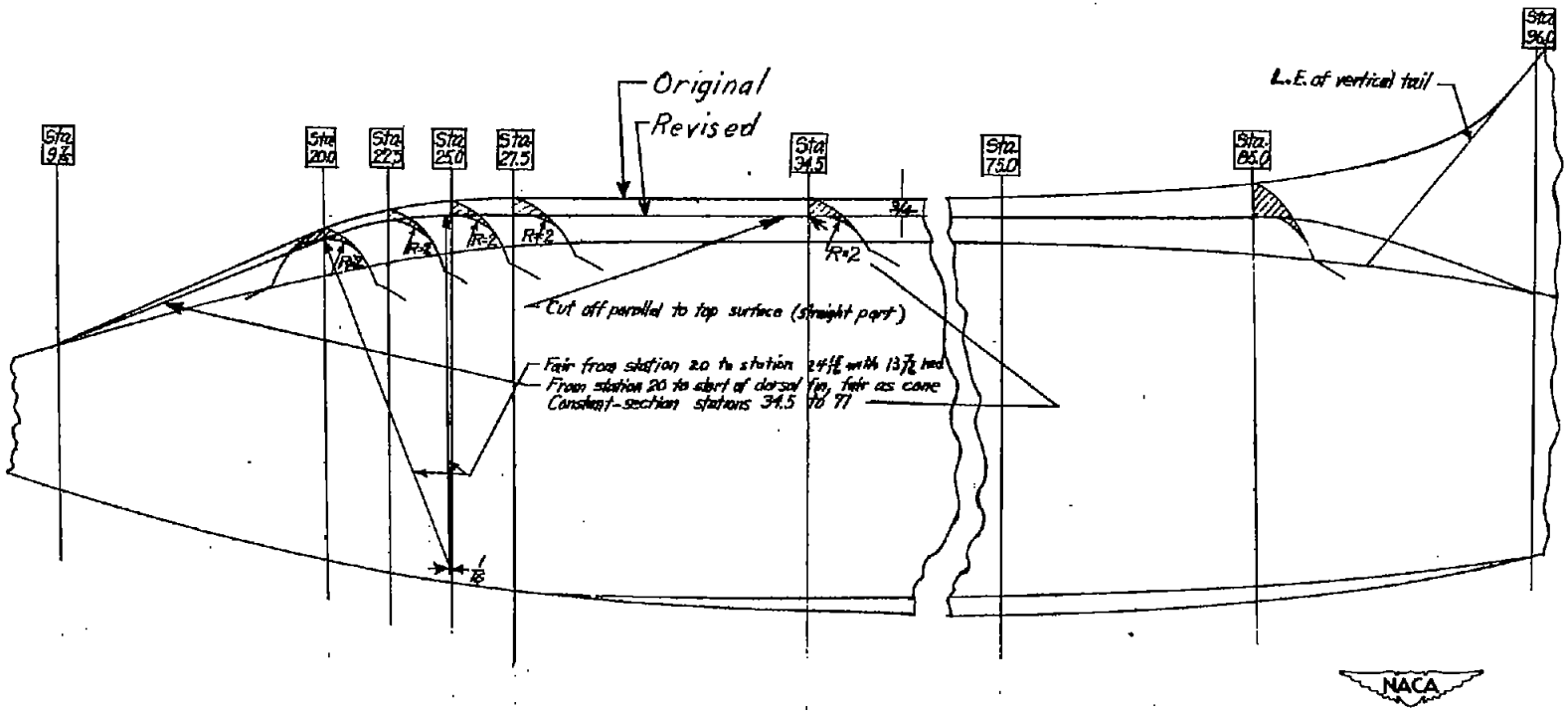

Figure 8.- Detail of revised dorsal for test model.

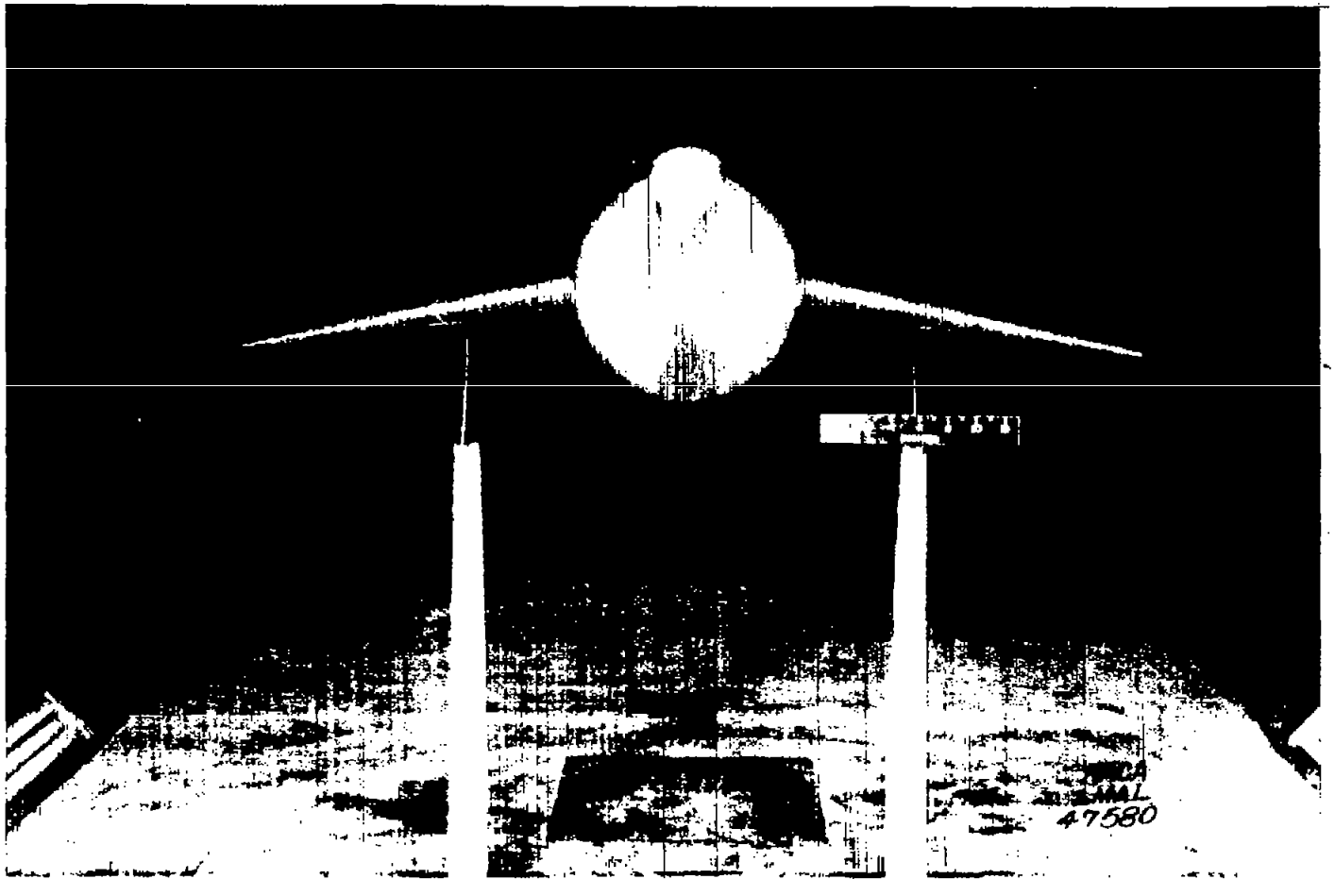

(a) Front view.

Figure 9.- Test model with revised dorsal mounted in the Langley 300 MPH 7- by 10-foot tunnel. Tail off; $\delta_f = 0^\circ$; $\Gamma = -10^\circ$.

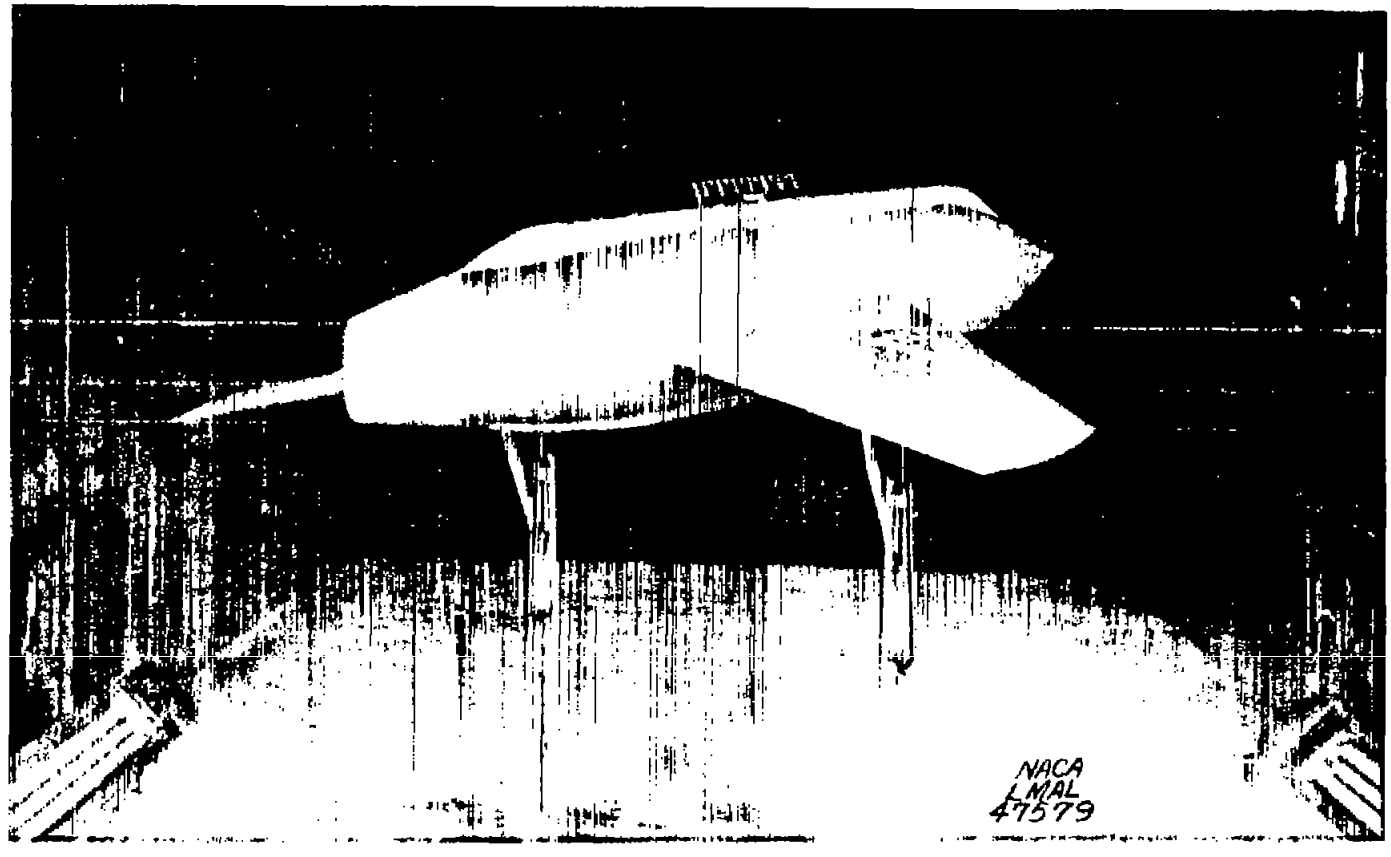

(b) Three-quarter rear view.

Figure 9.- Concluded.

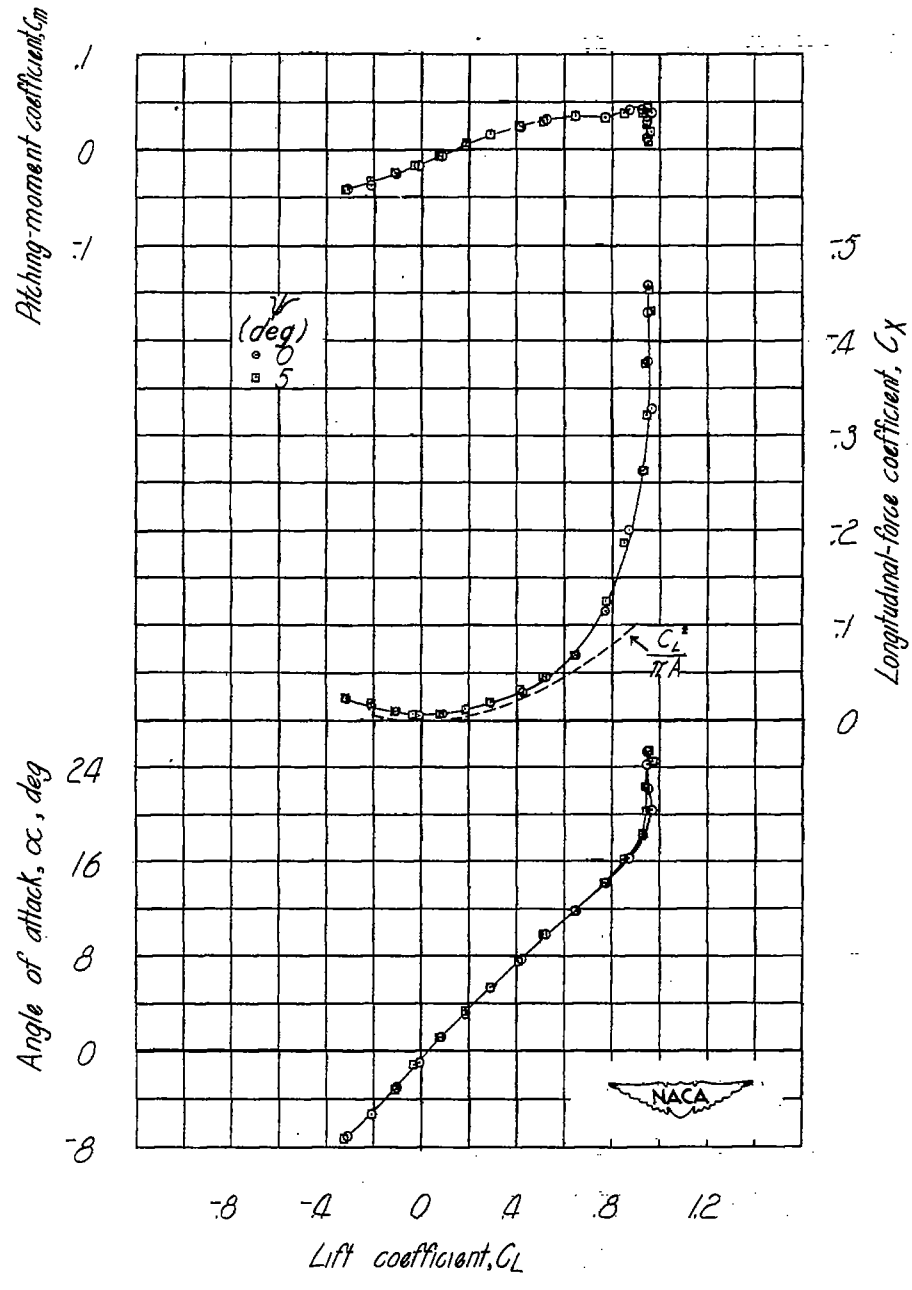

Figure 10.- Wing-alone characteristics in pitch of test model. $\delta_f = 0^\circ$; $\Gamma = 0^\circ$; test center of gravity at 35.9 percent M.A.C.

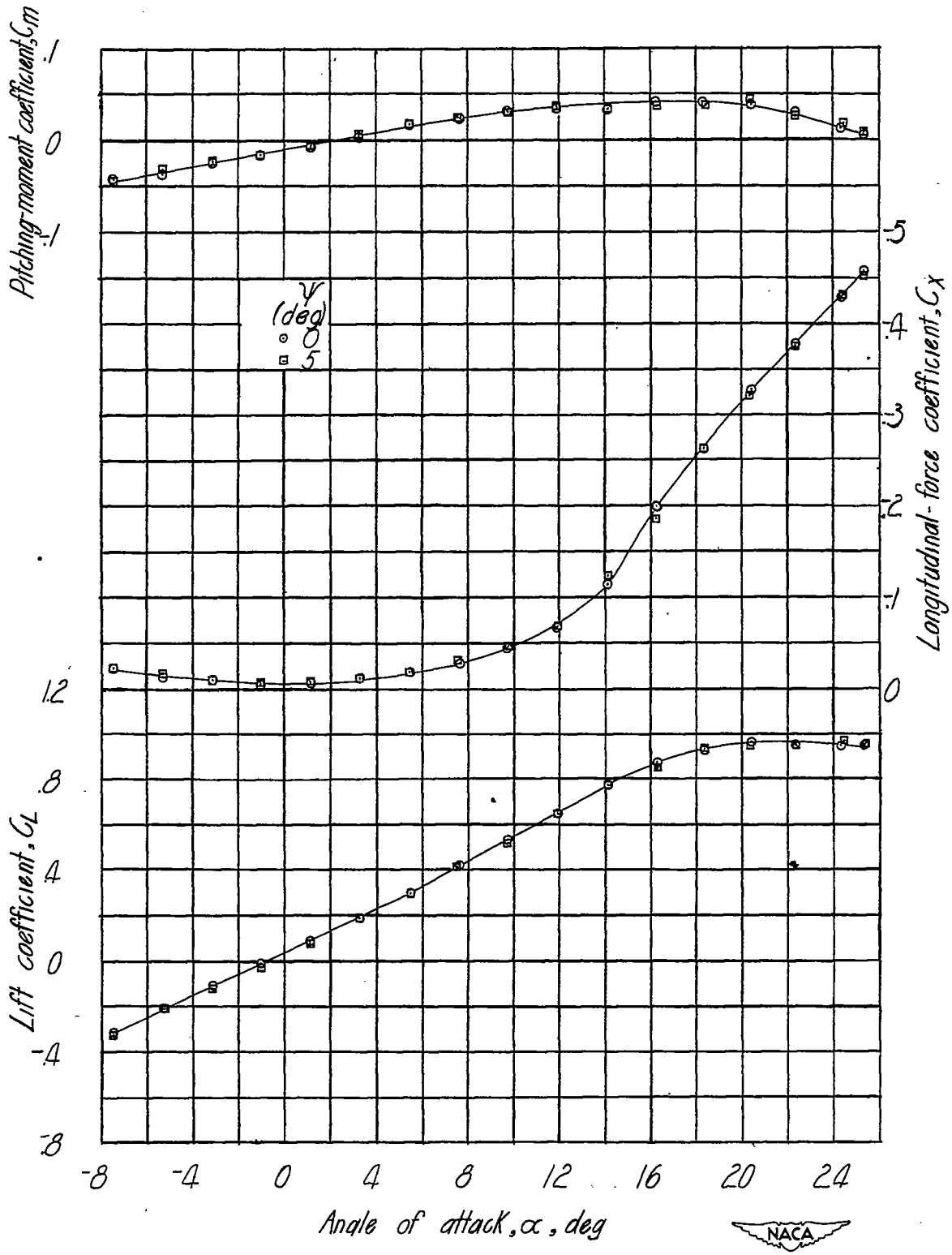

Figure 10.- Concluded.

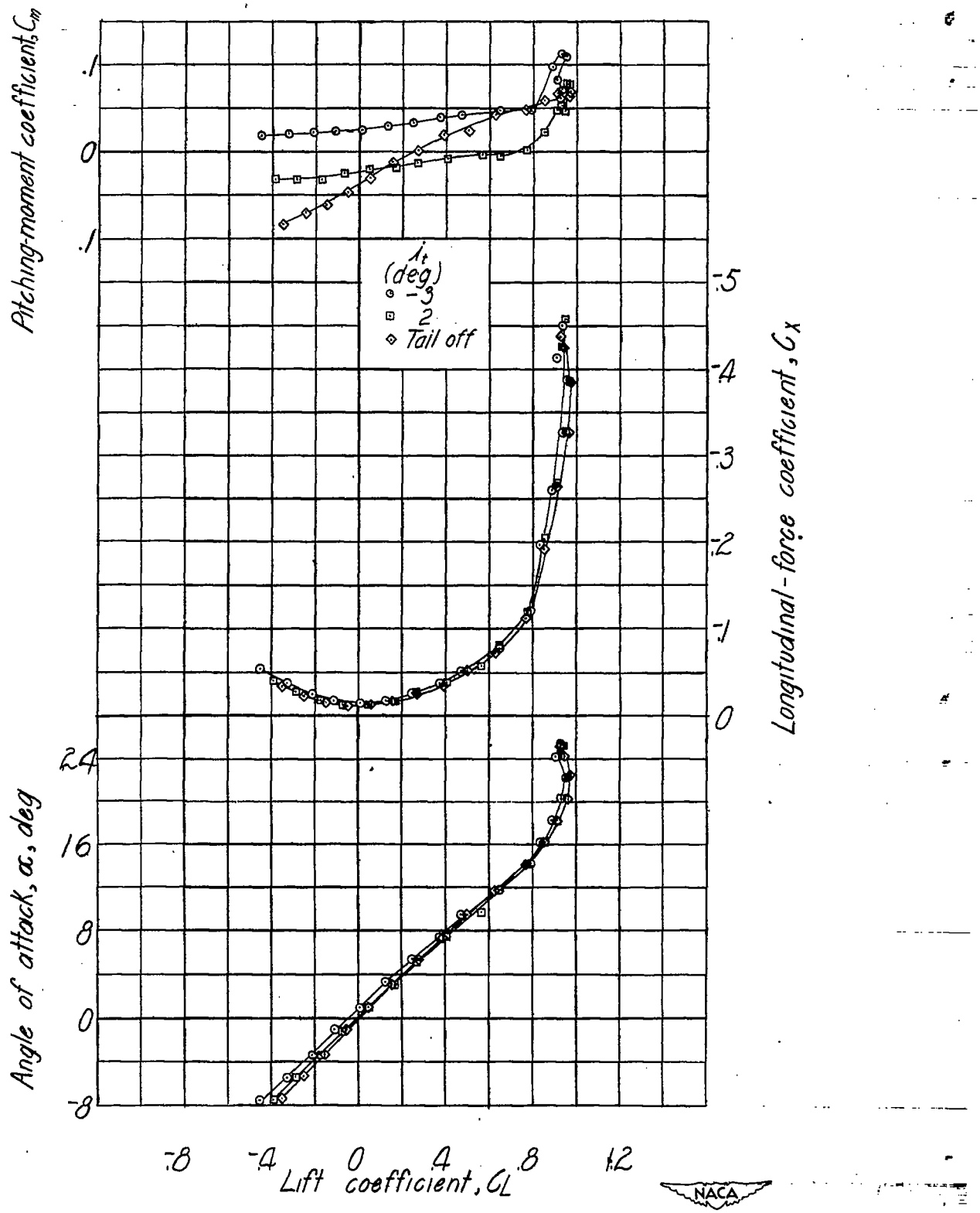

Figure 11.- Effect of stabilizer on the aerodynamic characteristics in pitch of test model. $\delta_f = 0^\circ$; $\Psi = 0^\circ$; $\Gamma = 0^\circ$; test center of gravity at 35.9 percent M.A.C.

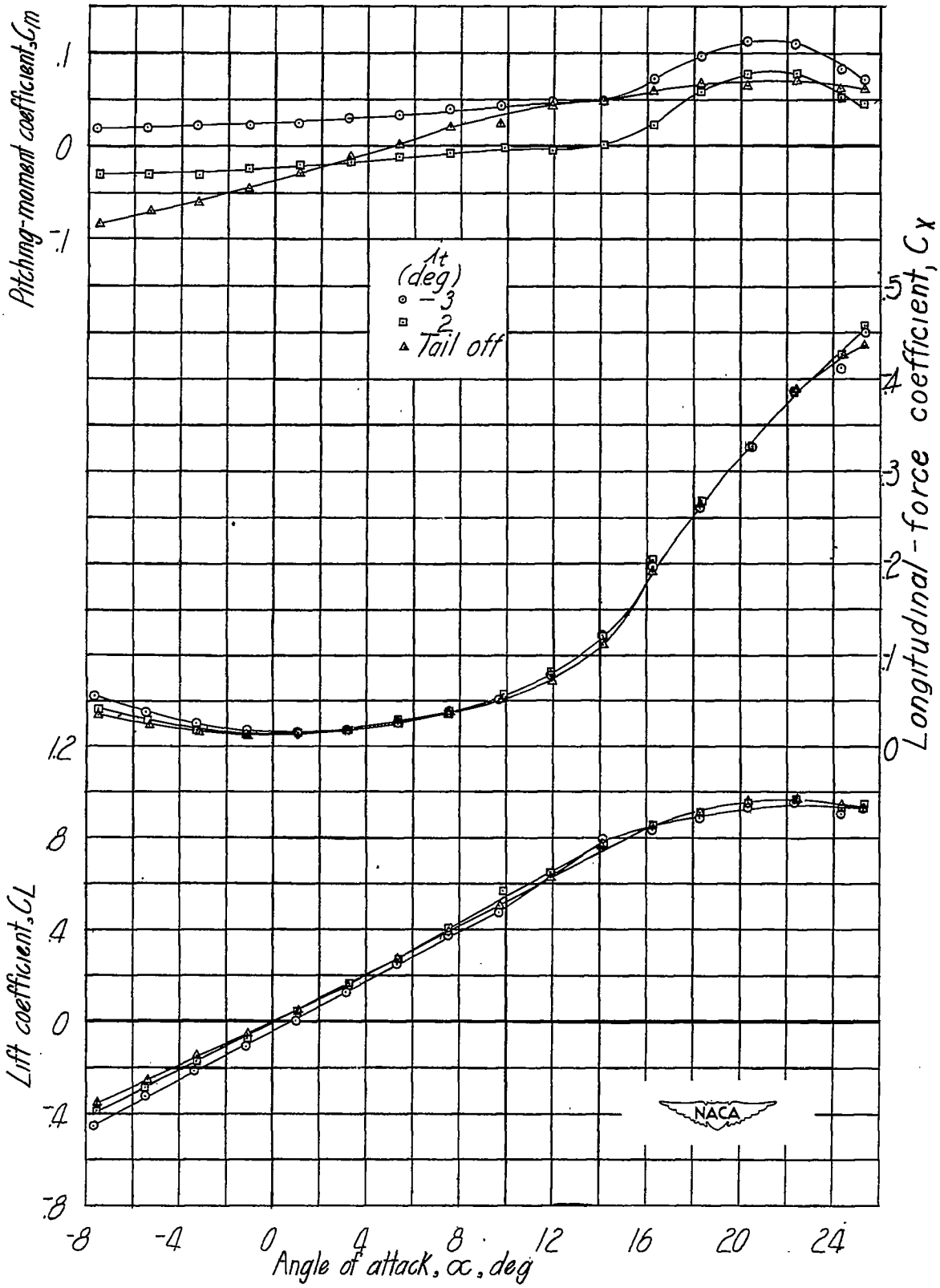

Figure 11.- Concluded.

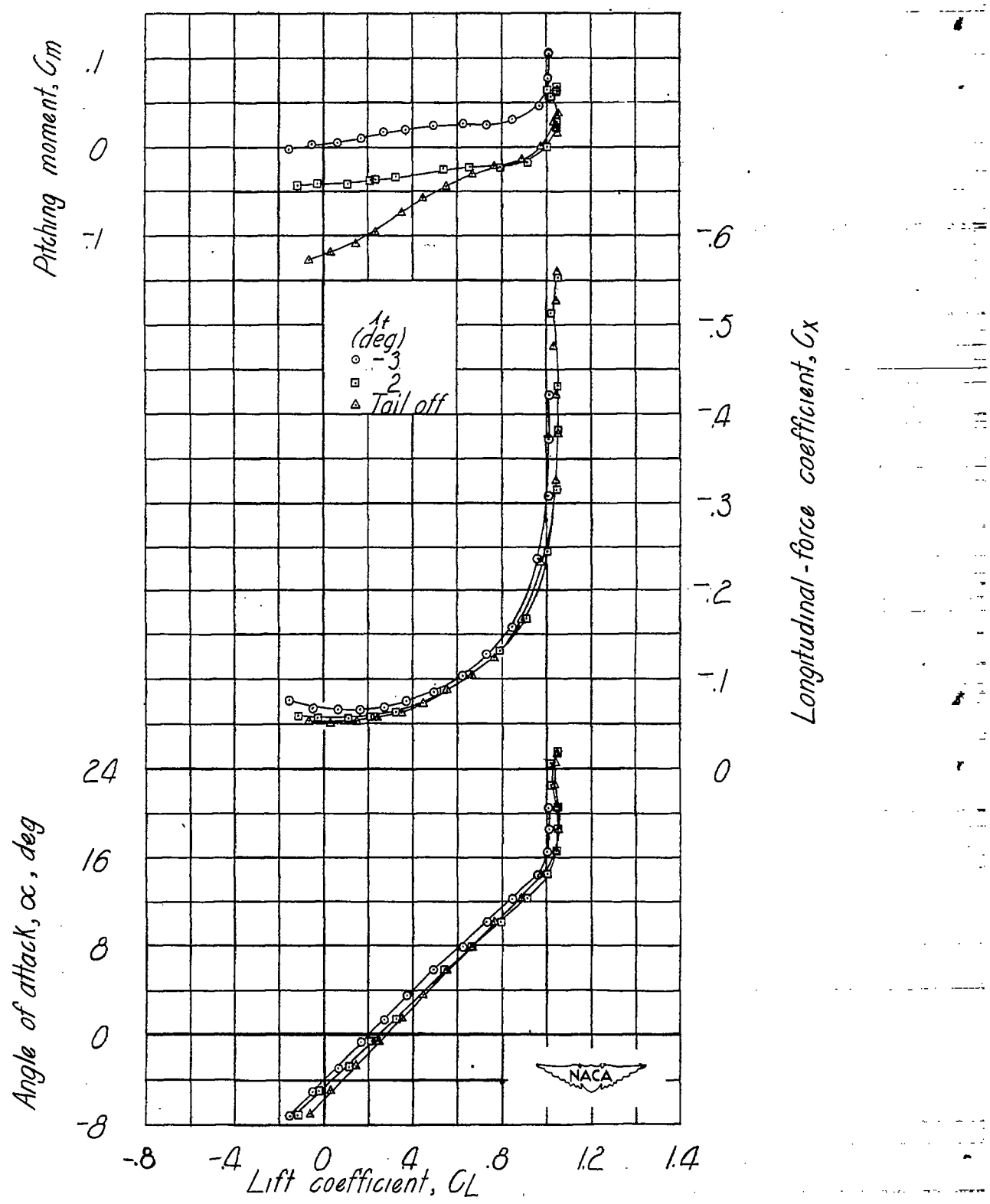

Figure 12.- Effect of stabilizer on the aerodynamic characteristics in pitch of test model. $\delta_f = 50^\circ$; $\psi = 0^\circ$; $\Gamma = 0^\circ$; test center of gravity at 35.9 percent M.A.C.

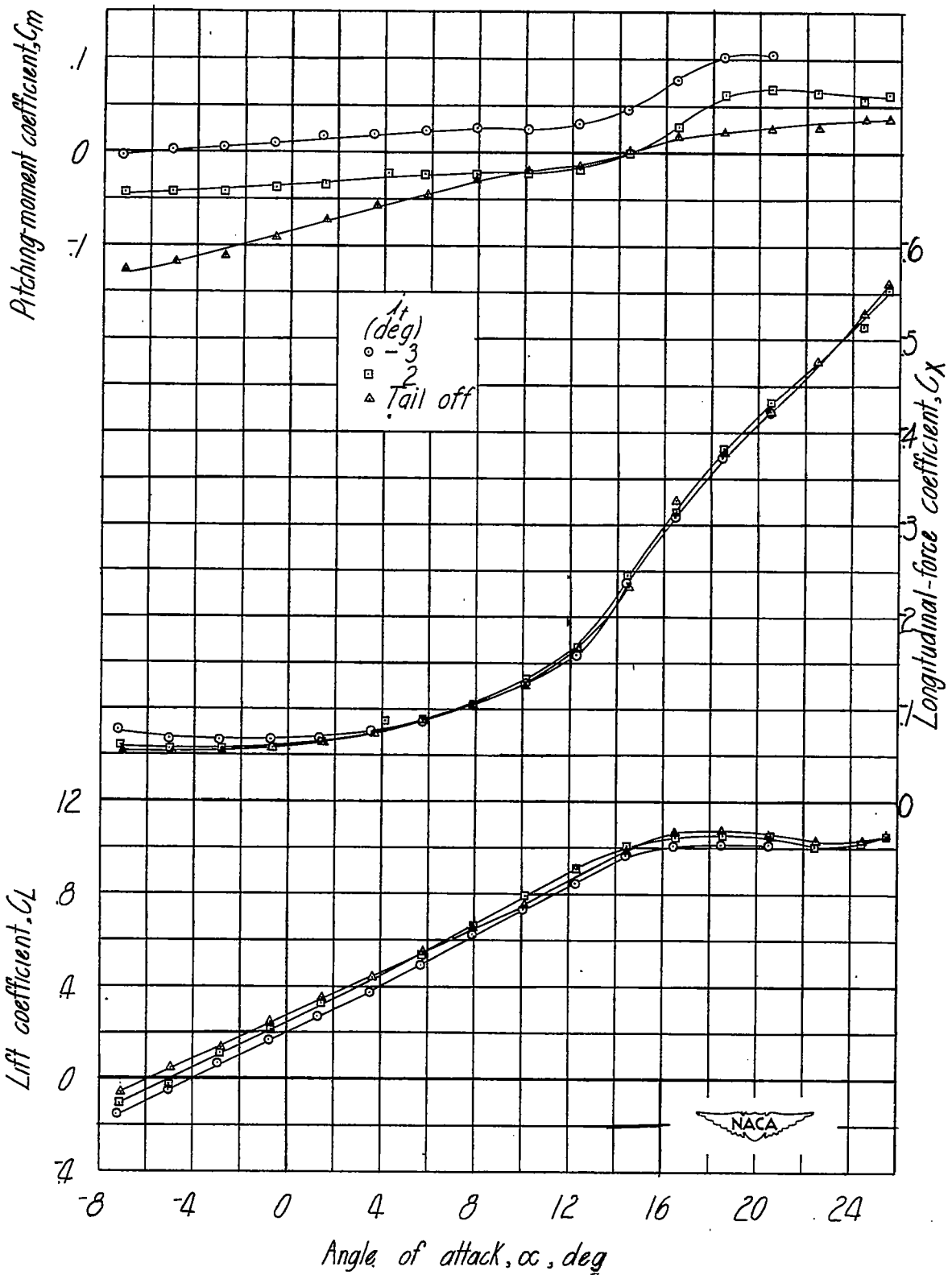

Figure 12.- Concluded.

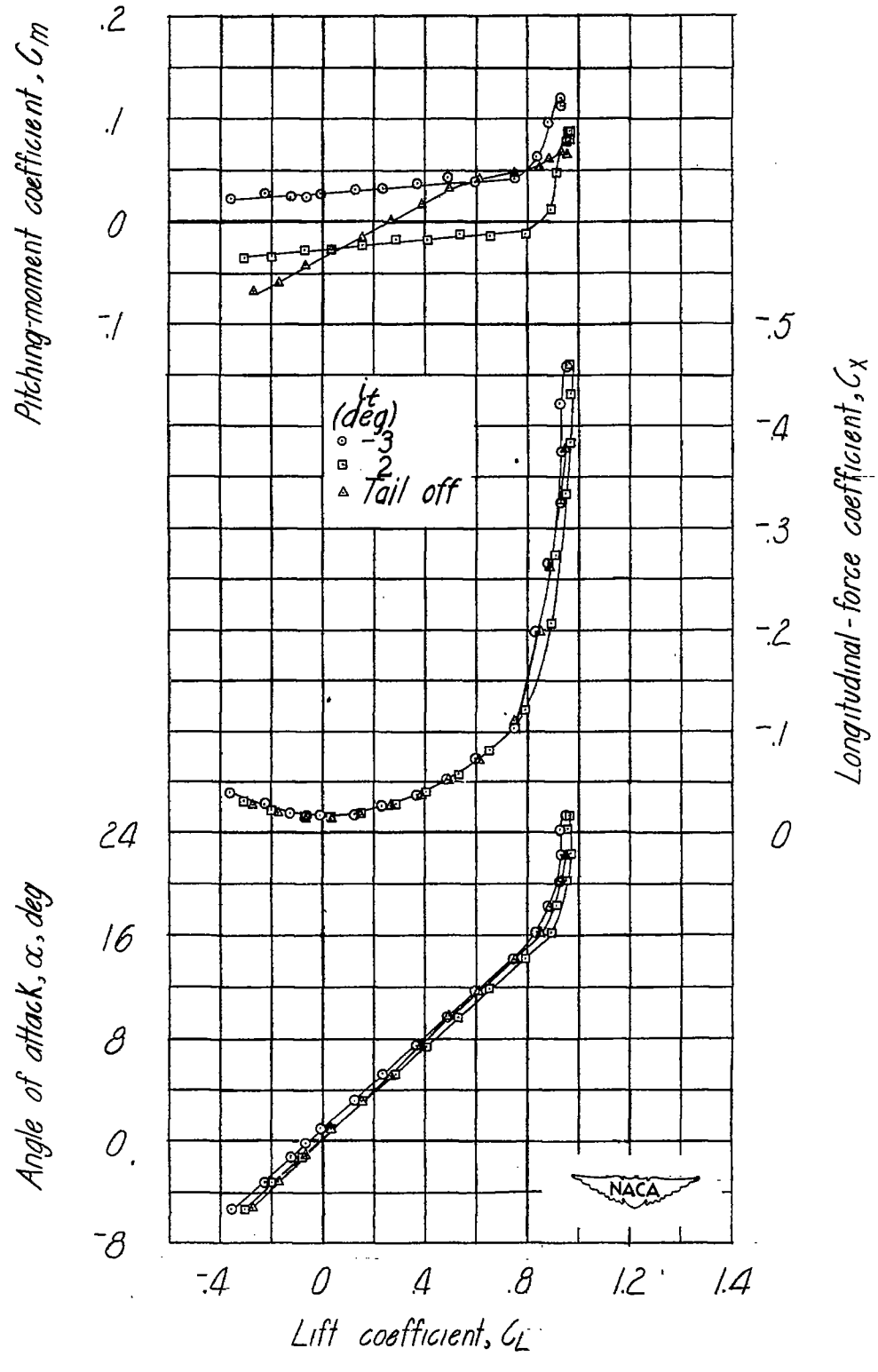

Figure 13.- Effect of stabilizer on the aerodynamic characteristics in pitch of test model. $\delta_f = 0^\circ$; $\psi = 0^\circ$; $\Gamma = -10^\circ$; test center of gravity at 35.9 percent M.A.C.

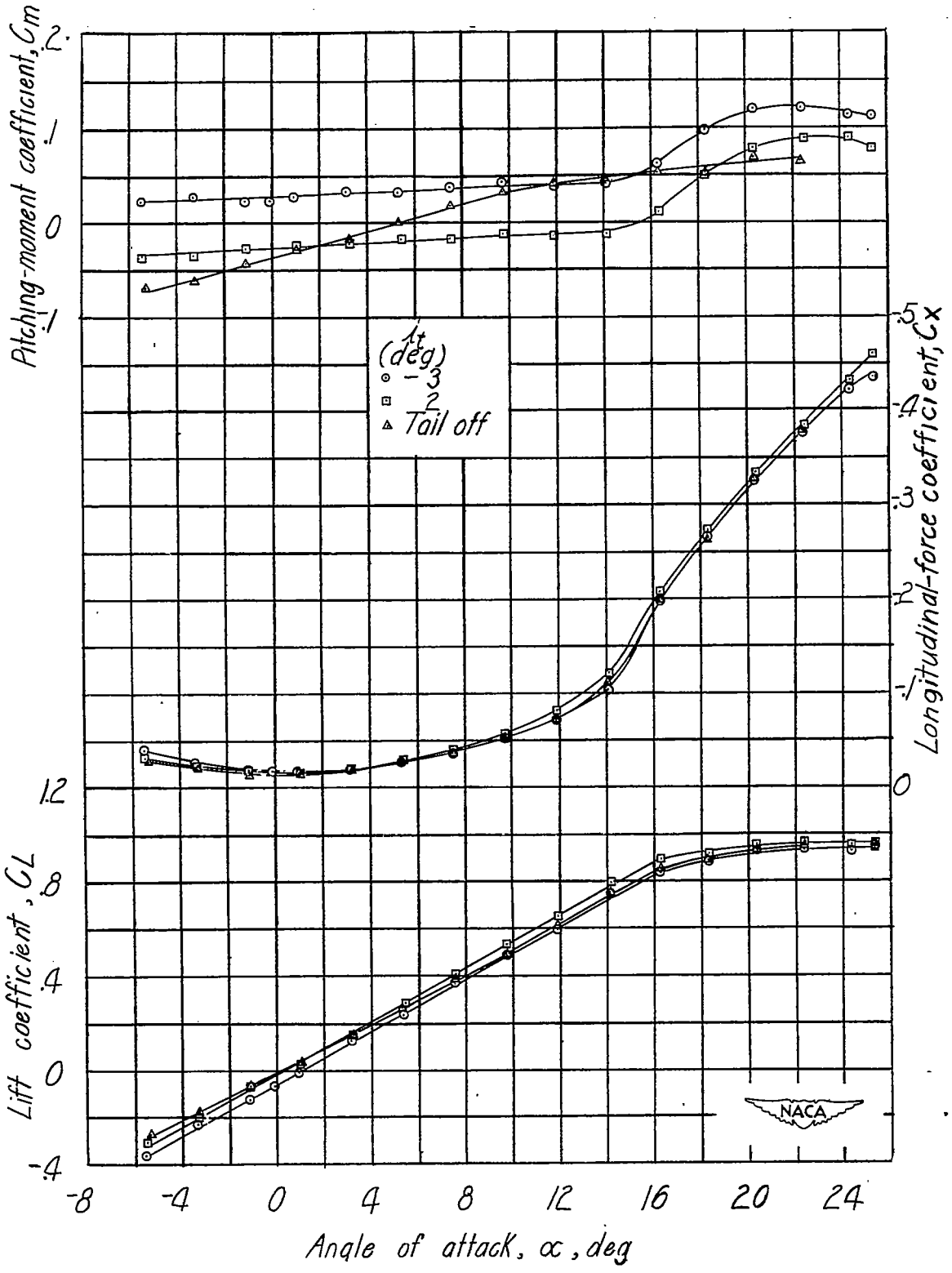

Figure 13.- Concluded.

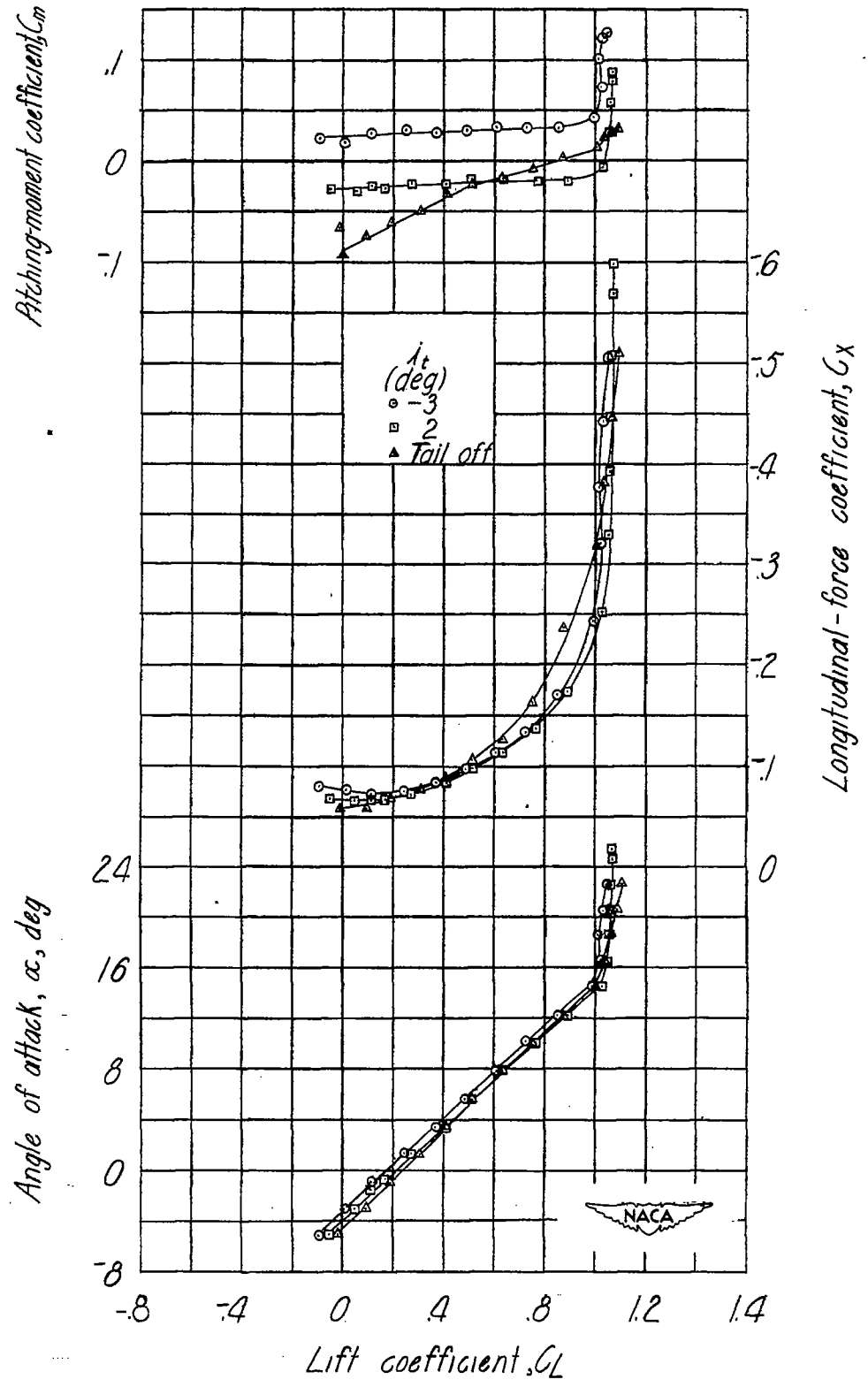

Figure 14.- Effect of stabilizer on the aerodynamic characteristics in pitch of test model. $\delta_f = 50^\circ$; $\Psi = 0^\circ$; $\Gamma = -10^\circ$; test center of gravity at 35.9 percent M.A.C.

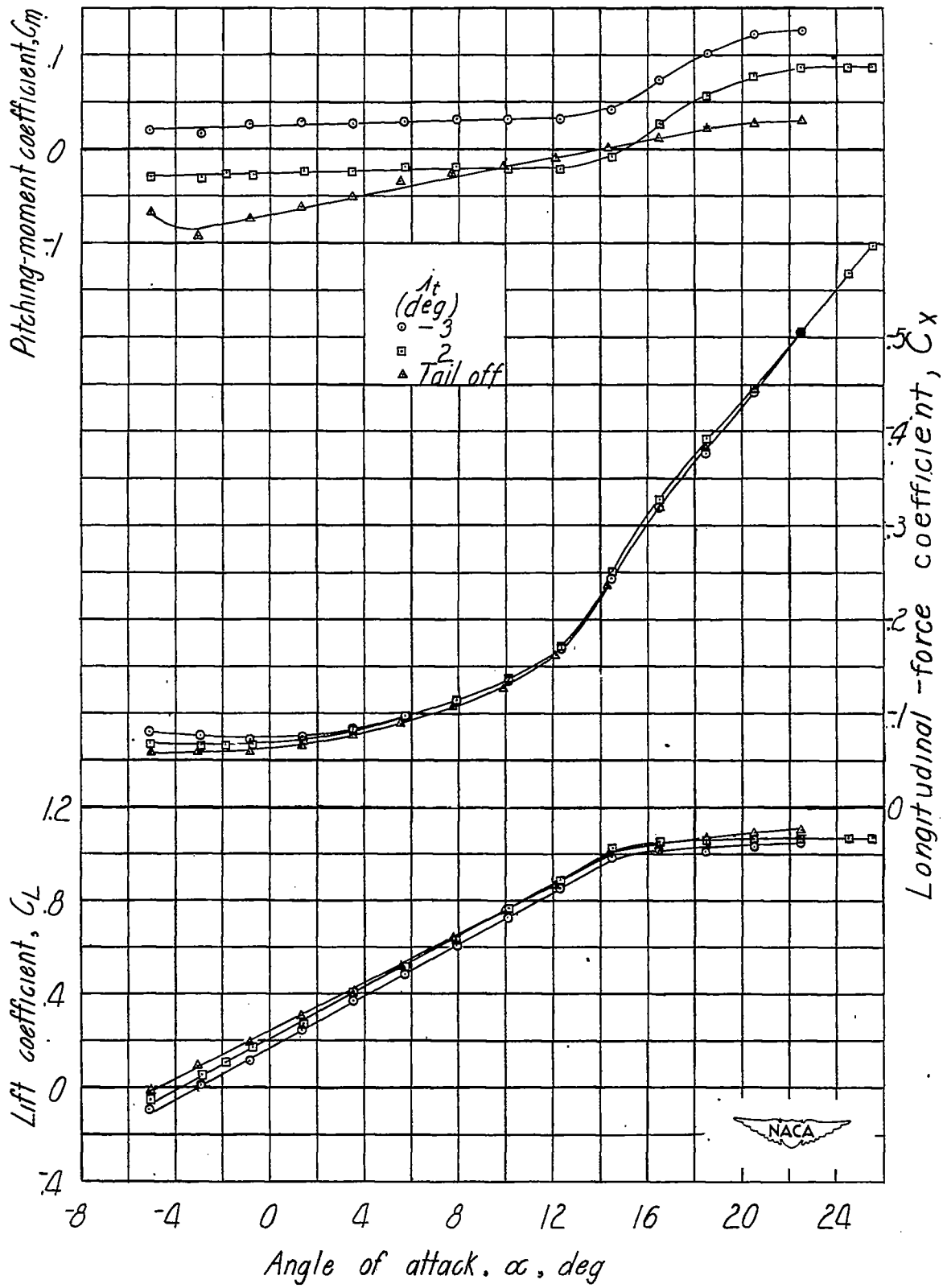

Figure 14.- Concluded.

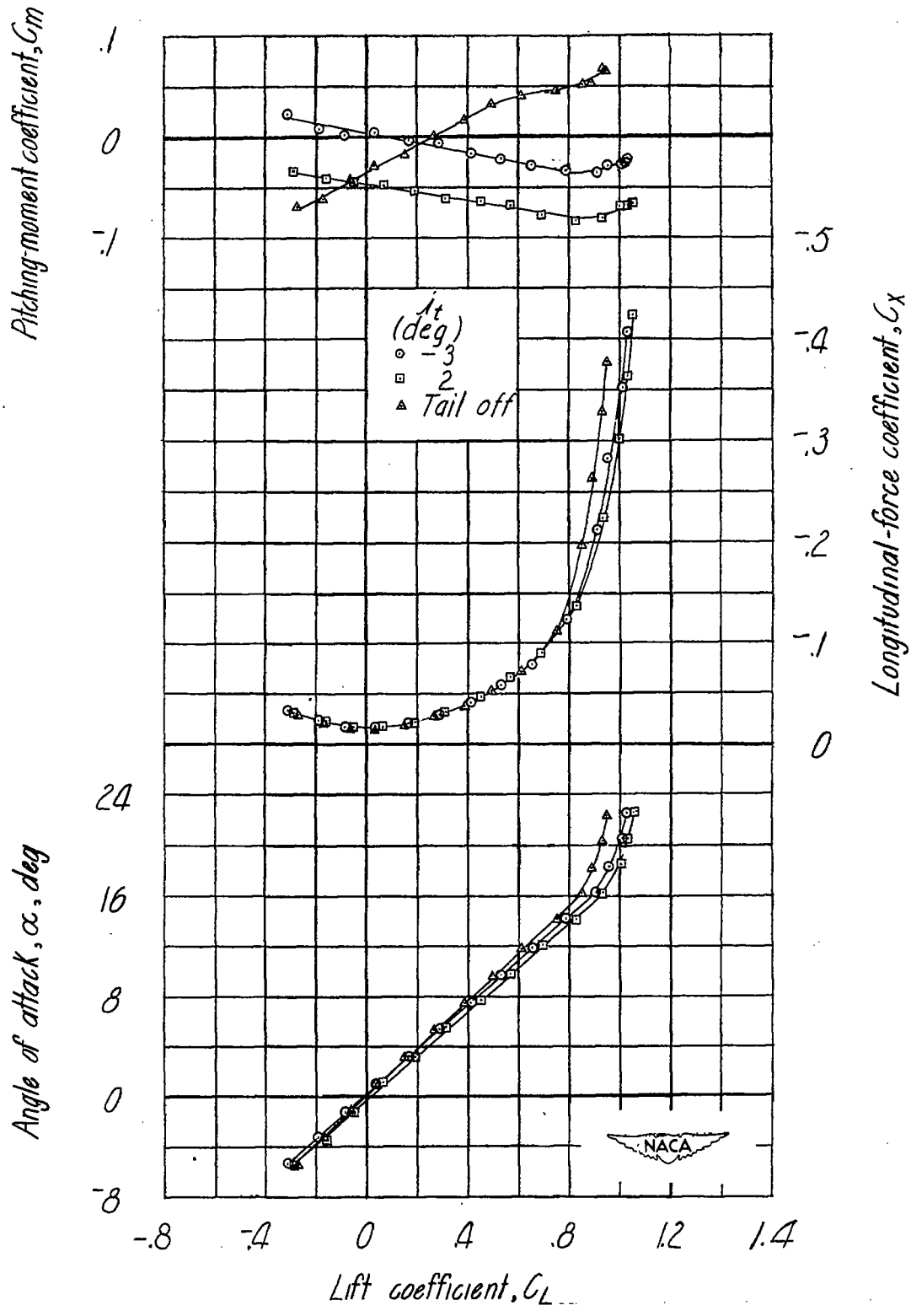

Figure 15.- Effect of stabilizer on the aerodynamic characteristics in pitch of test model. $\delta_f = 0^\circ$; $\psi = 0^\circ$; $\Gamma = -10^\circ$; test center of gravity at 35.9 percent M.A.C; high-horizontal-tail location.

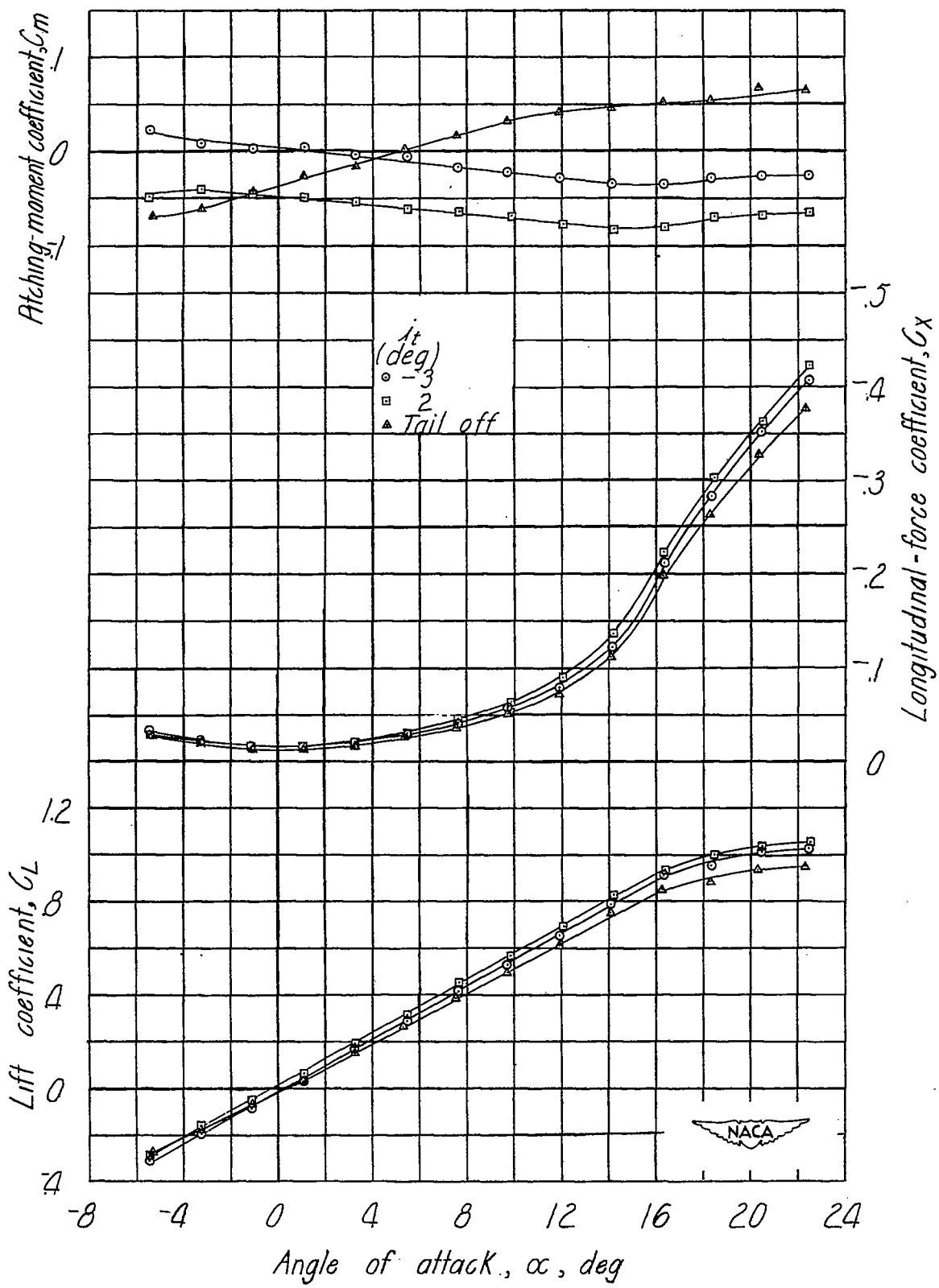

Figure 15.- Concluded.

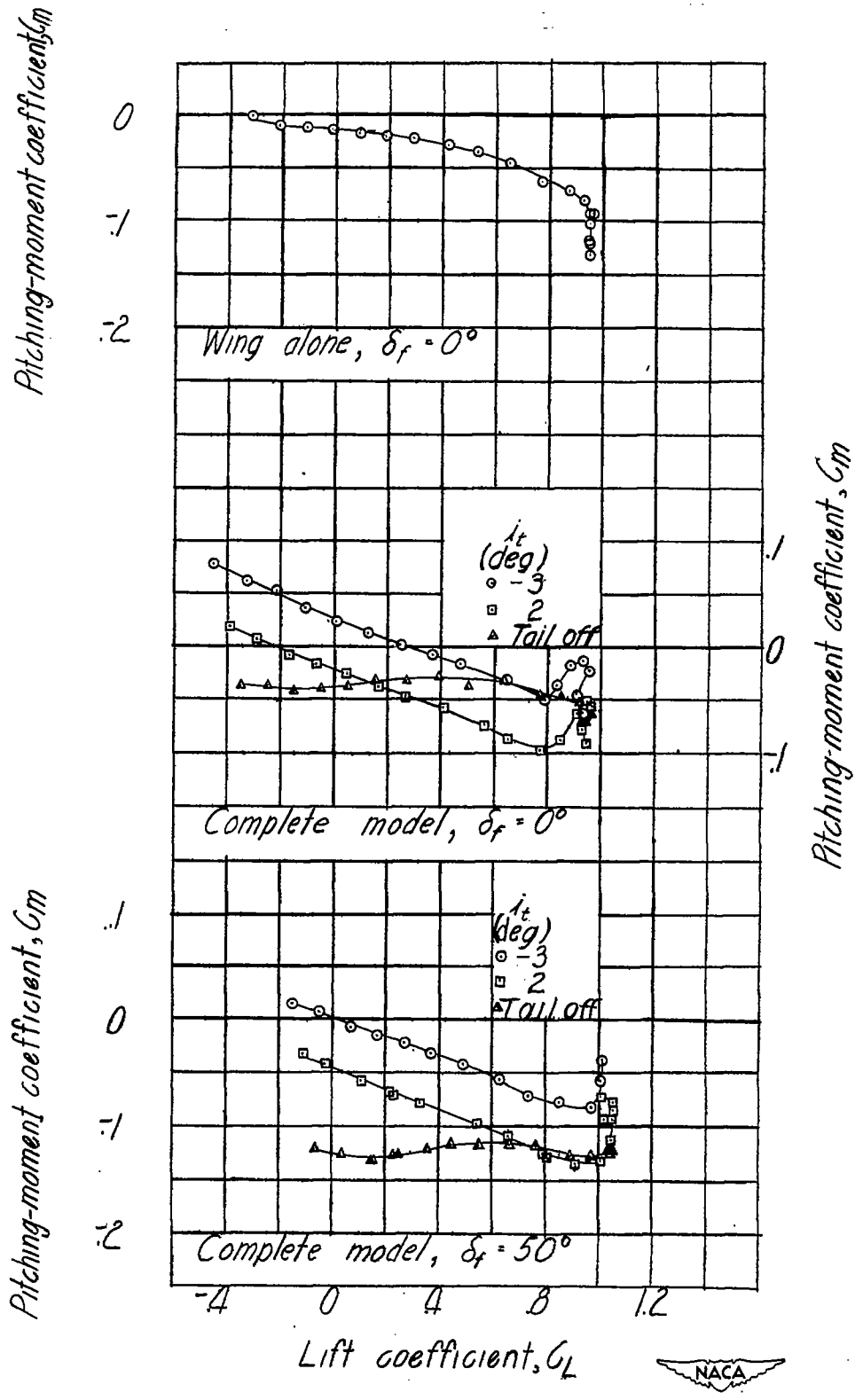

Figure 16.- Effect of stabilizer on the aerodynamic characteristics in pitch of test model. $\psi = 0°$; $\Gamma = 0°$; center of gravity transferred to 23.0 percent M.A.C.

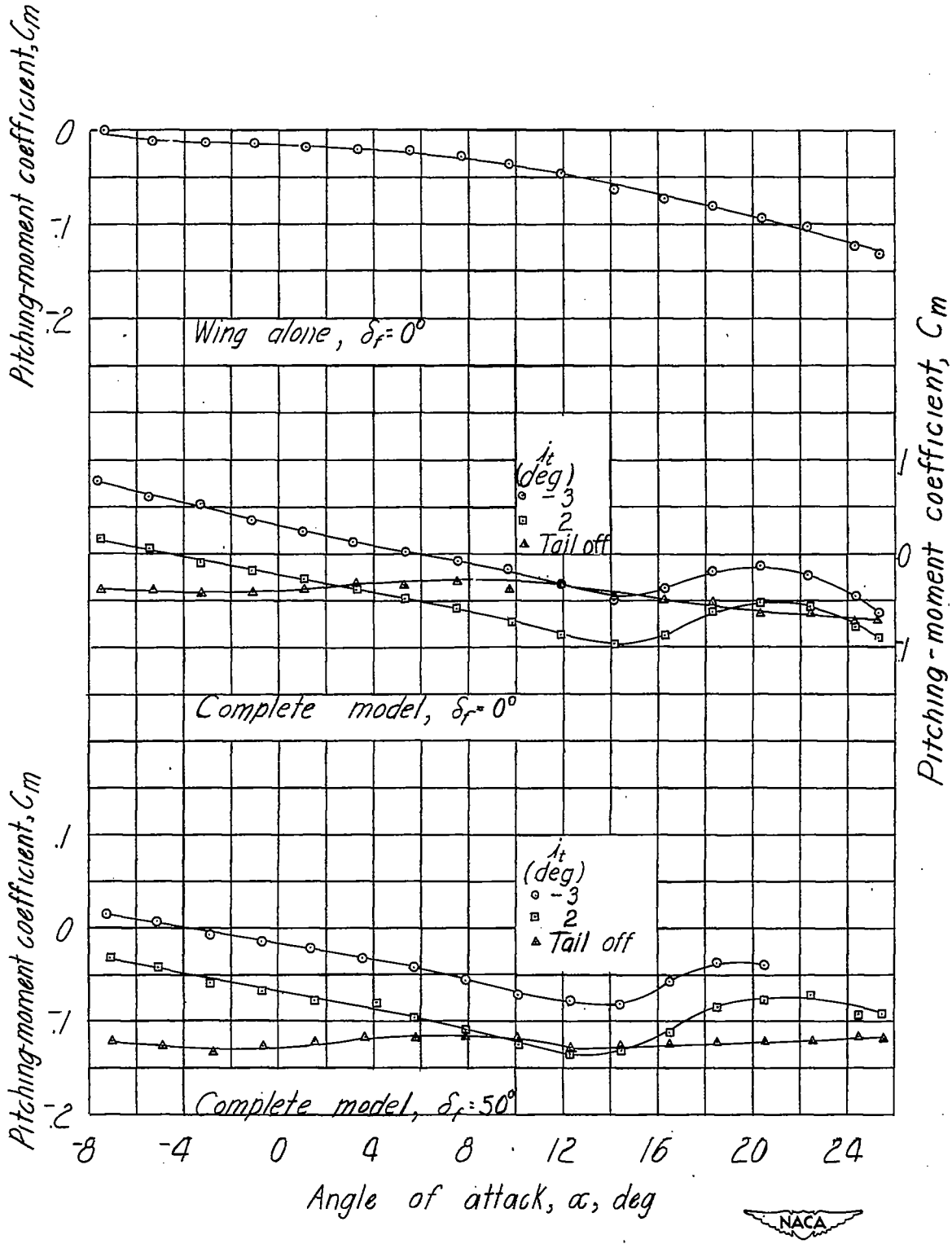

Figure 16.- Concluded.

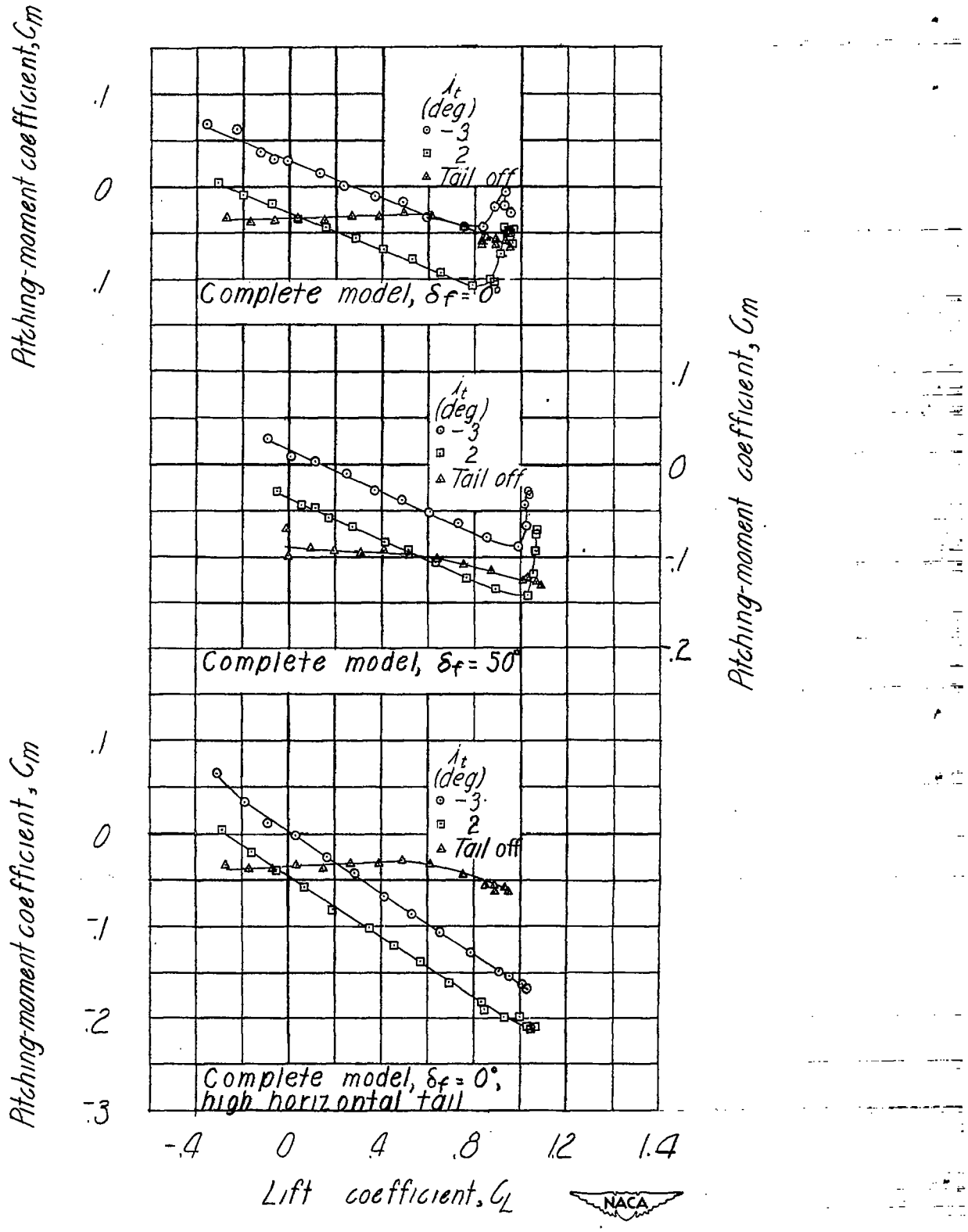

Figure 17.- Effect of stabilizer on the aerodynamic characteristics in pitch of test model. $\Psi = 0^\circ$; $\Gamma = -10^\circ$; center of gravity transferred to 23.0 percent M.A.C.

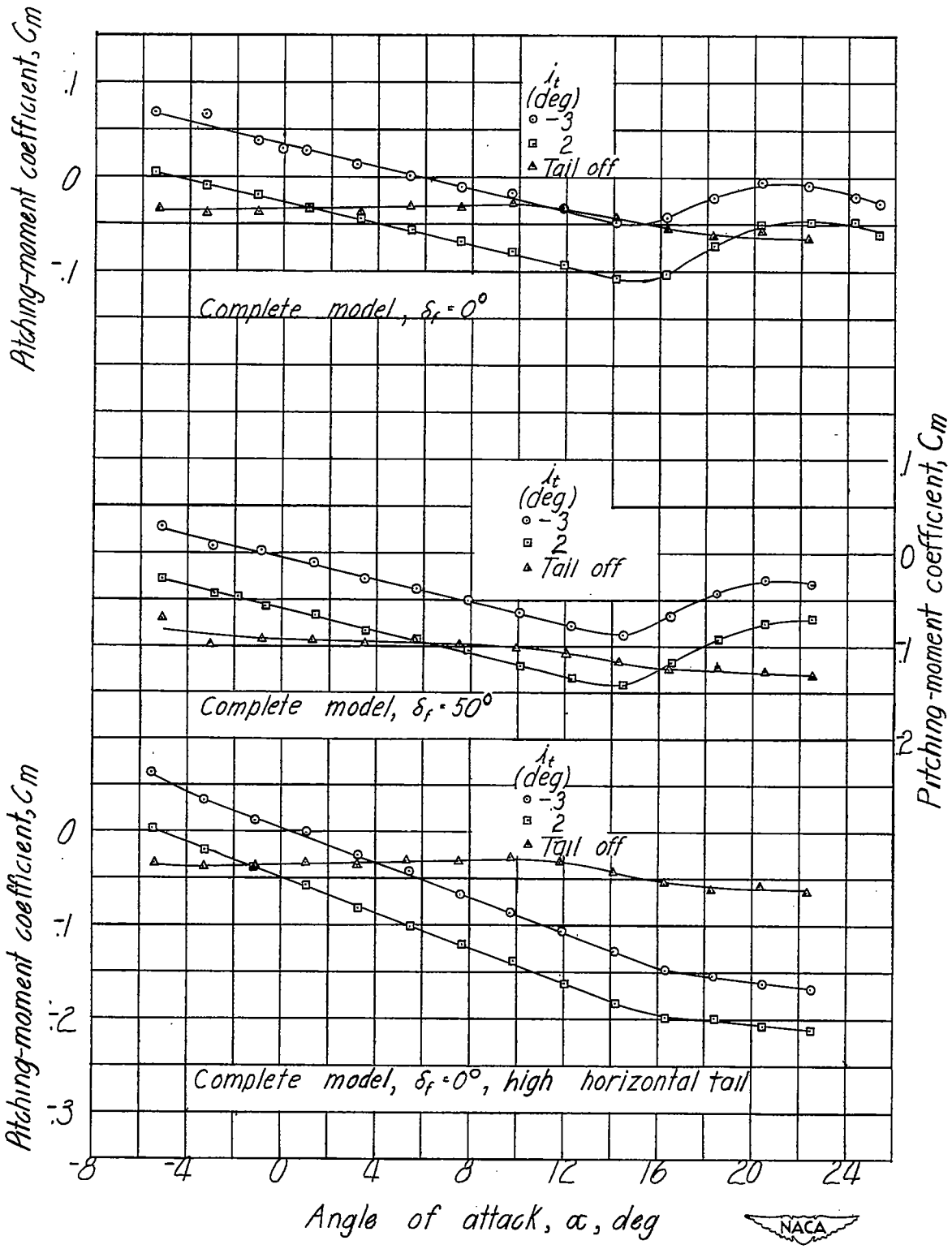

Figure 17.- Concluded

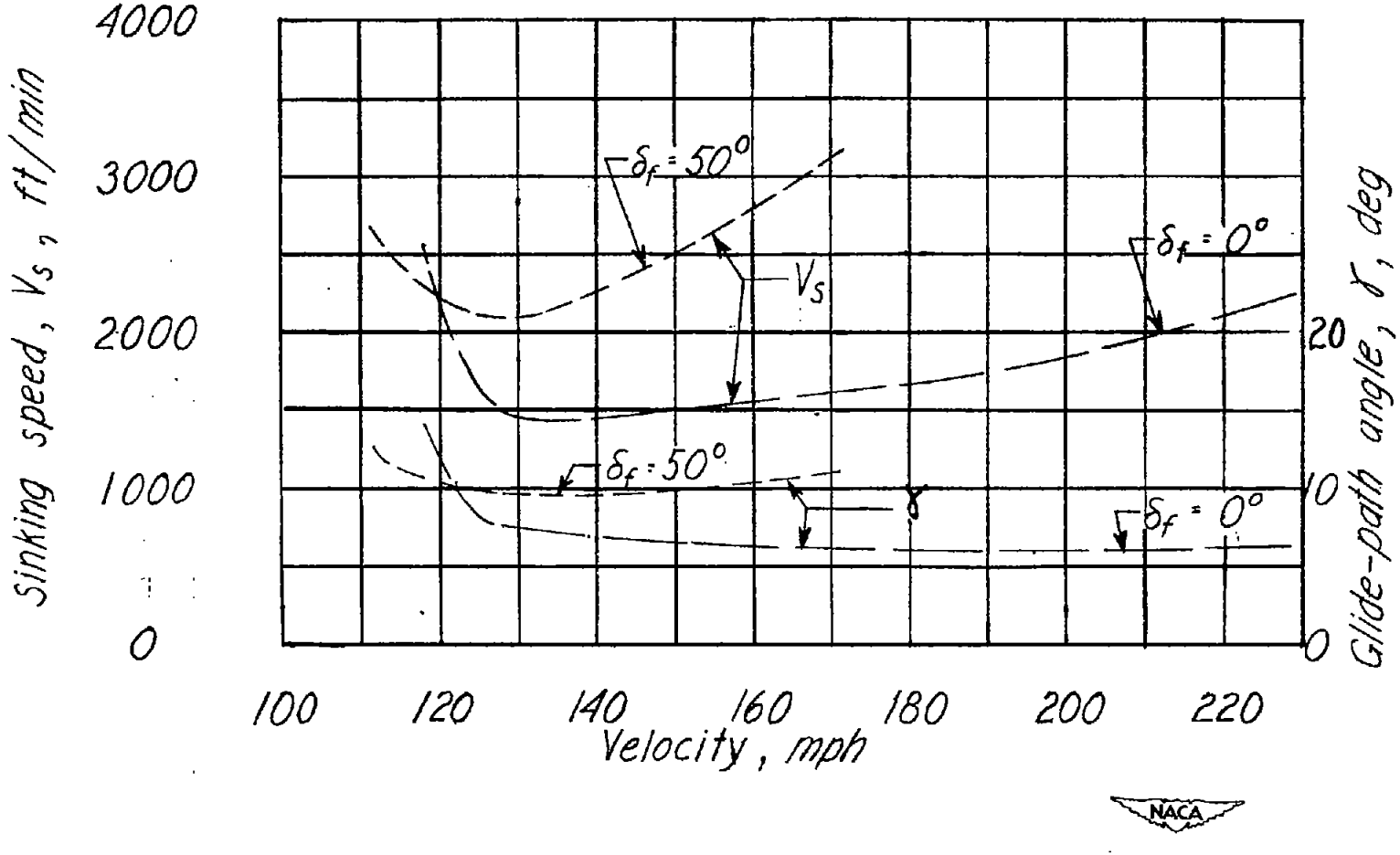

Figure 18.- Effect of flap deflection on the estimated sinking speed and glide-path angle for a full-scale model. $\frac{W}{S}$ = 30.5 pounds per square foot at sea level.

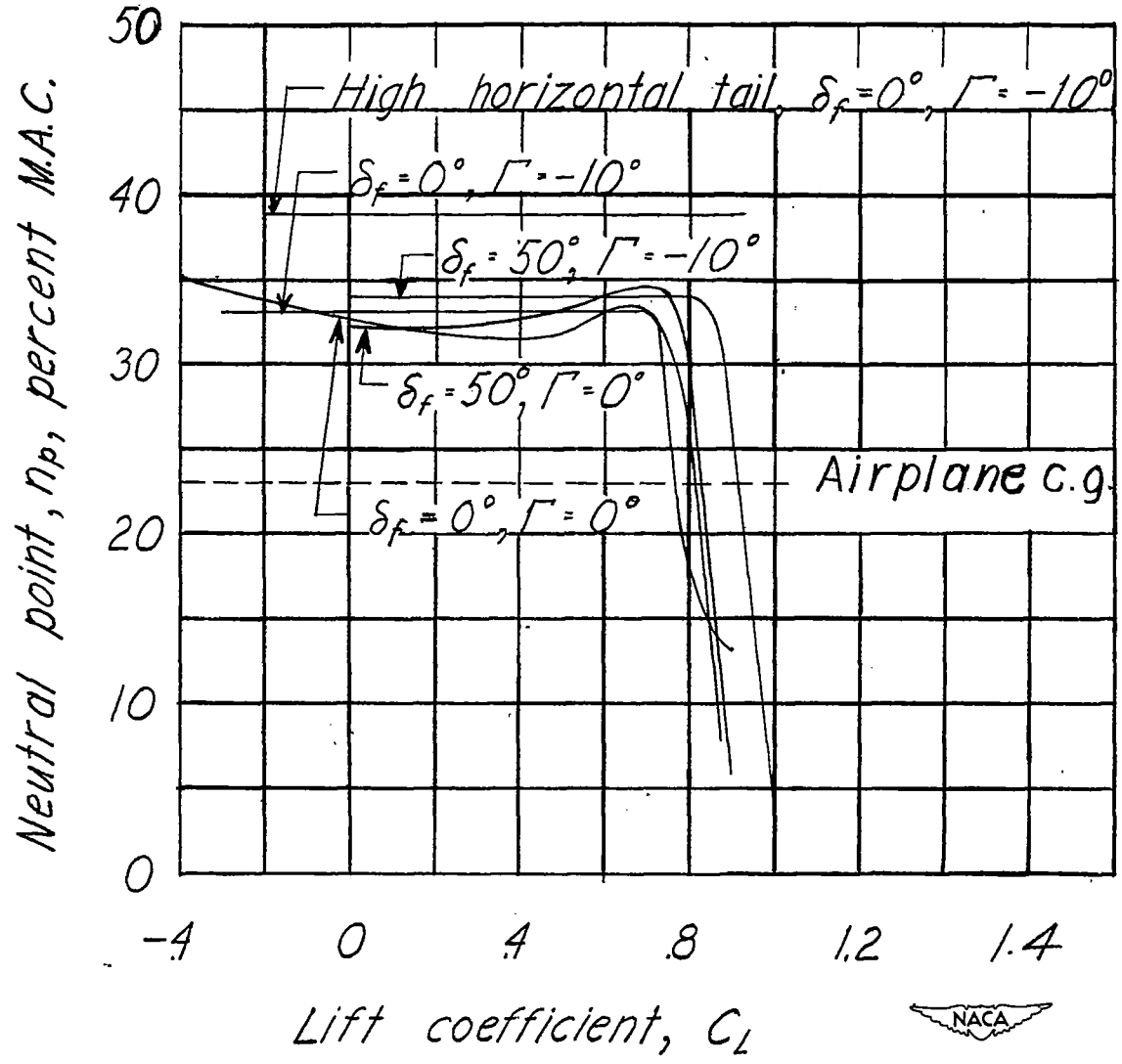

Figure 19.- Neutral points for test model.

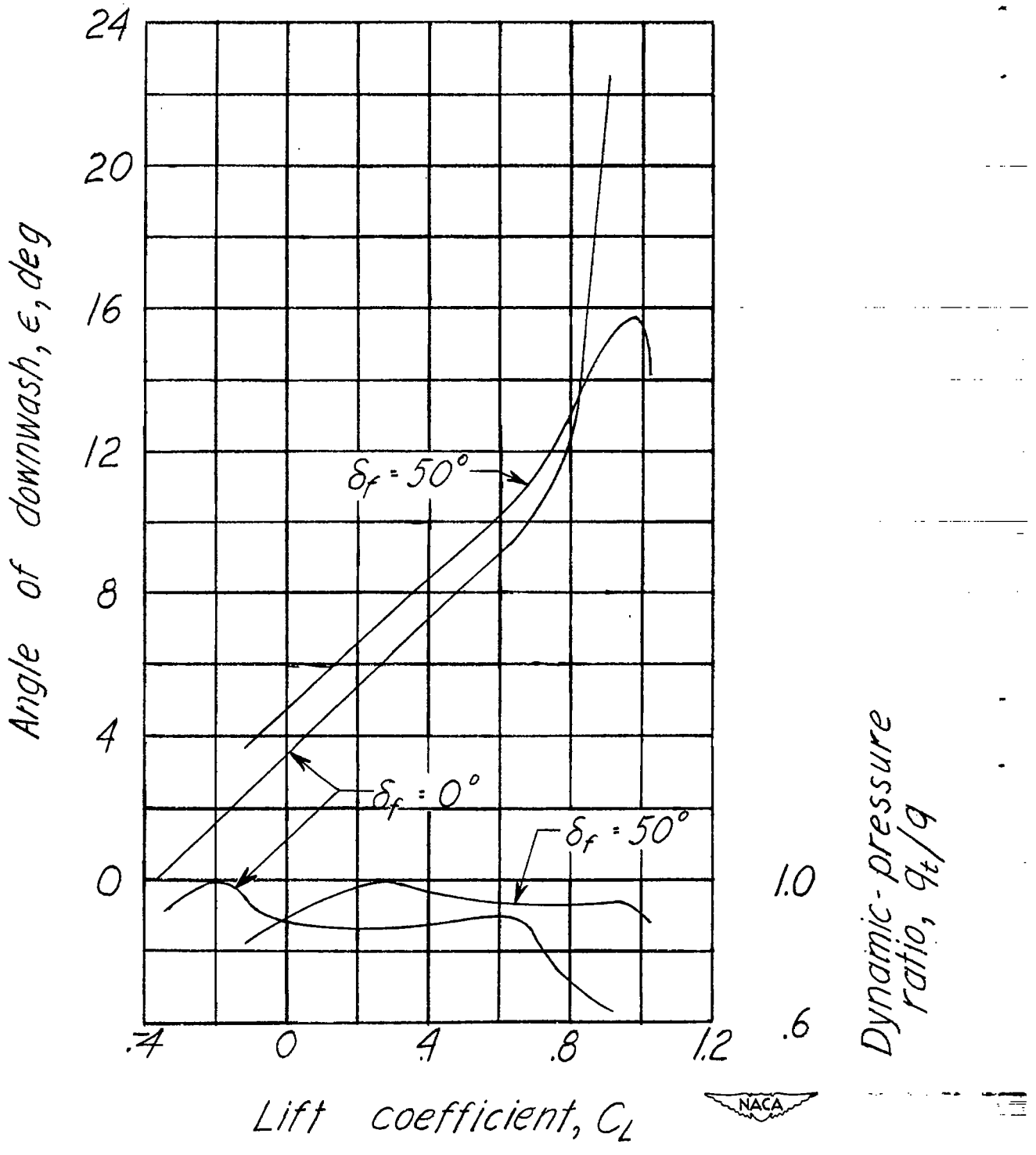

(a) $\Gamma = 0^\circ$.

Figure 20.- The effect of flap deflection on the downwash angles and the dynamic-pressure ratios at the horizontal tail for test model.

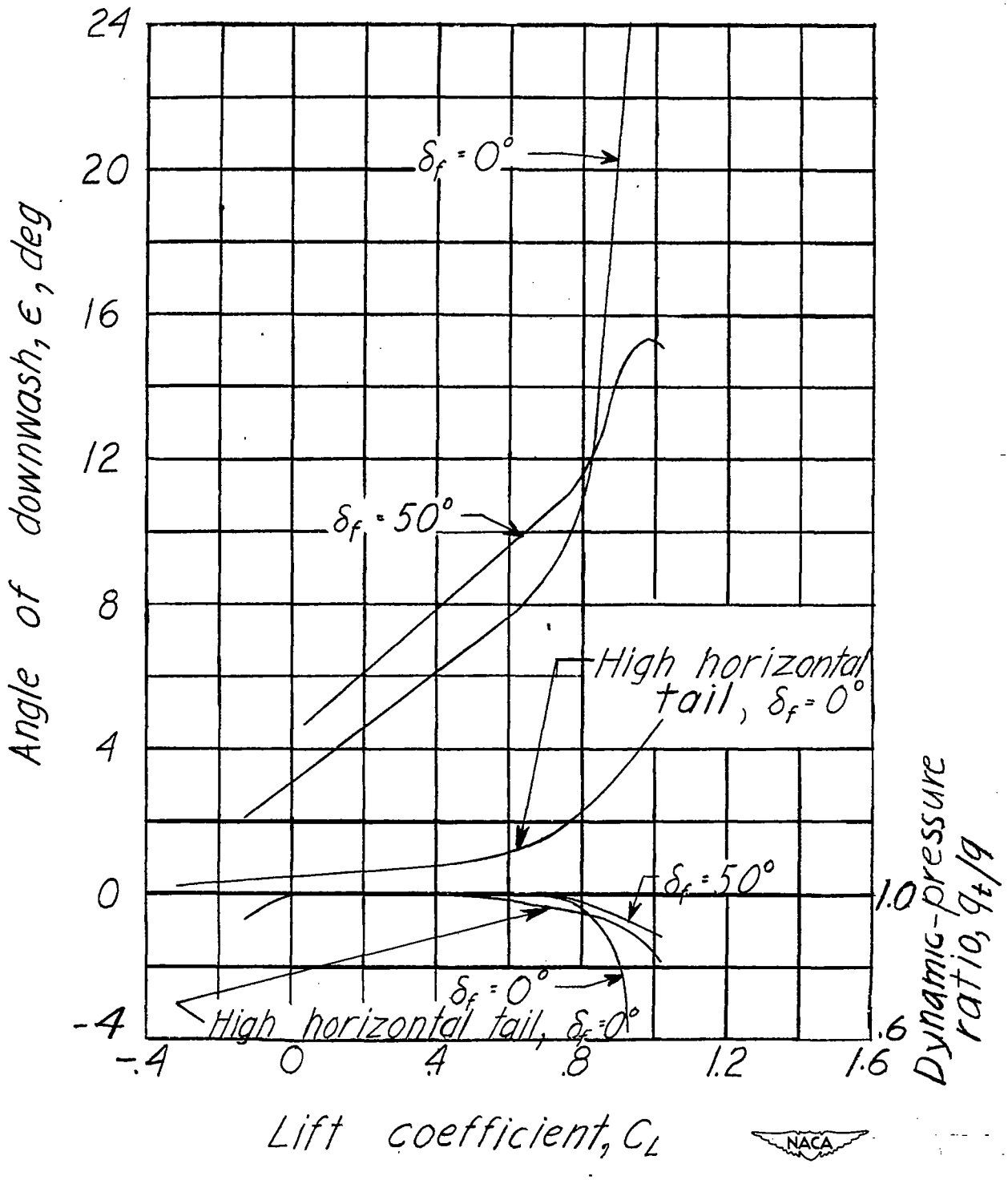

(b) $\Gamma = -10°$.

Figure 20.- Concluded.

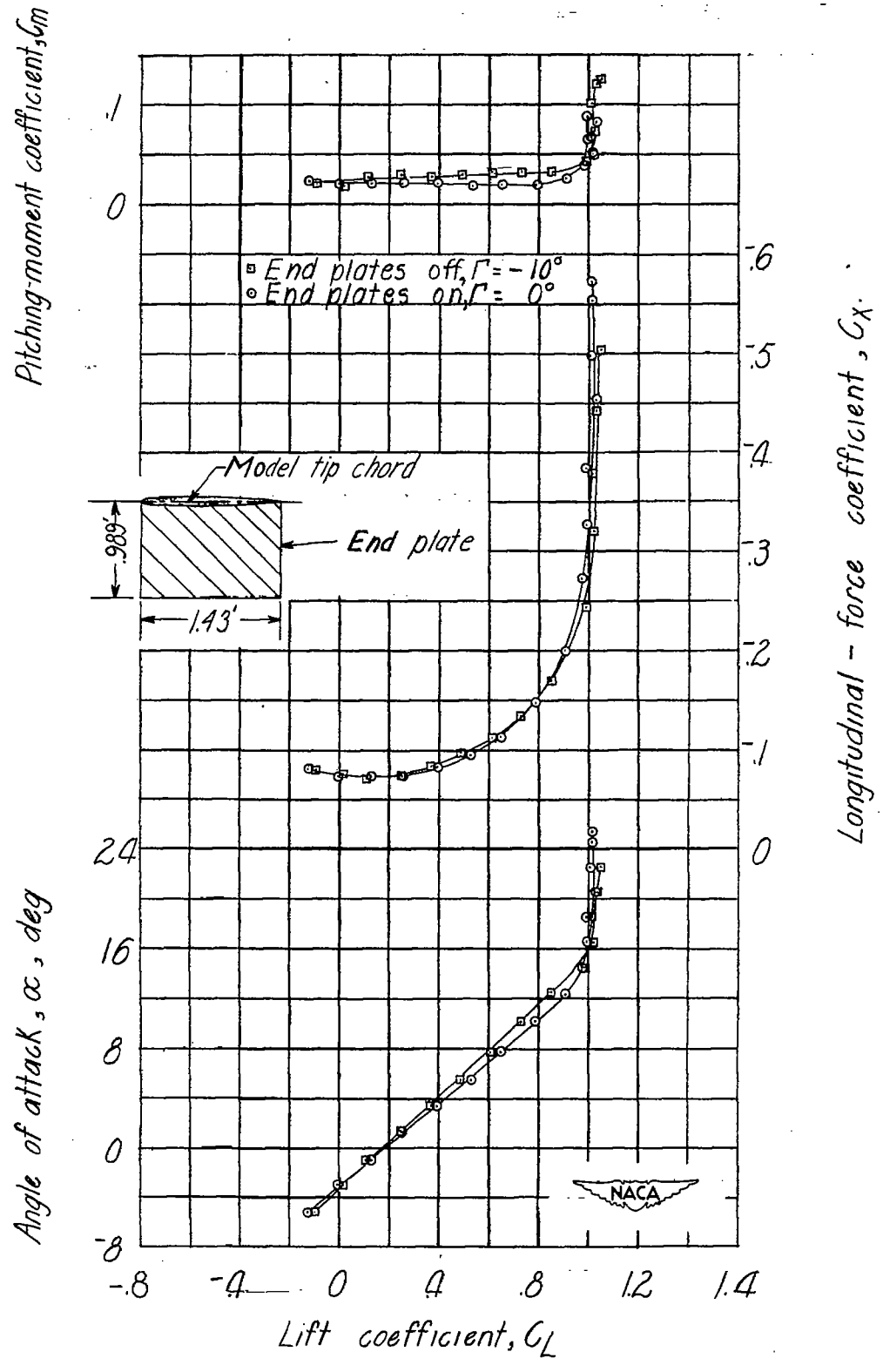

Figure 21.- Effect of end plates on the aerodynamic characteristics in pitch of test model. $\delta_f = 50°$; $\psi = 0°$; test center of gravity at 35.9 percent M.A.C.

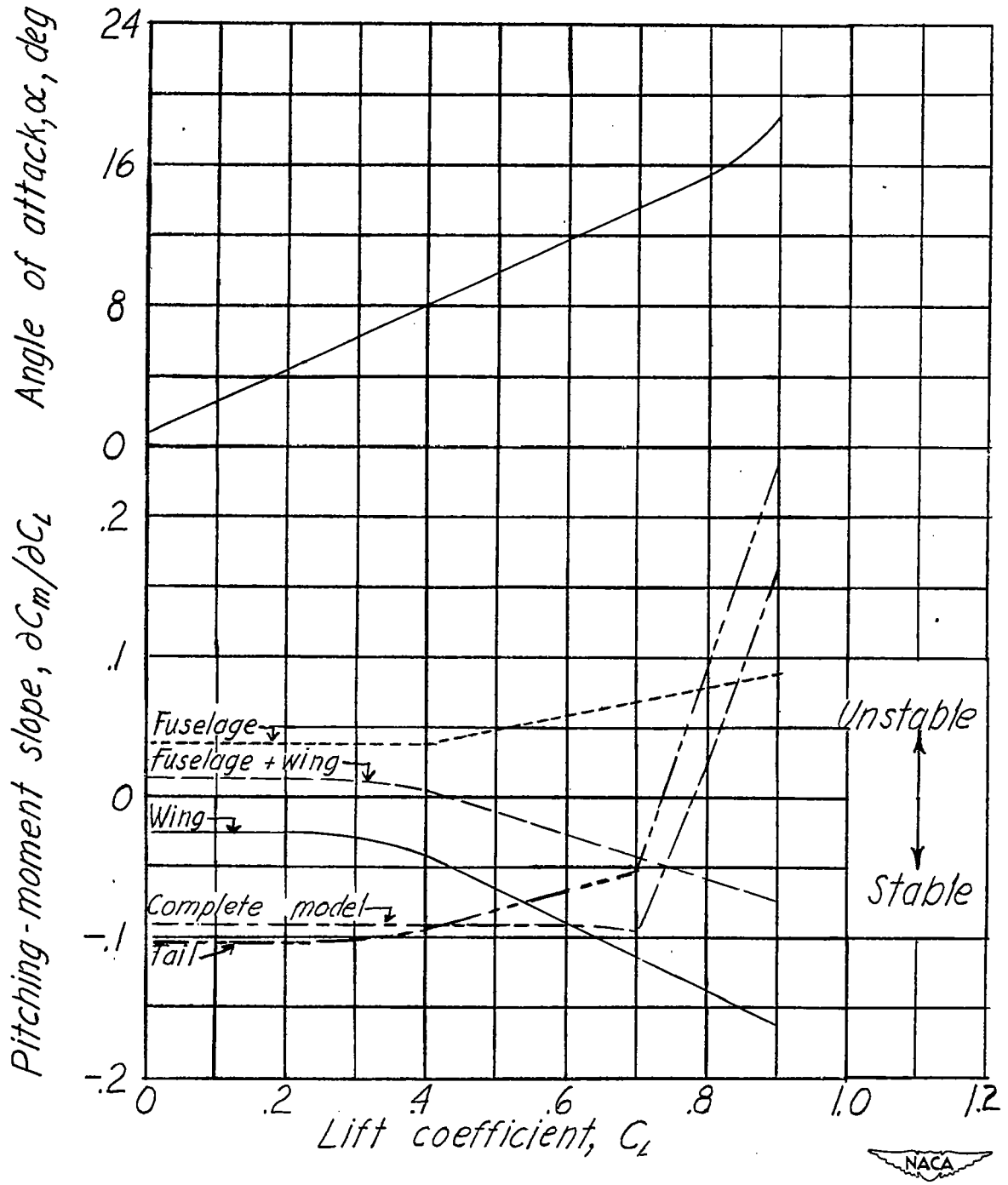

Figure 22.- Contribution of the various components to longitudinal stability of test model. $\delta_f = 0^\circ$; $\Gamma = 0^\circ$; center of gravity at 23.0 percent M.A.C.

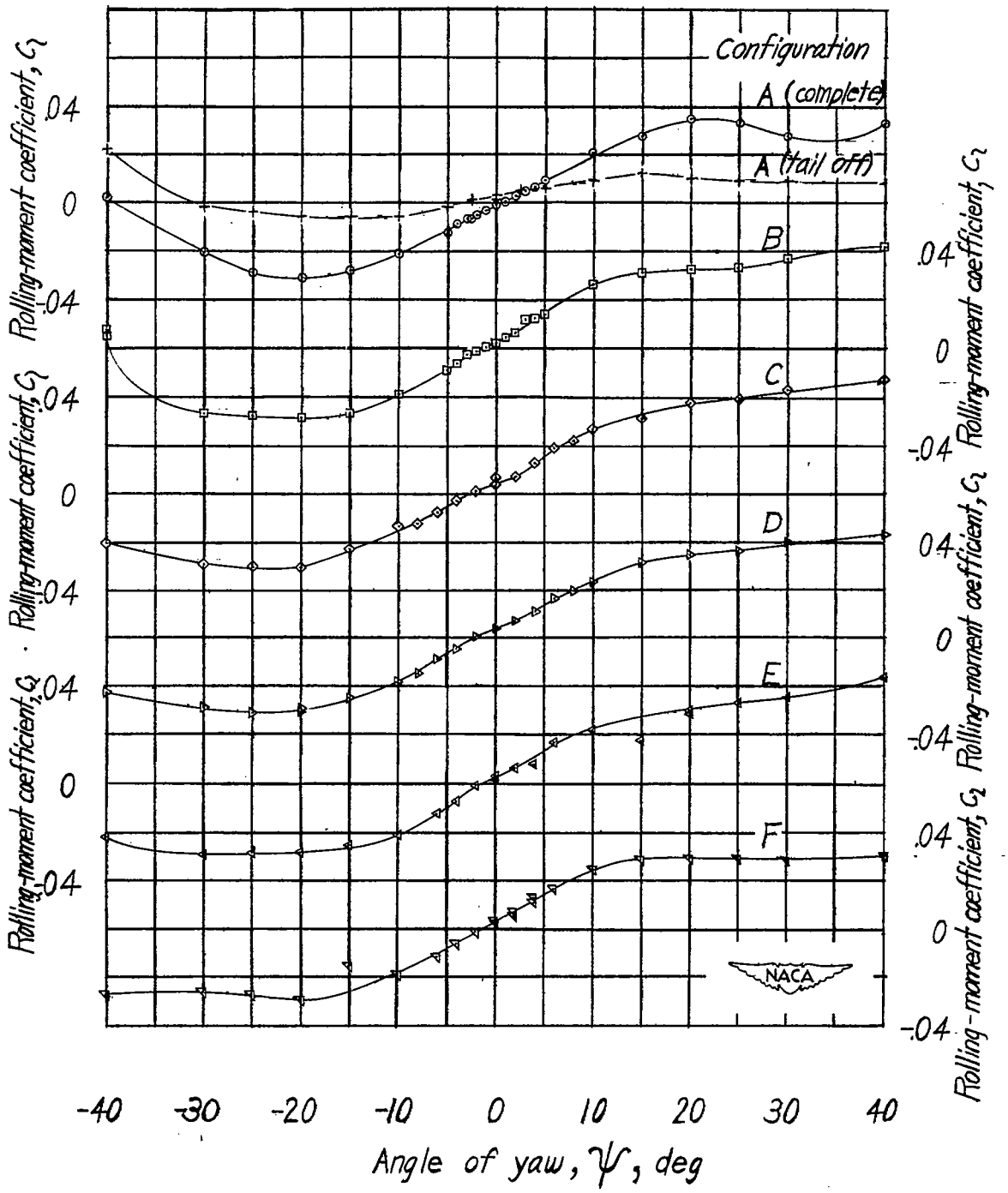

(a) $\alpha = 5.4^\circ$; rolling-moment coefficients.

Figure 23.- Effect of dorsal and vertical-tail modifications on the lateral stability characteristics in yaw of test model. $\delta_f = 0^\circ$.

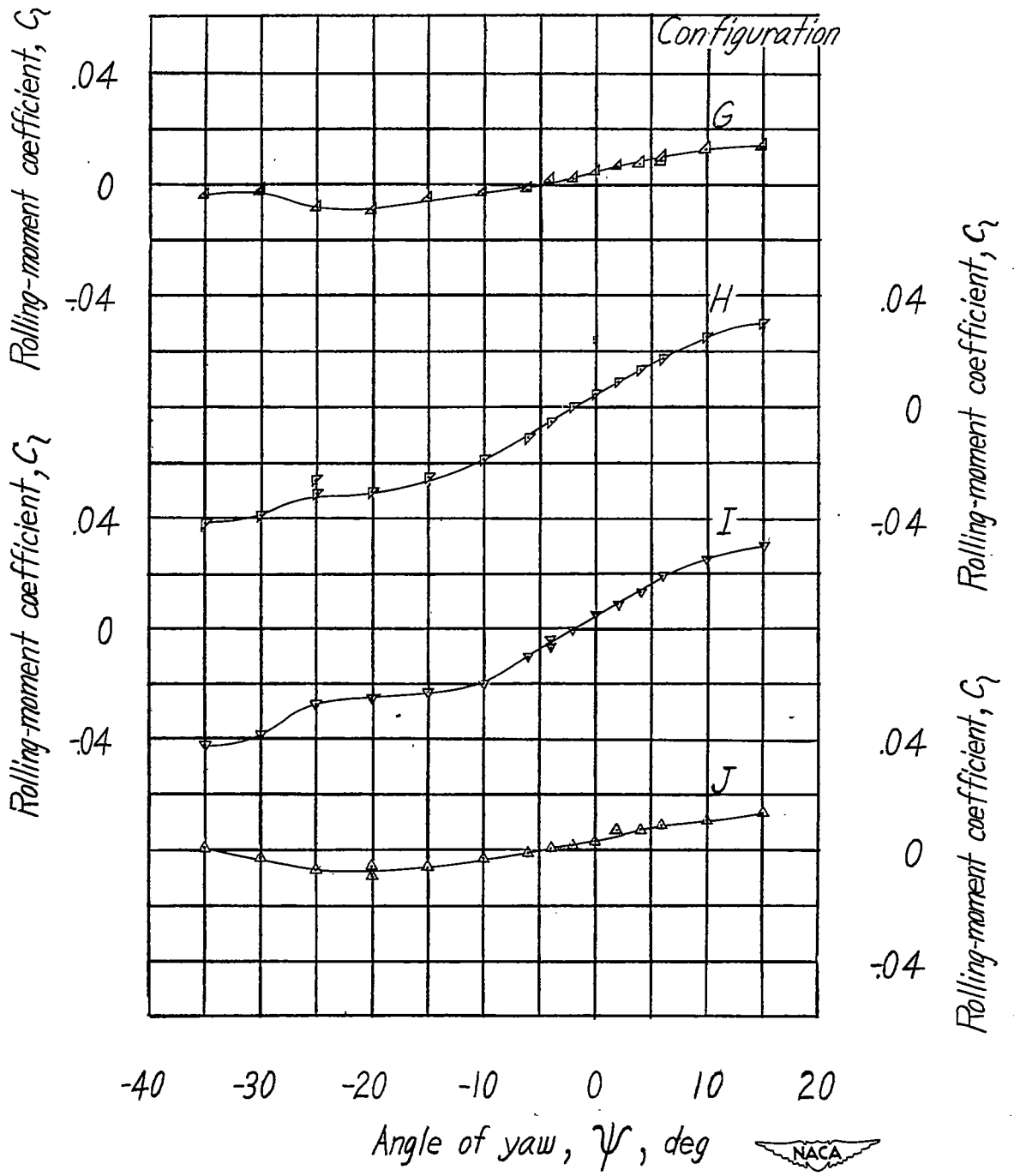

(a) Concluded.

Figure 23.- Continued.

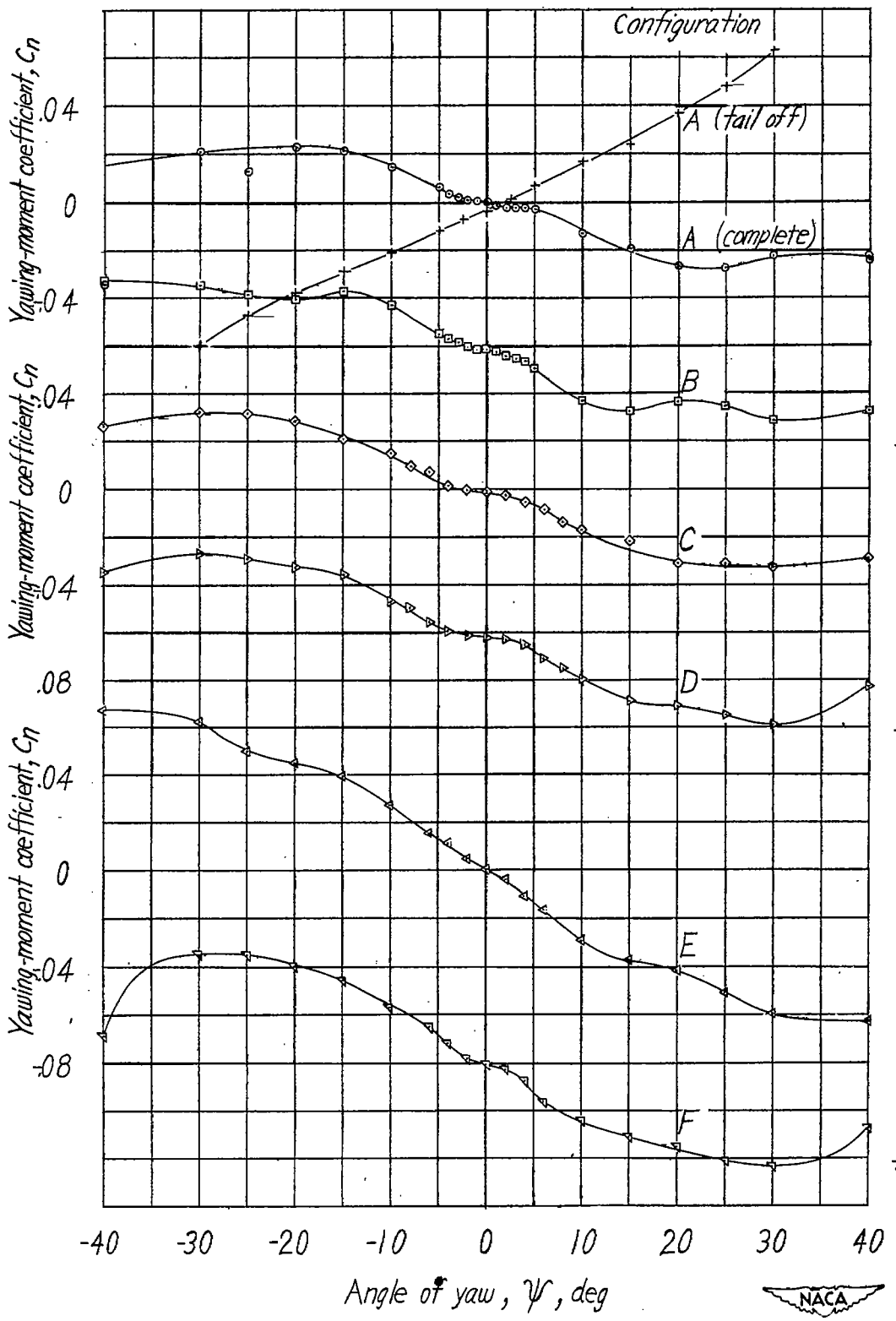

(b) $\alpha = 5.4^\circ$; yawing-moment coefficients.

Figure 23.- Continued.

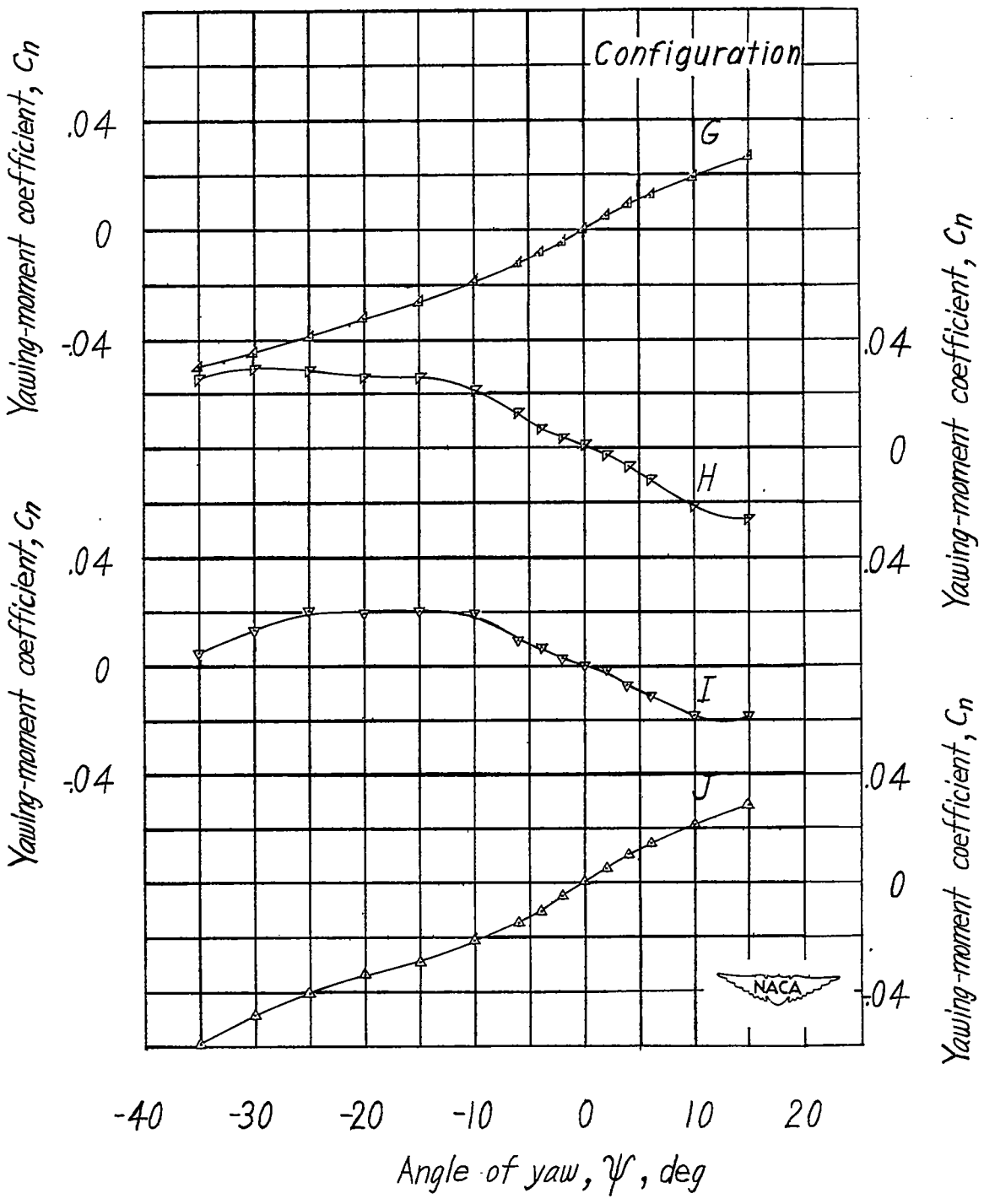

(b) Concluded.

Figure 23.- Continued.

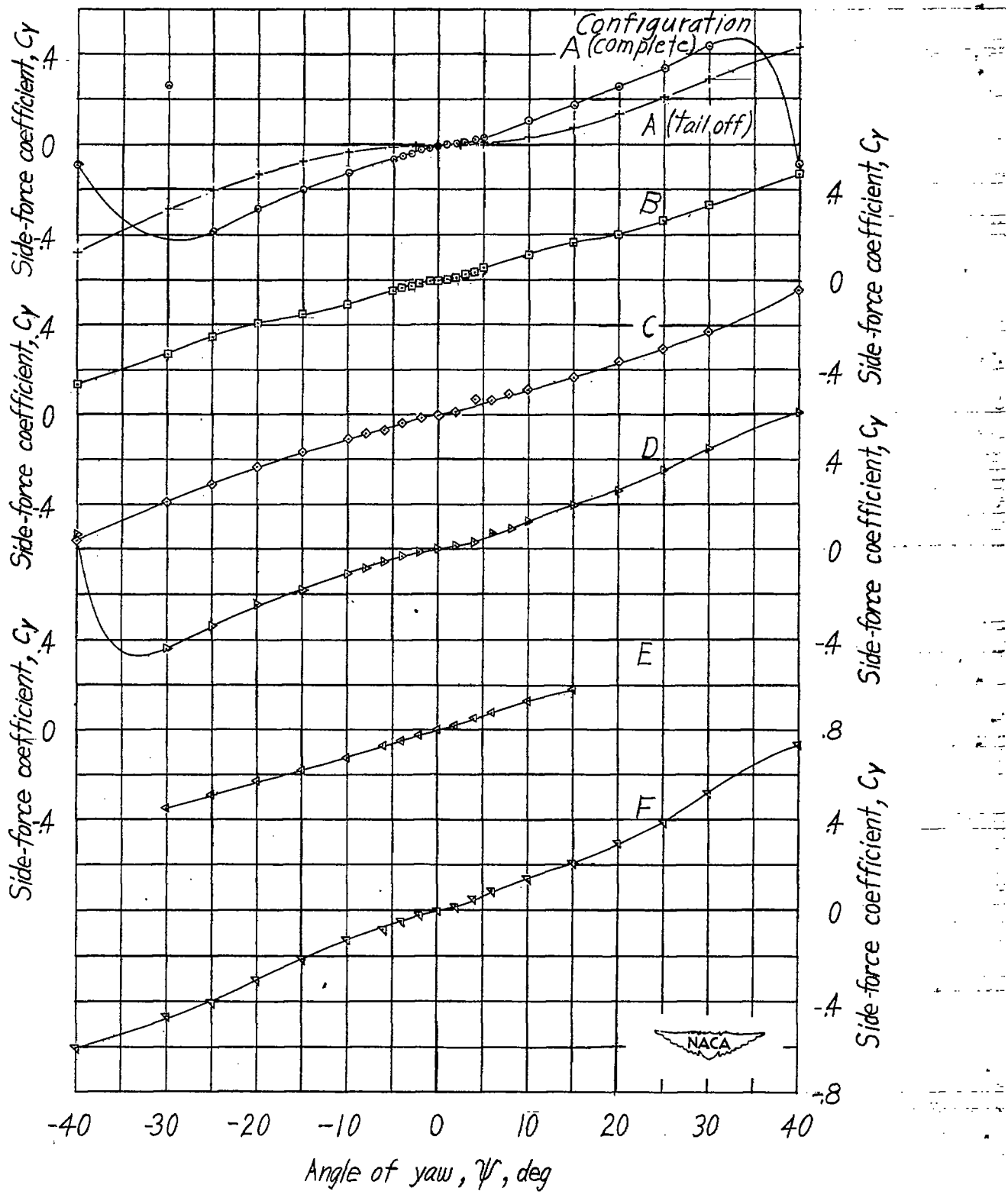

(c) $\alpha = 5.4^\circ$; side-force coefficients.

Figure 23.- Continued.

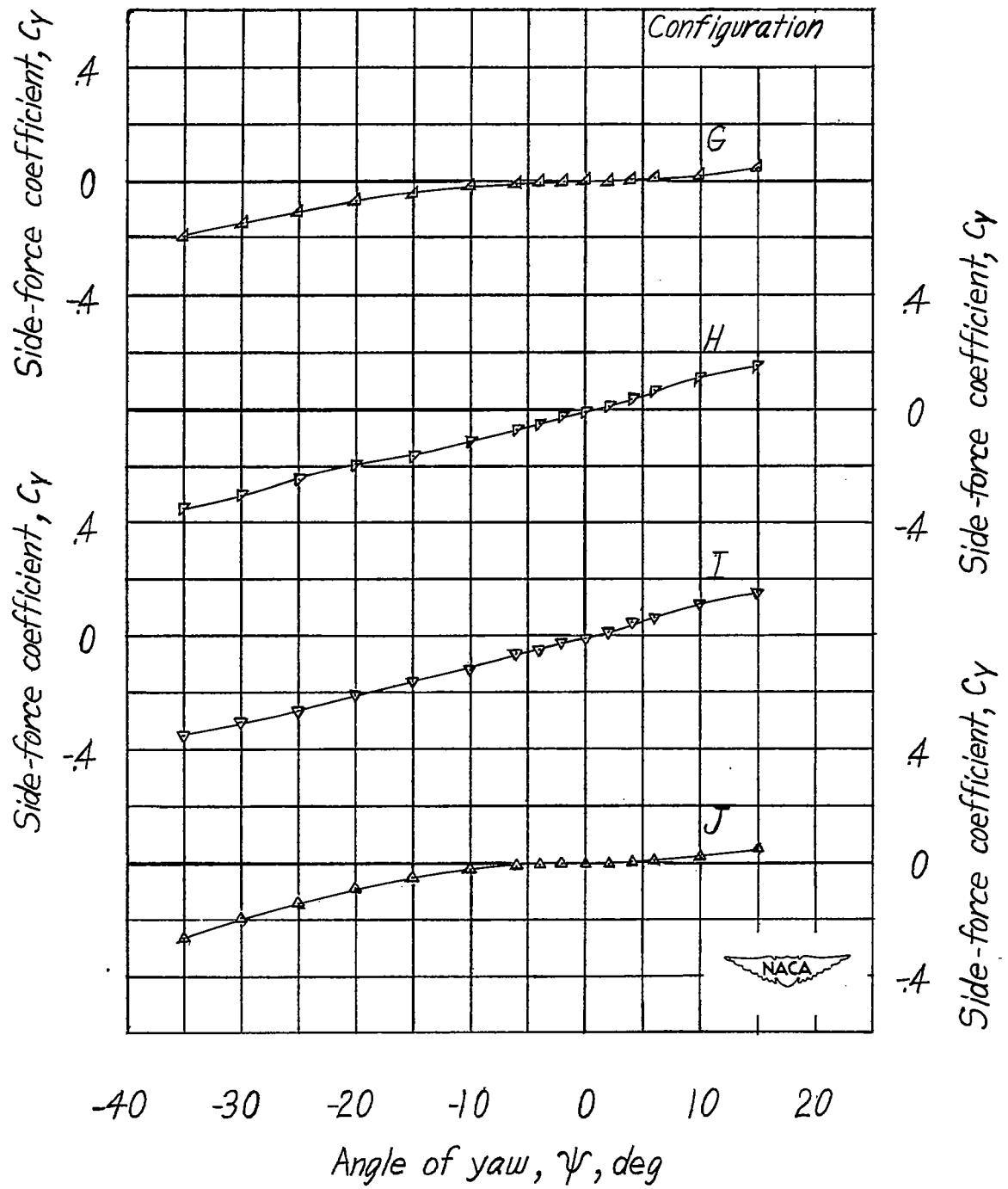

(c) Concluded.

Figure 23.- Continued.

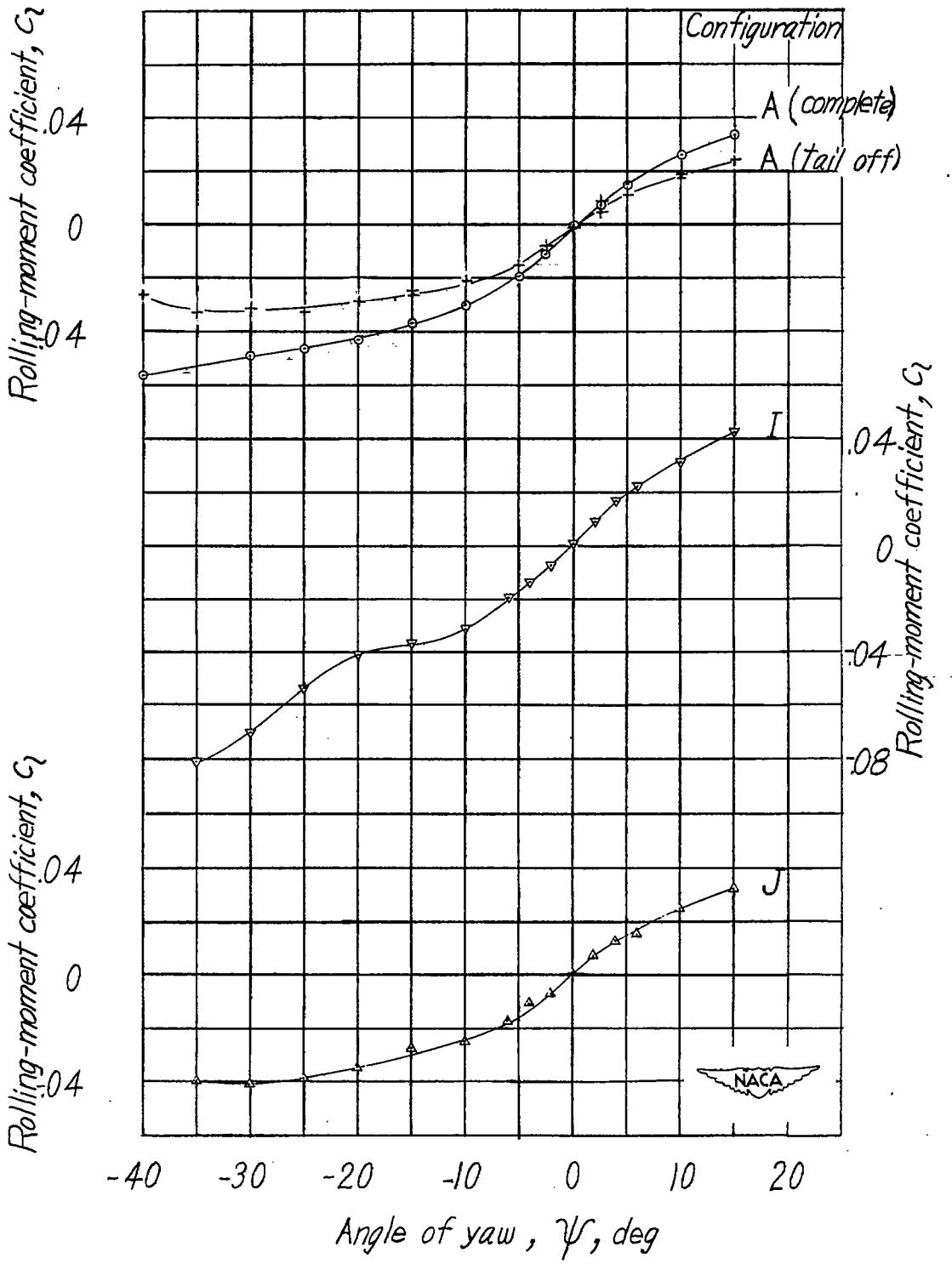

(d) $\alpha = 13.0^\circ$; rolling-moment coefficients.

Figure 23.- Continued.

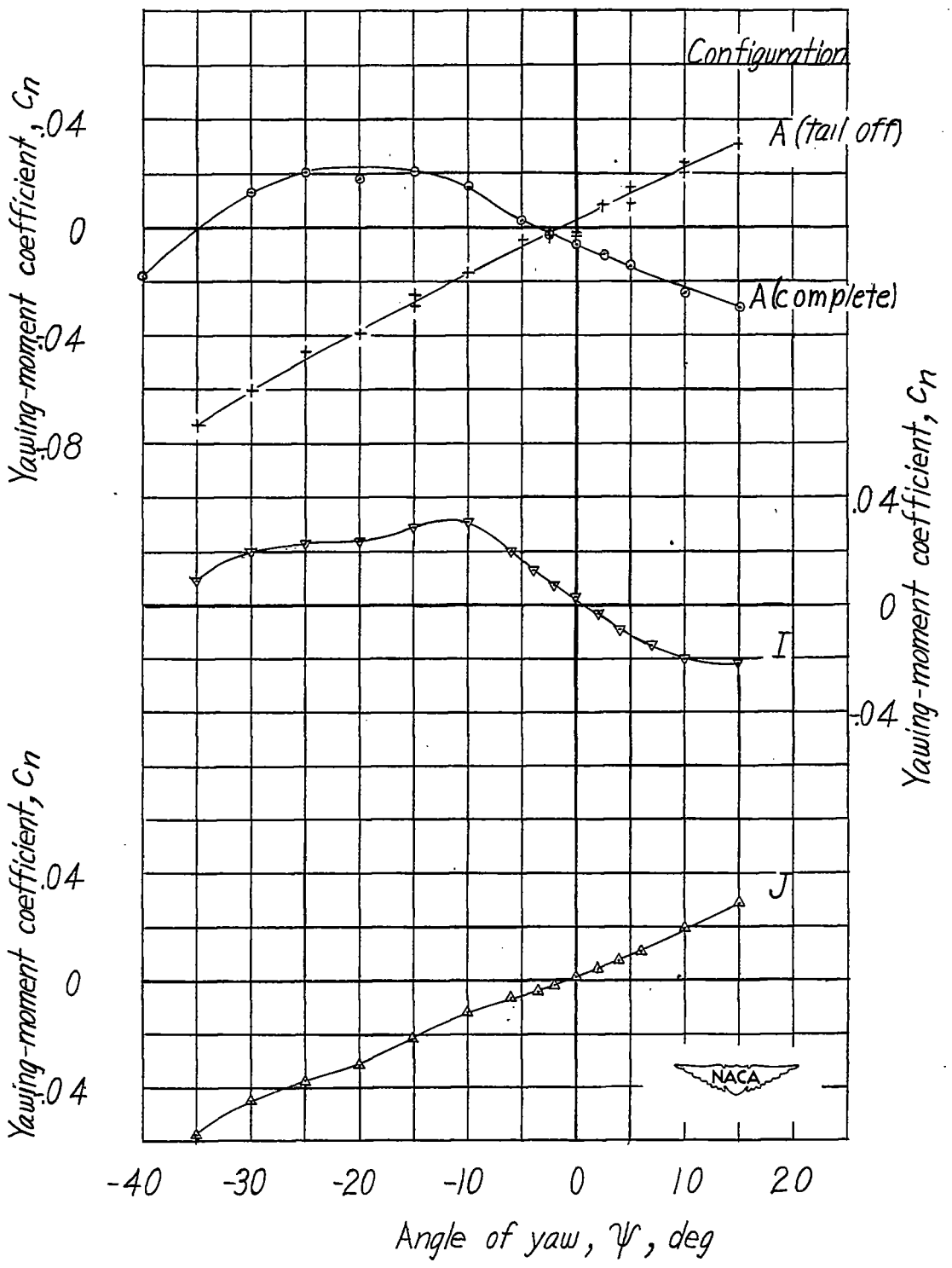

(e) $\alpha = 13.0^{\circ}$; yawing-moment coefficients.

Figure 23.- Continued.

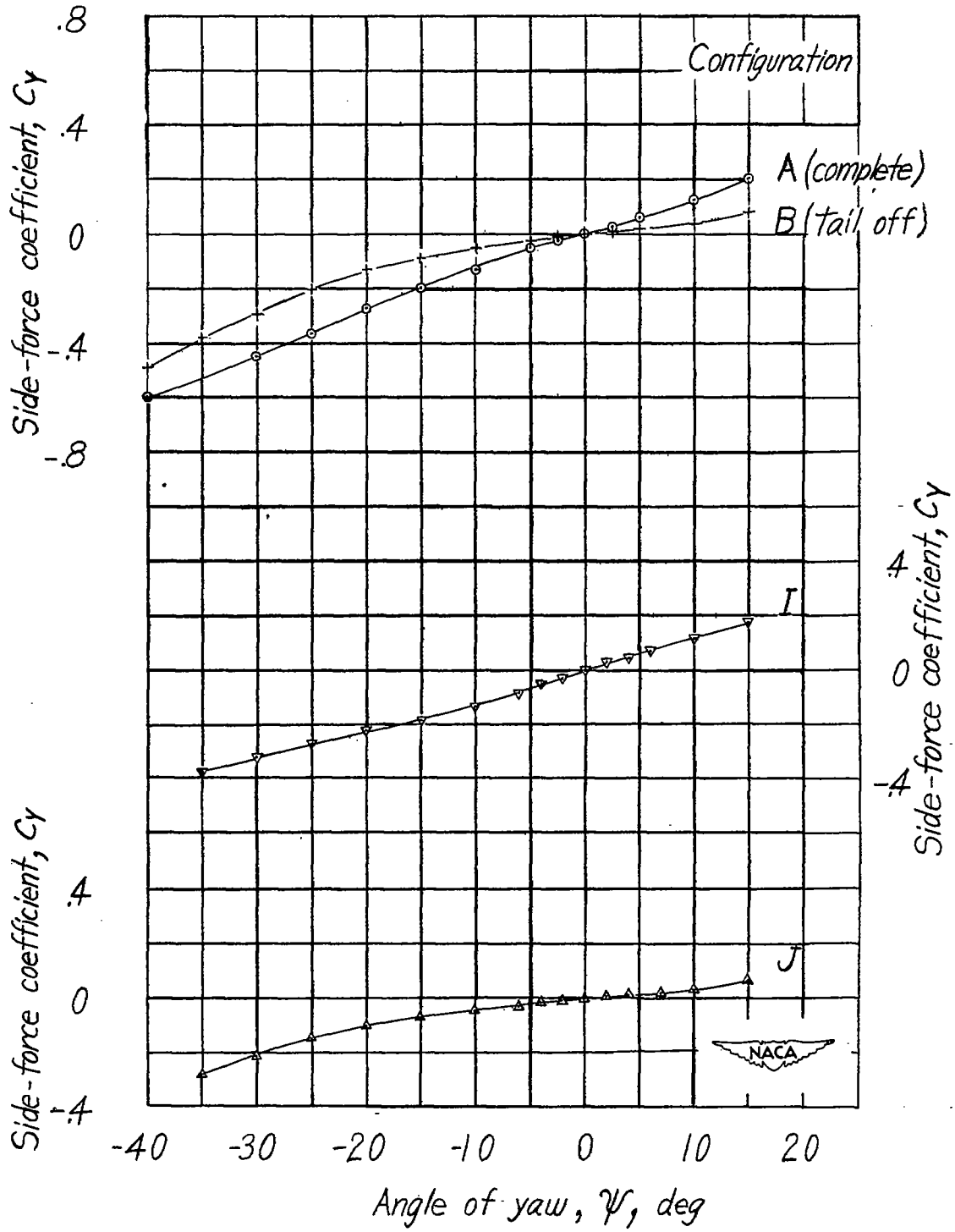

(f) $\alpha = 13.0^\circ$; side-force coefficients

Figure 23.- Concluded.

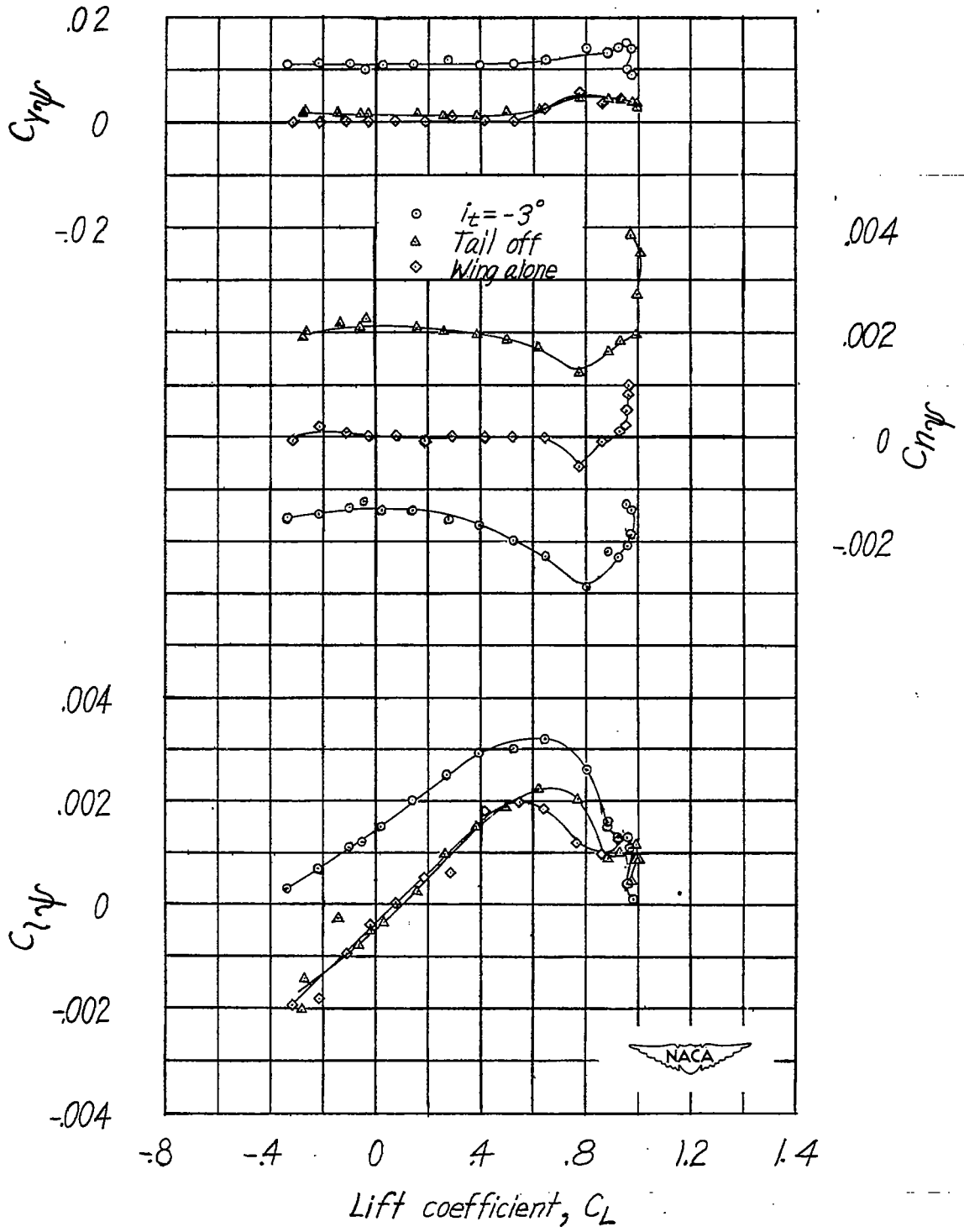

(a) $\delta_f = 0°$.

Figure 24.- Variation of lateral-stability derivatives with lift coefficient for test model. Revised dorsal; steel vertical tail; $\Gamma = 0°$.

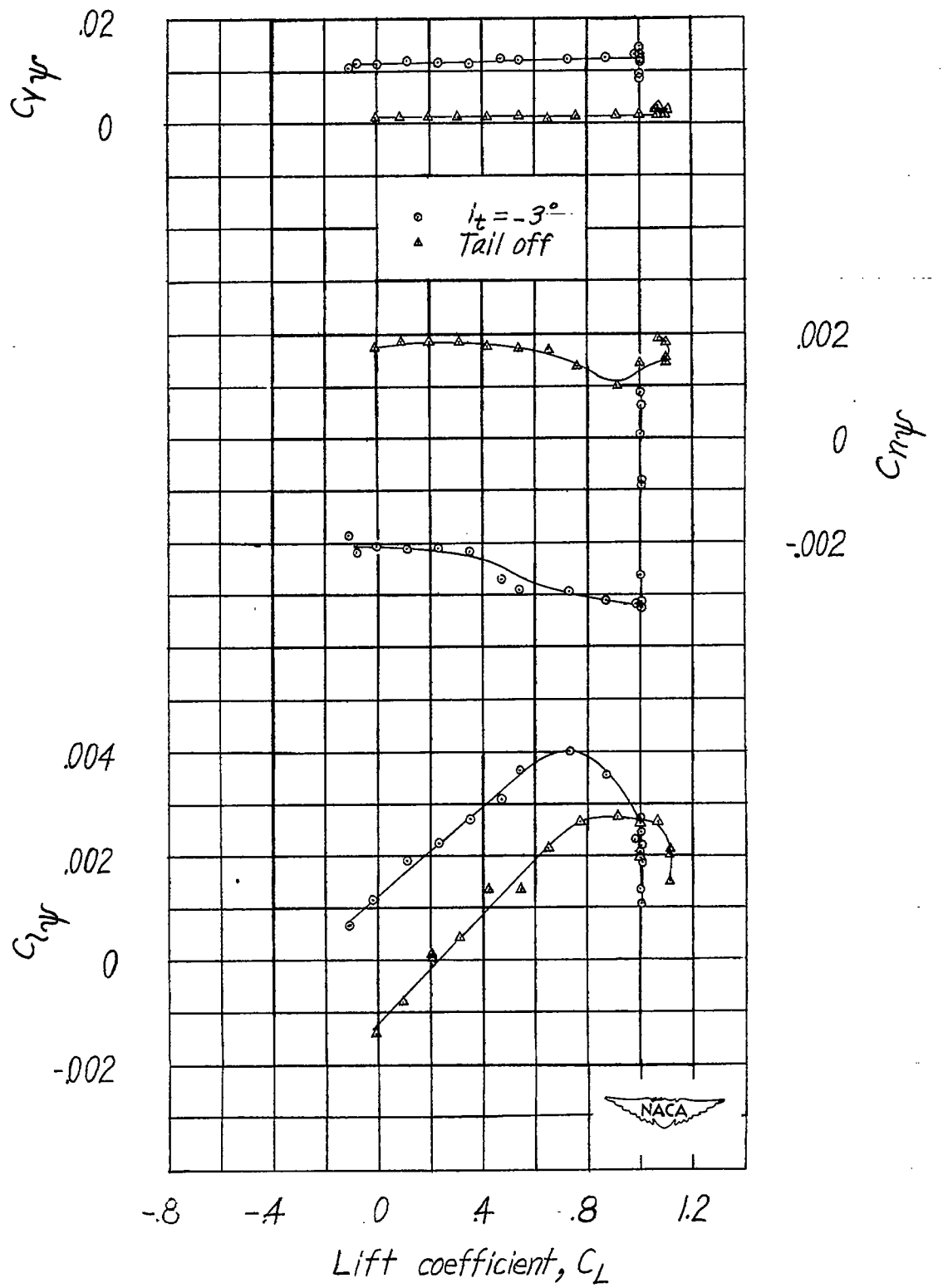

(b) $\delta_f = 50°$.

Figure 24.- Concluded.

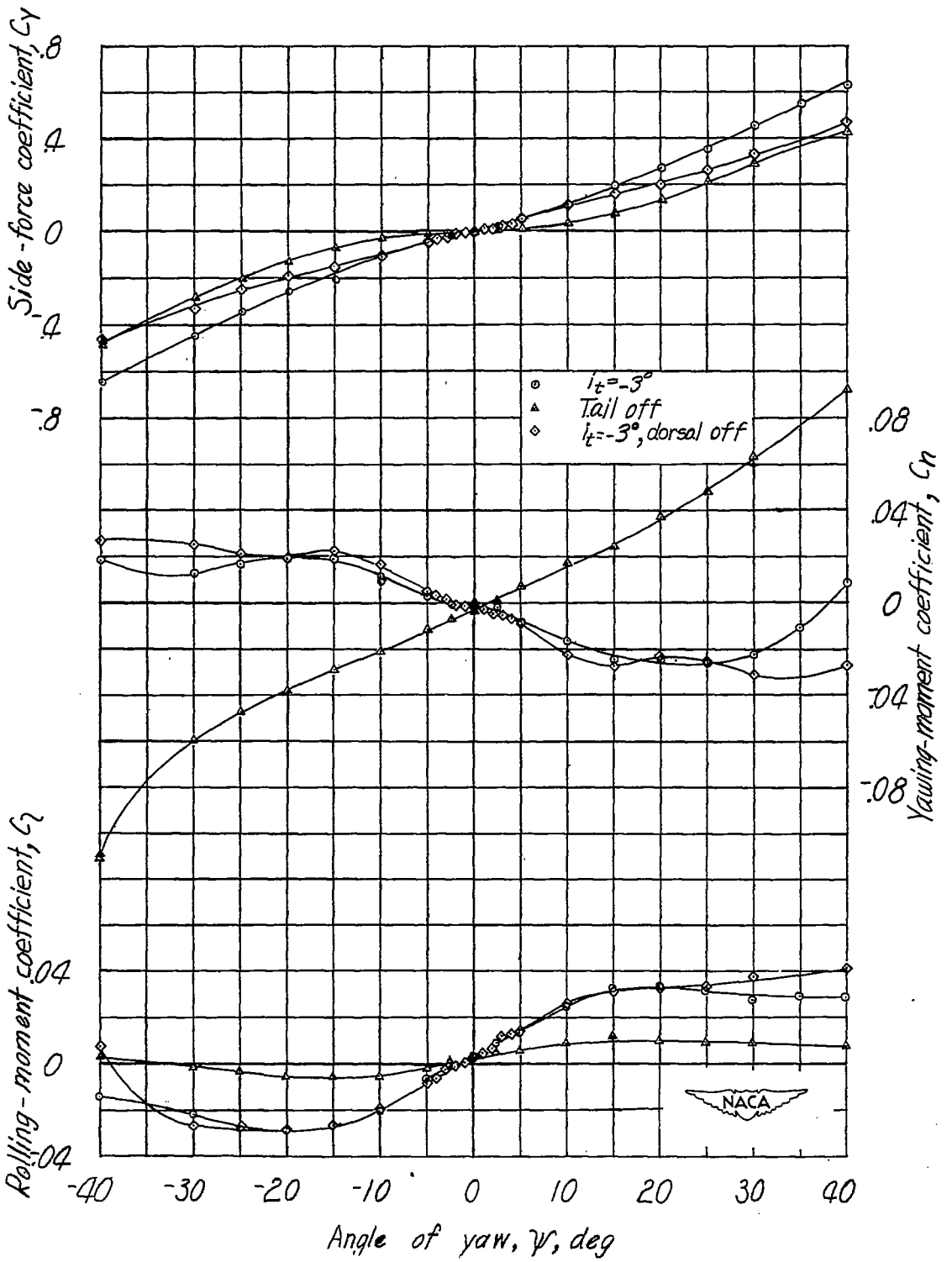

(a) $\delta_f = 0°$; $\alpha = 5.4°$.

Figure 25.- Variation of the aerodynamic characteristics with angle of yaw for test model. Original wing; $\Gamma = 0°$.

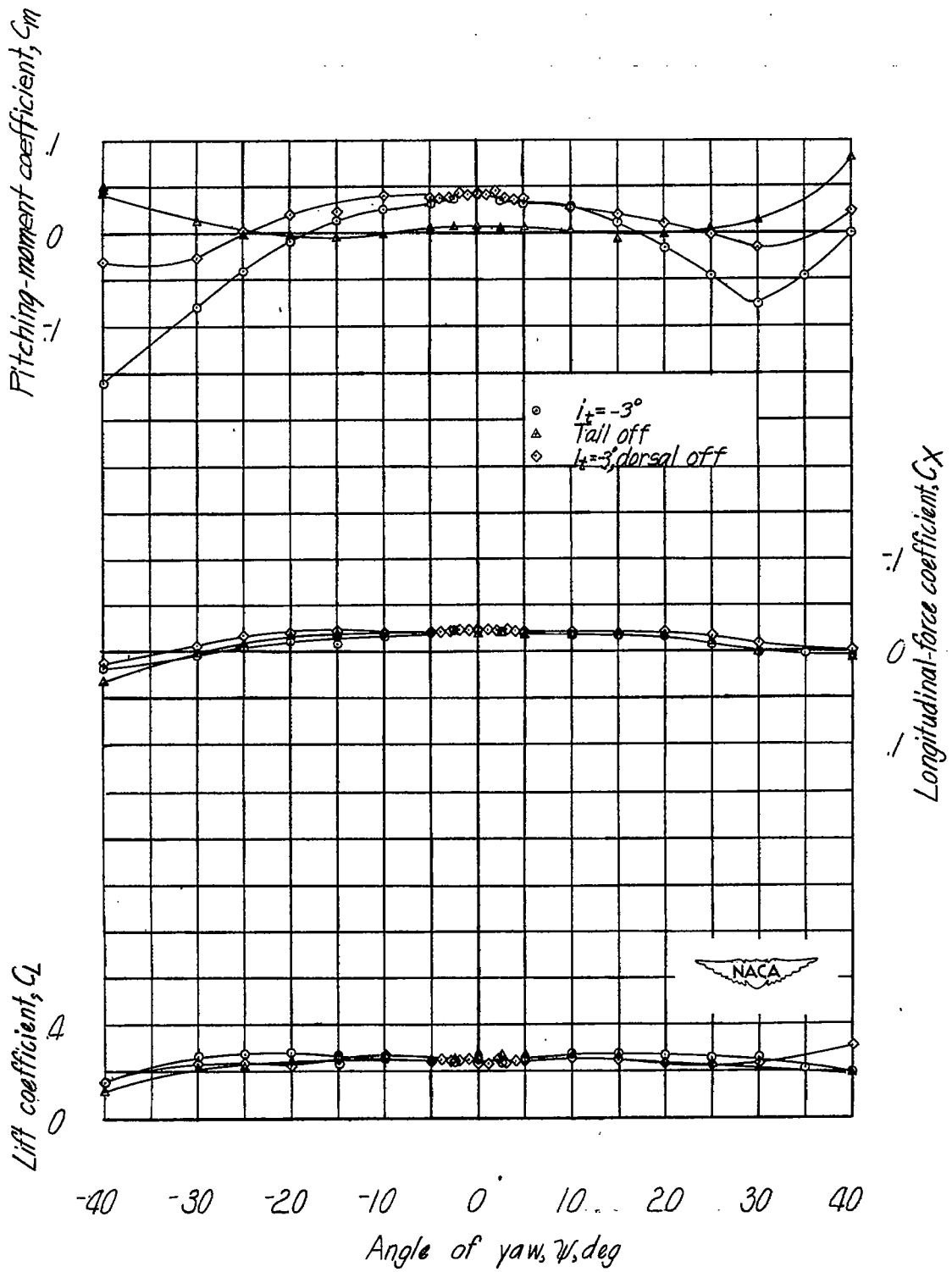

(a) Concluded.

Figure 25.- Continued.

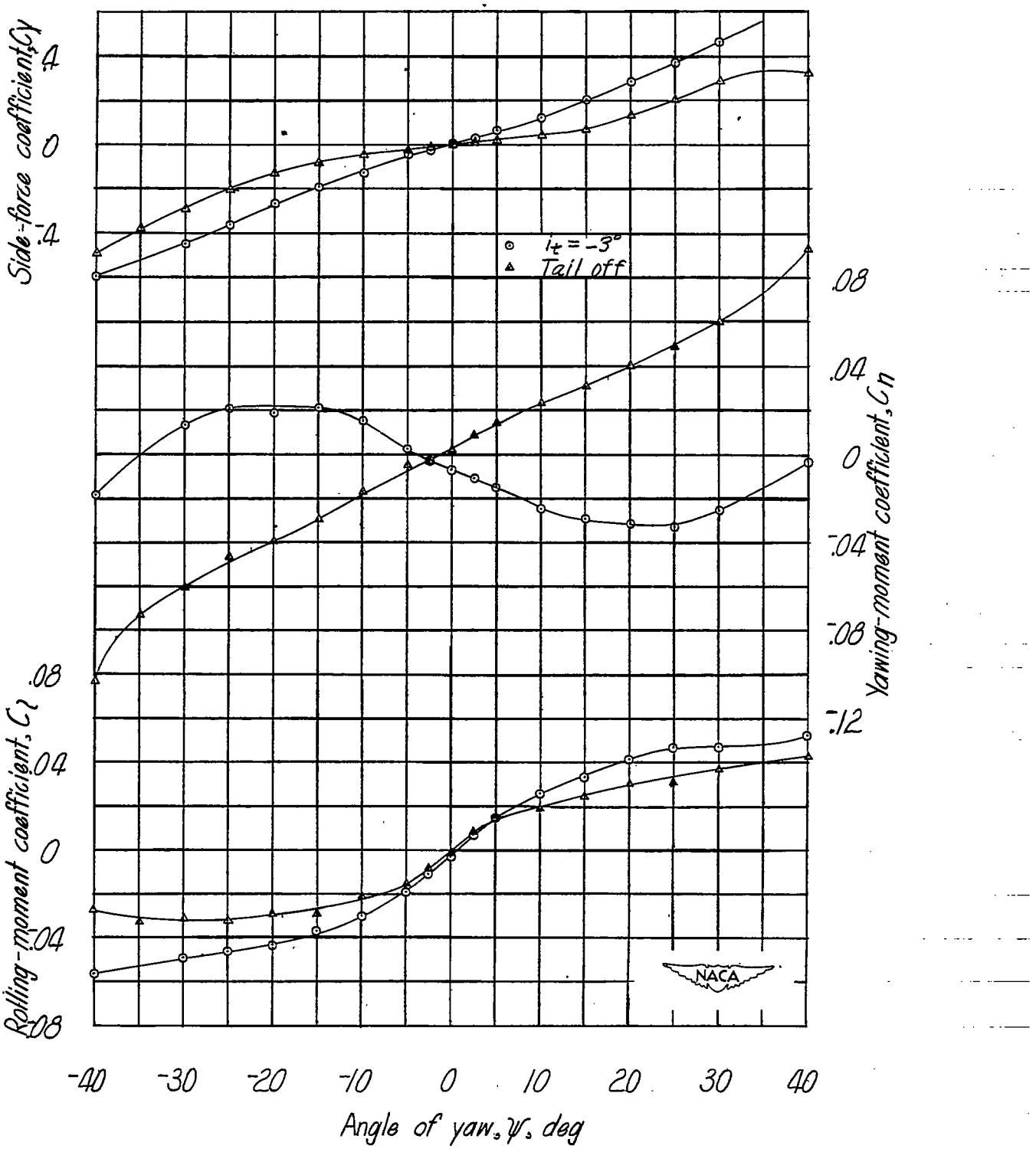

(b) $\delta_f = 0°$; $\alpha = 13.0°$.

Figure 25.- Continued.

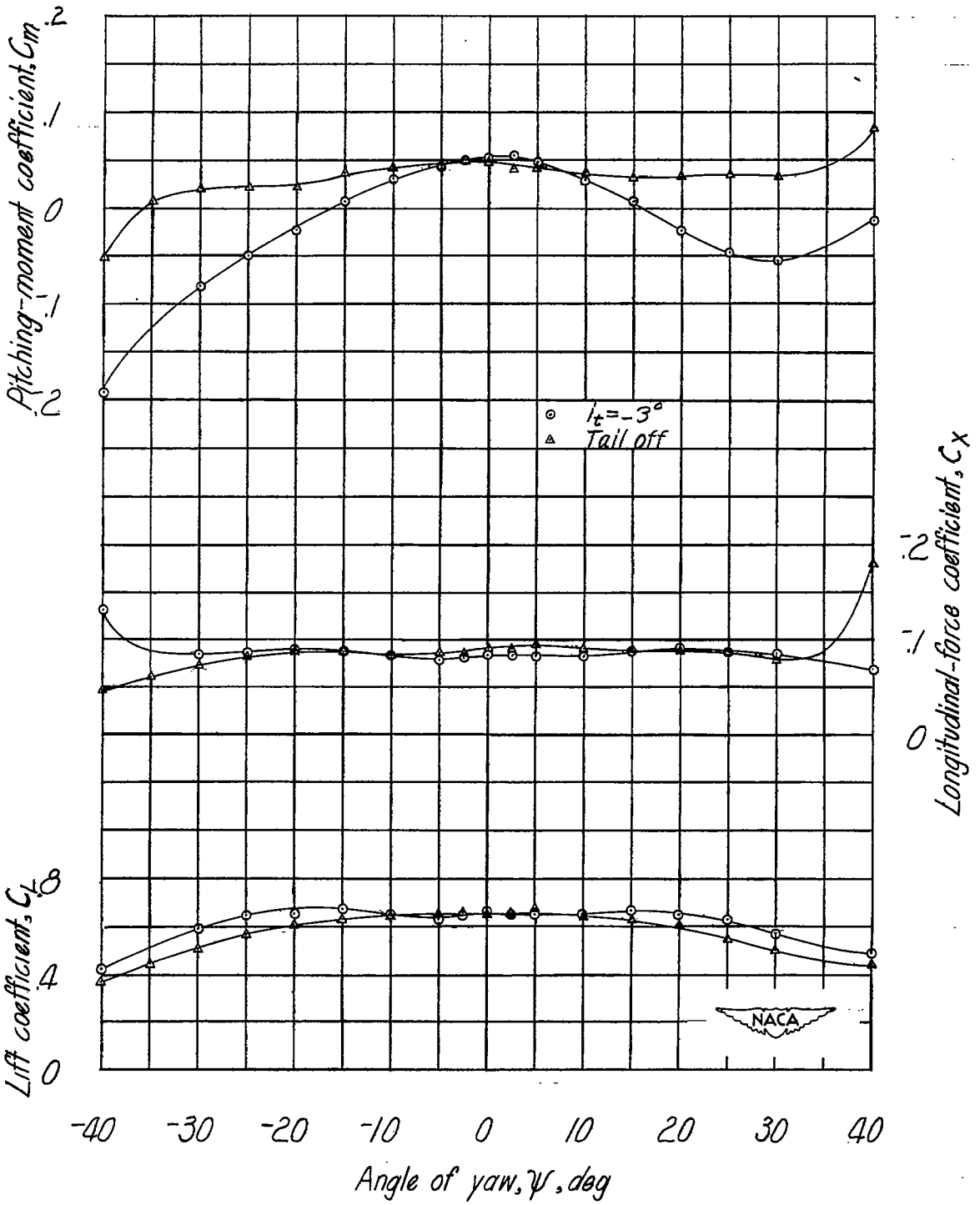

(b) Concluded.

Figure 25.- Continued.

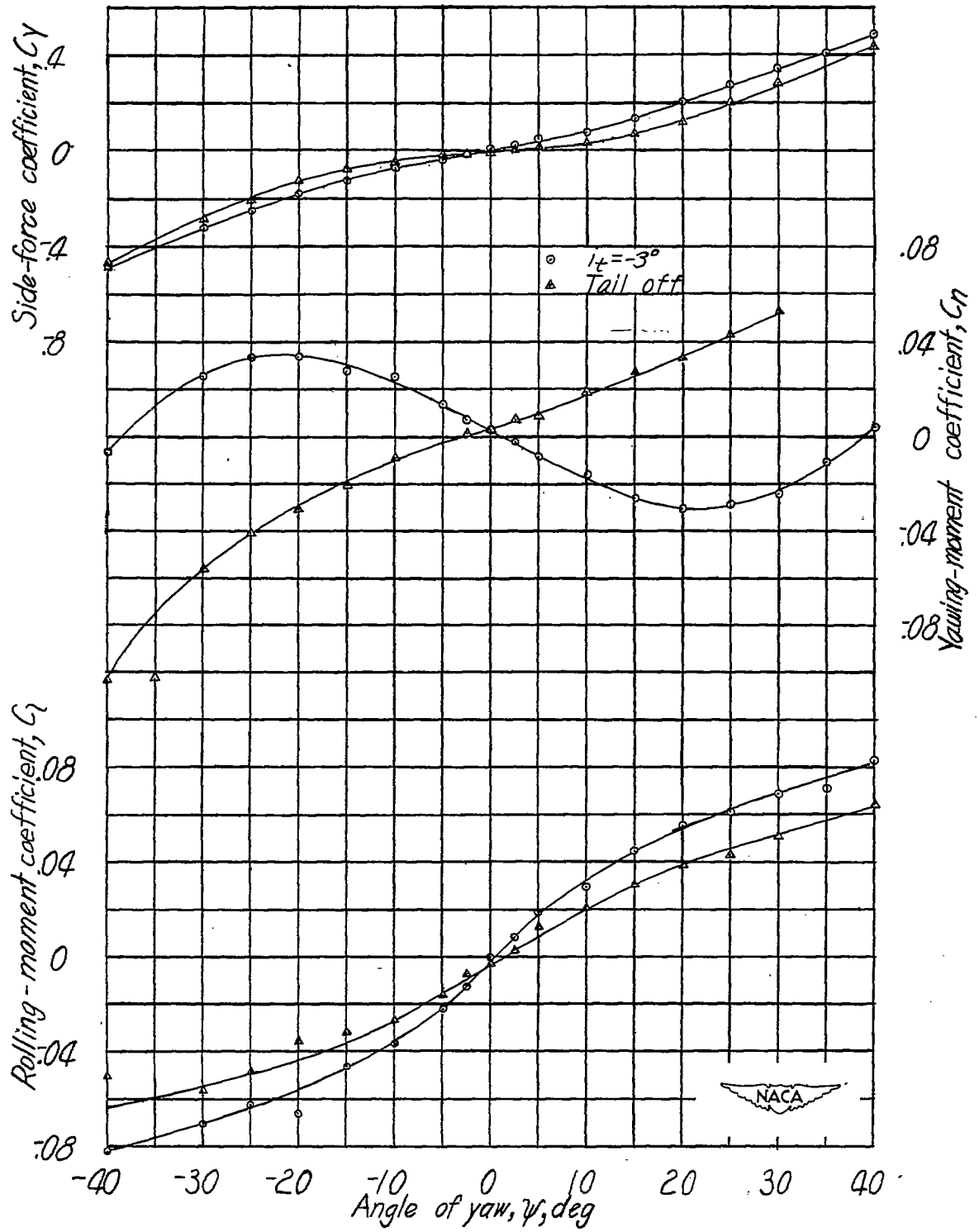

(c) $\delta_f = 50°$; $\alpha = 11.2°$.

Figure 25.- Continued.

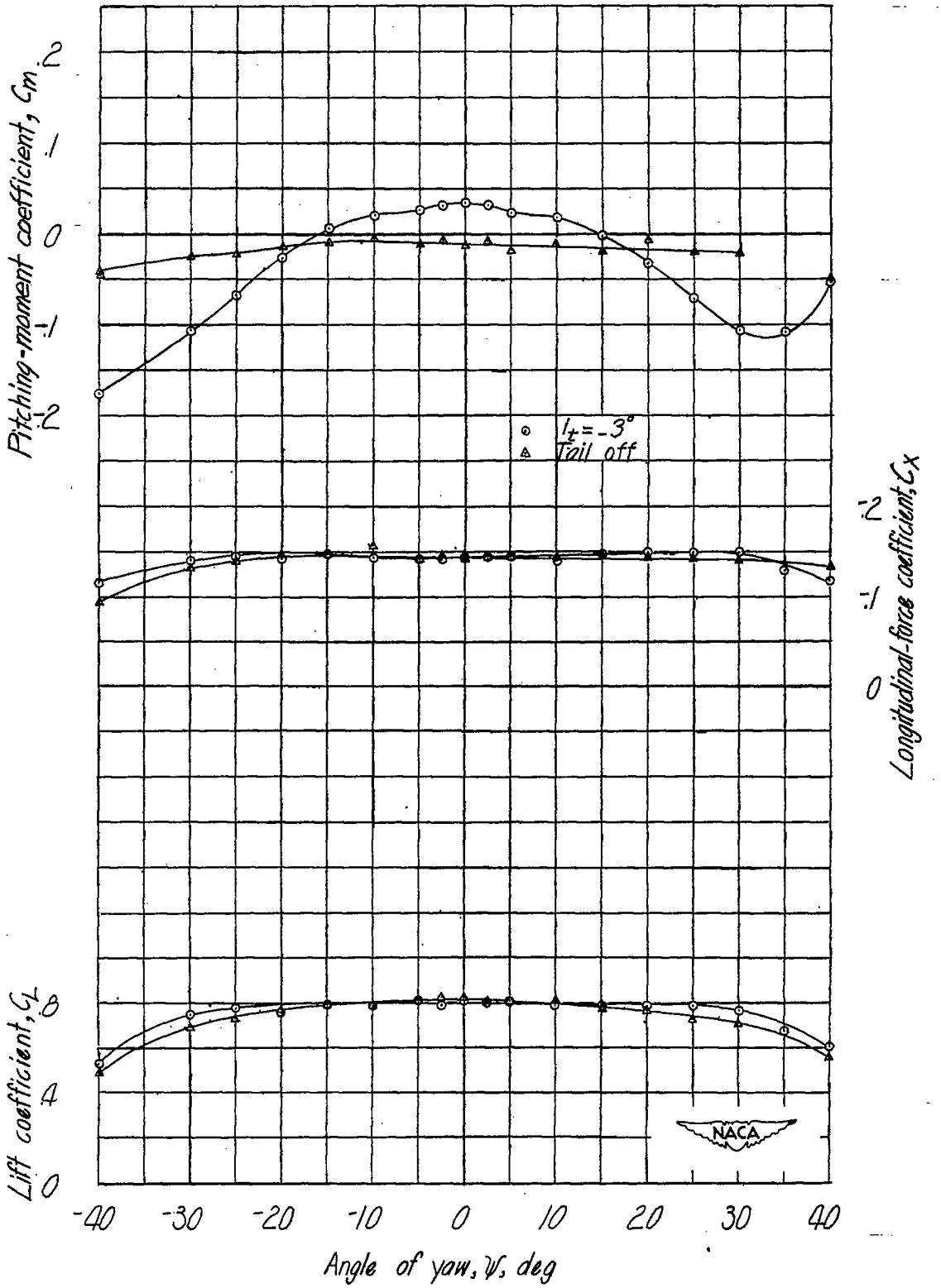

(c) Concluded.

Figure 25.- Concluded.

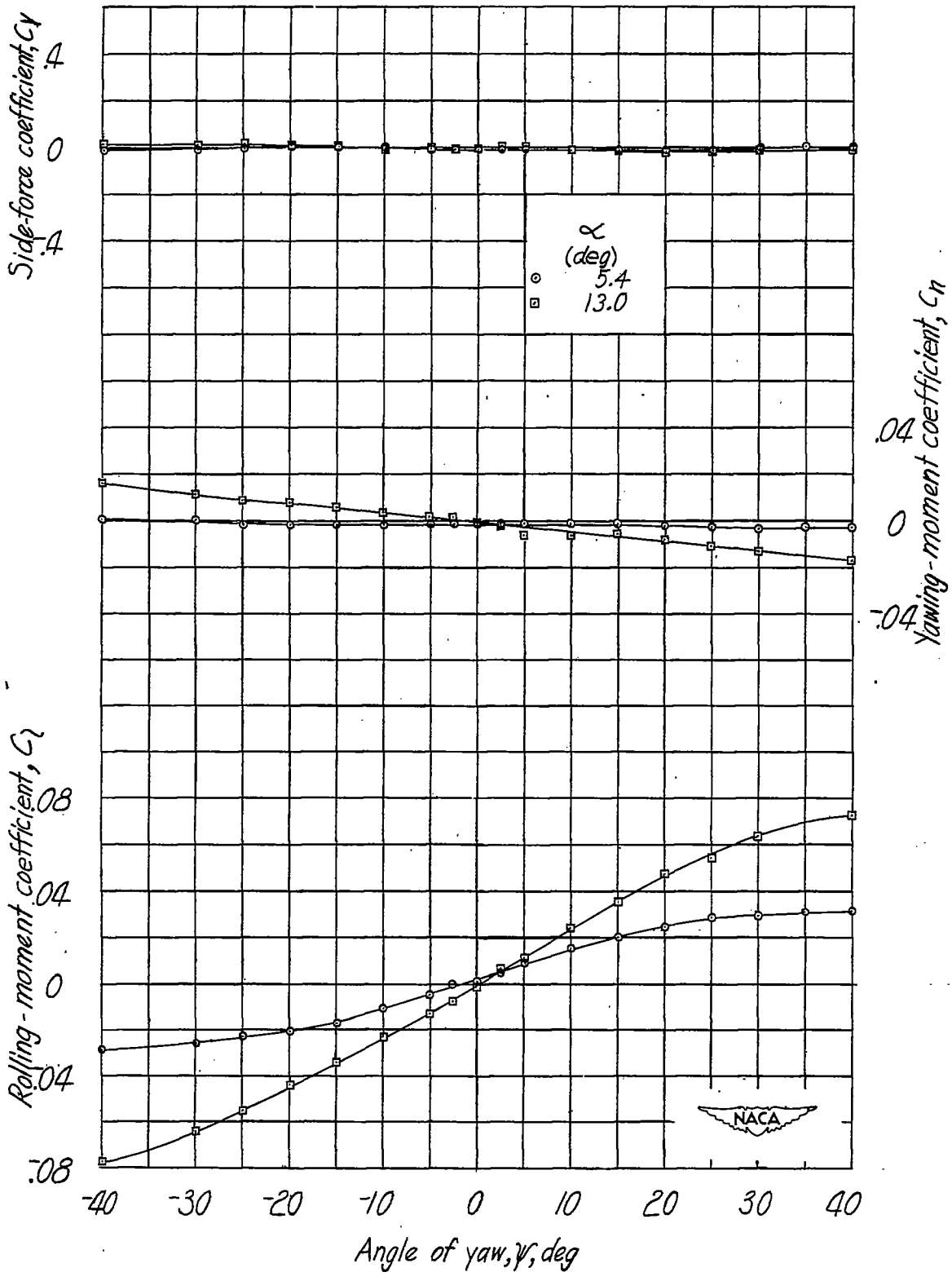

Figure 26.- The wing-alone aerodynamic characteristics in yaw of test model. $\Gamma = 0^\circ$.

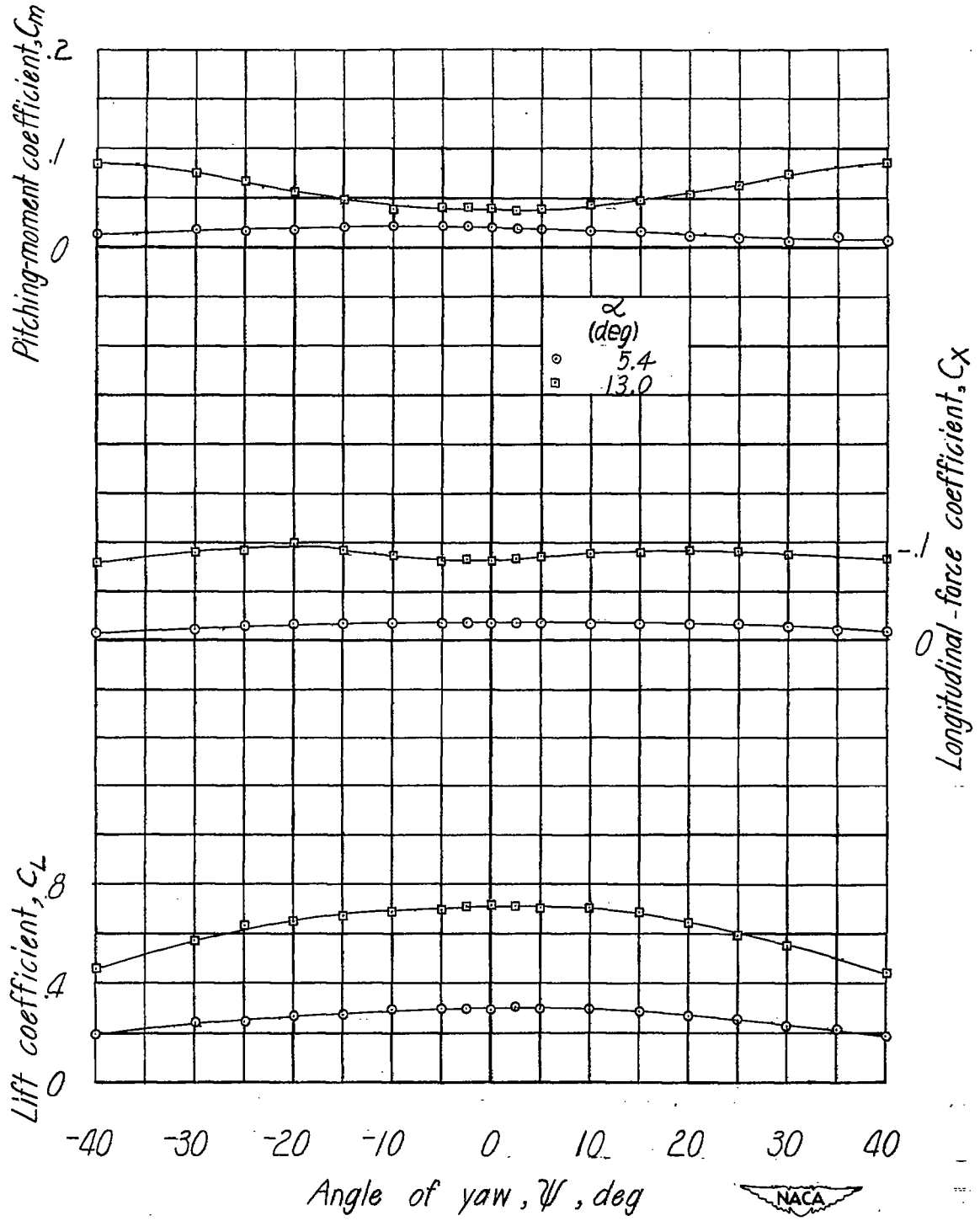

Figure 26.- Concluded.

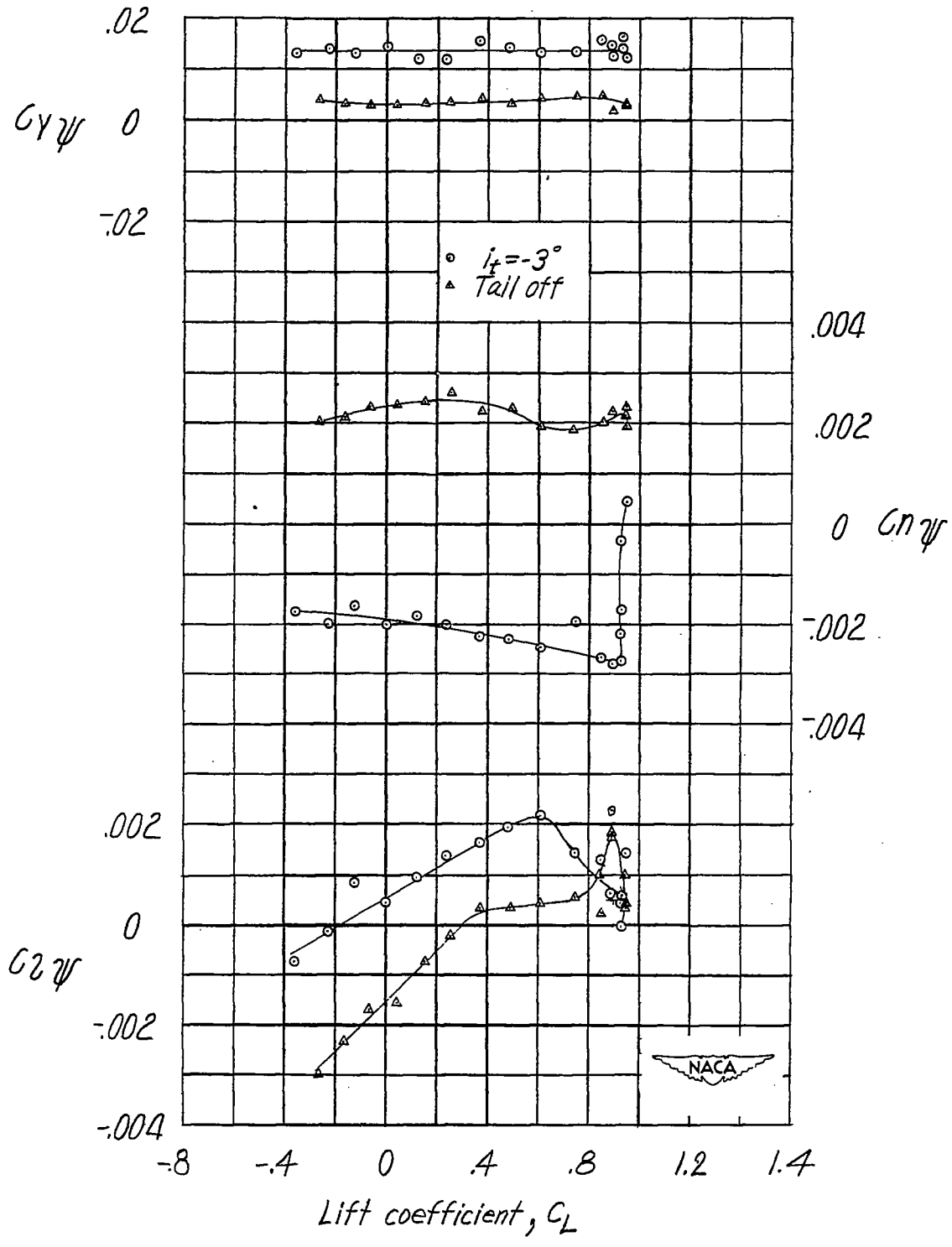

(a) $\delta_f = 0°$.

Figure 27.- Variation of lateral-stability derivatives with lift coefficient for test model. Revised dorsal, steel vertical tail; $\Gamma = -10°$.

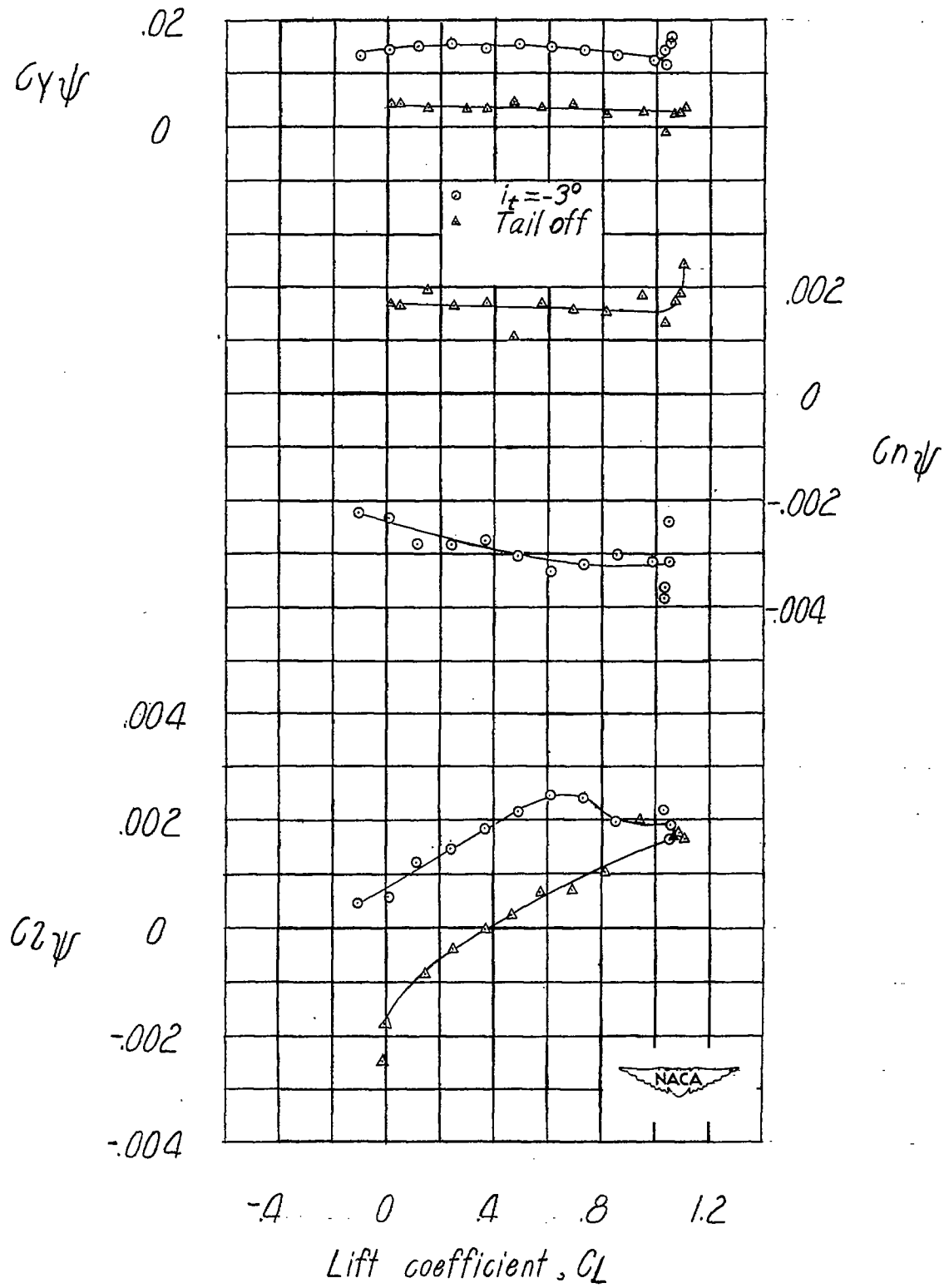

(b) $\delta_f = 50°$.

Figure 27.- Concluded.

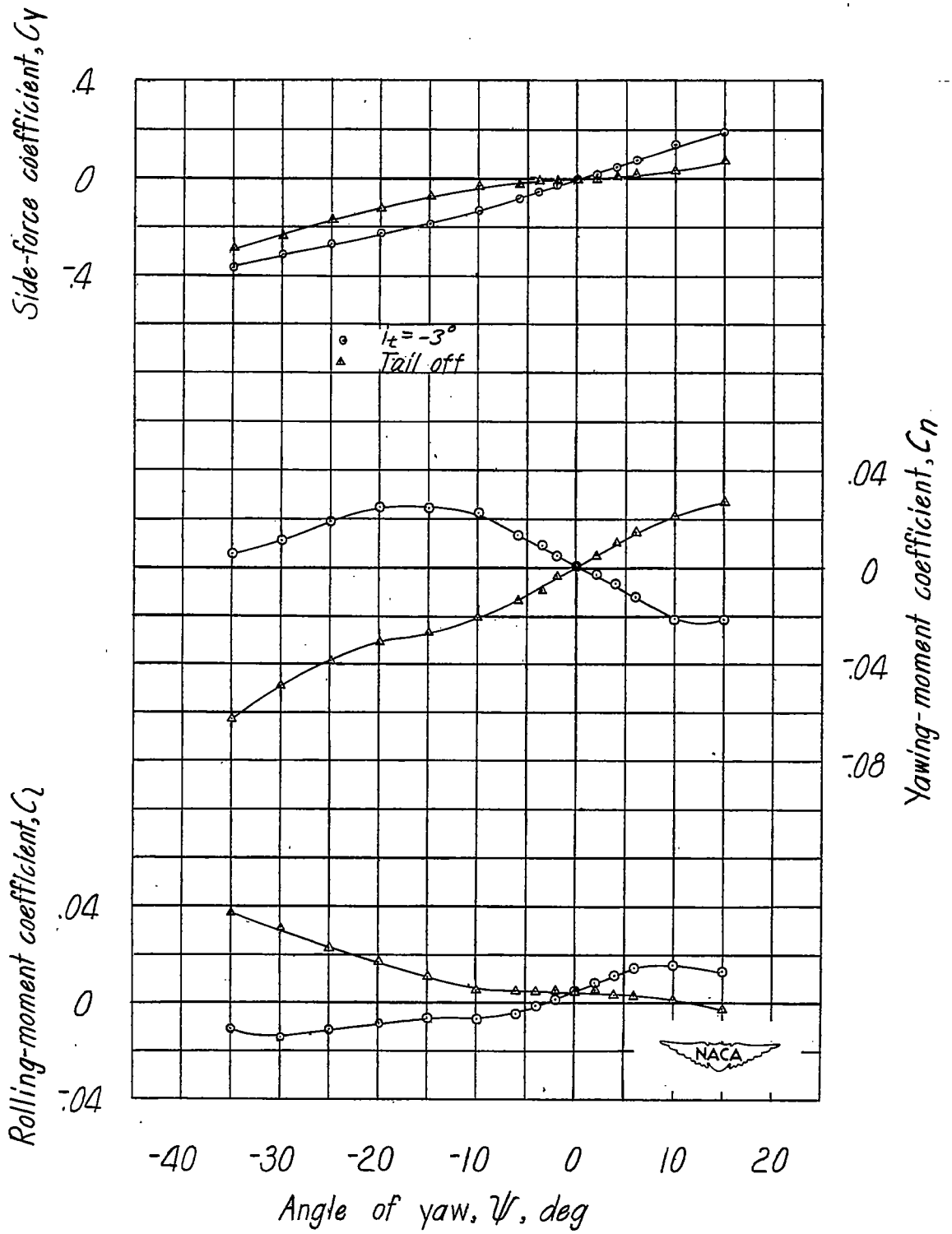

(a) $\delta_f = 0°$; $\alpha = 5.4°$.

Figure 28.- Variation of the aerodynamic characteristics with angle of yaw for test model. $\Gamma = -10°$.

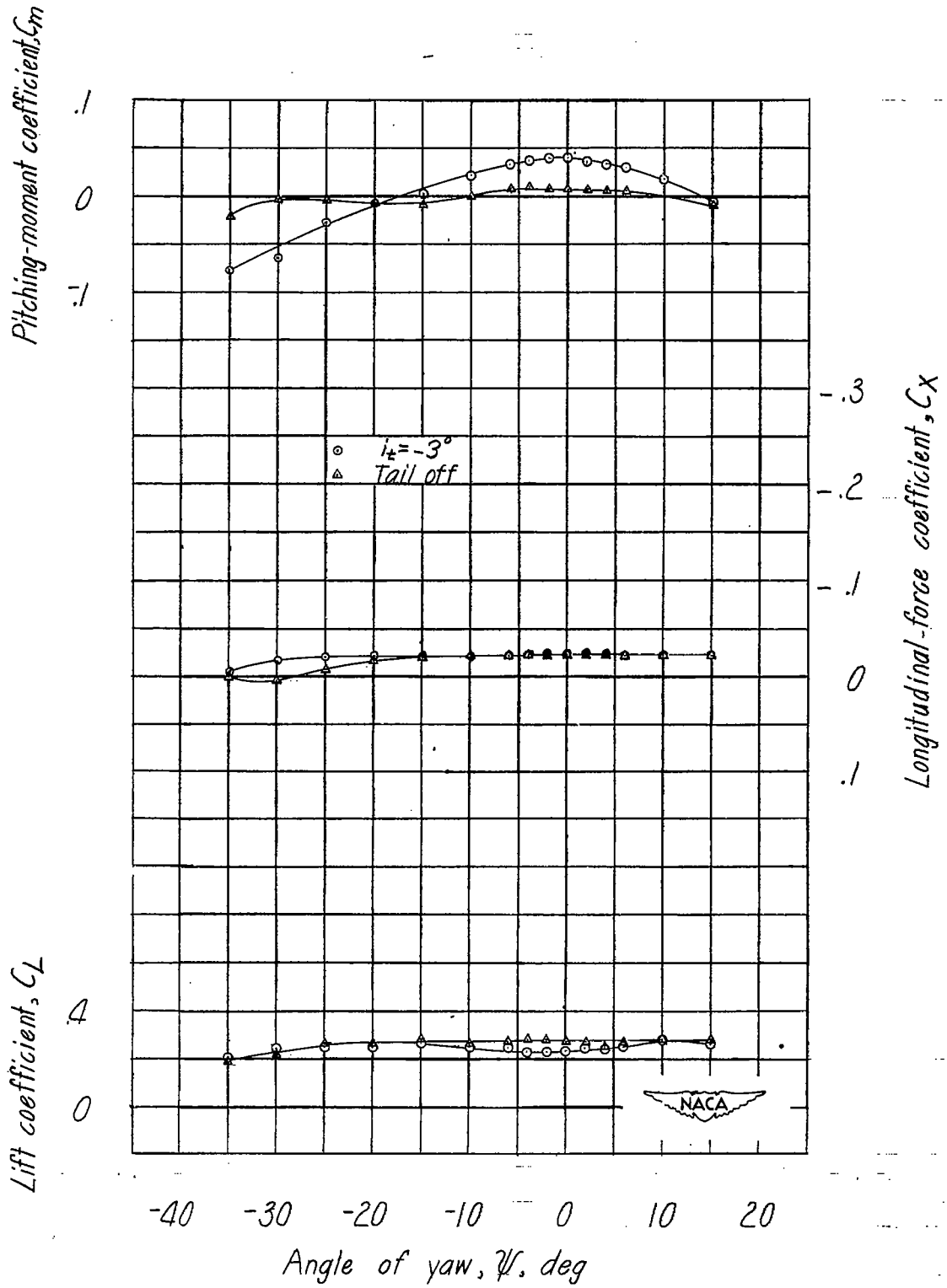

(a) Concluded.

Figure 28.- Continued.

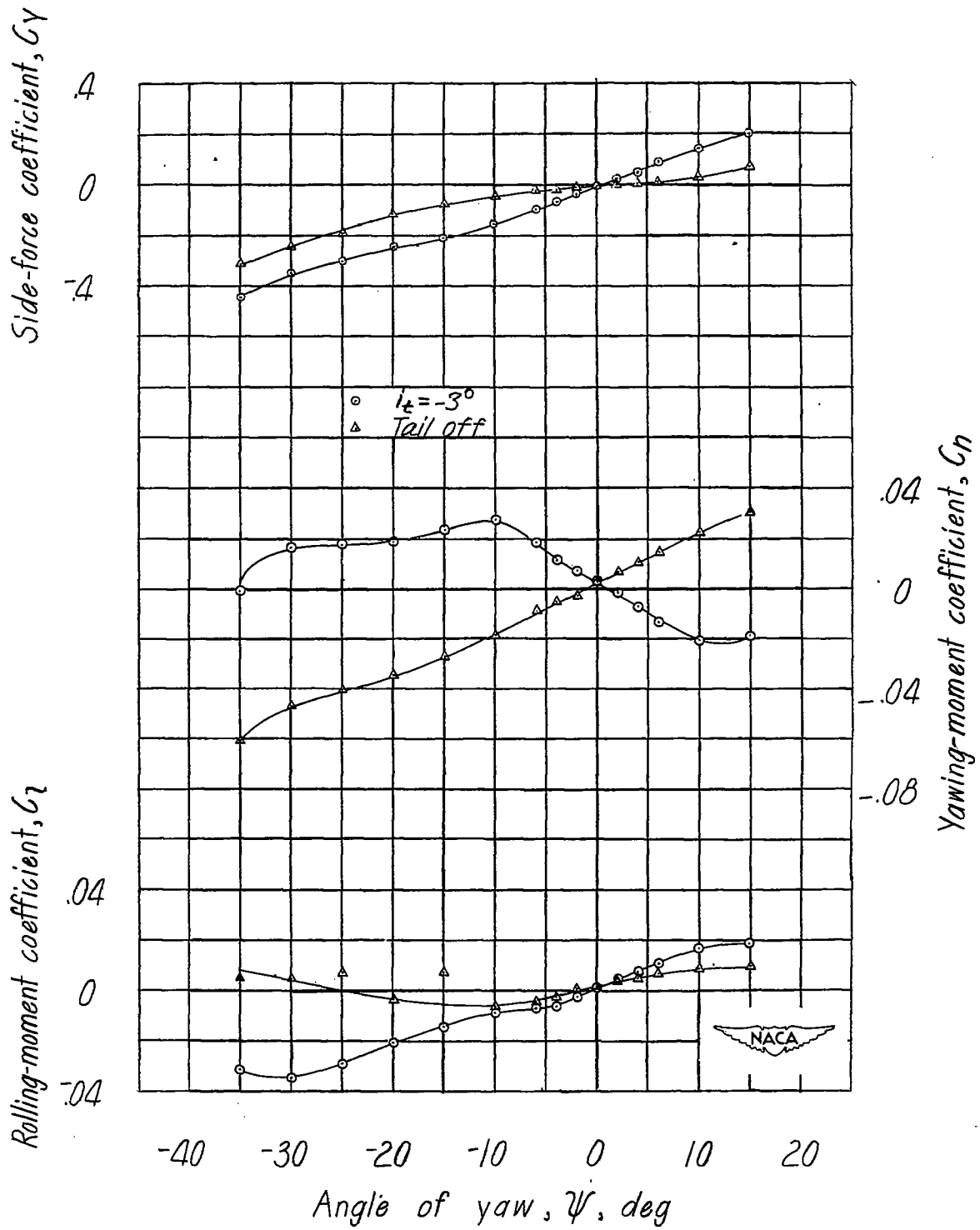

(b) $\delta_f = 0°$; $\alpha = 13.0°$.

Figure 28.- Continued.

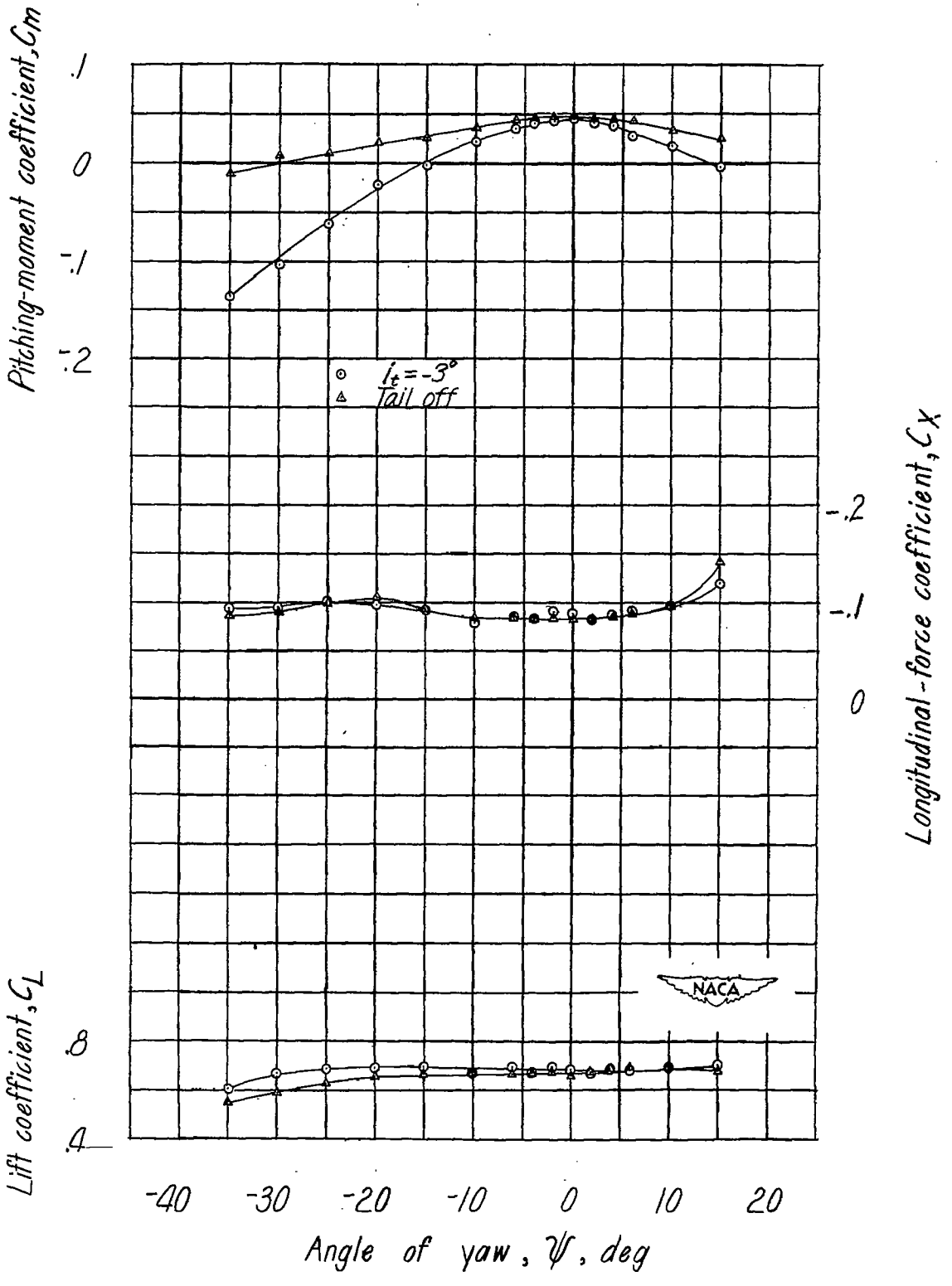

(b) Concluded.

Figure 28.- Continued.

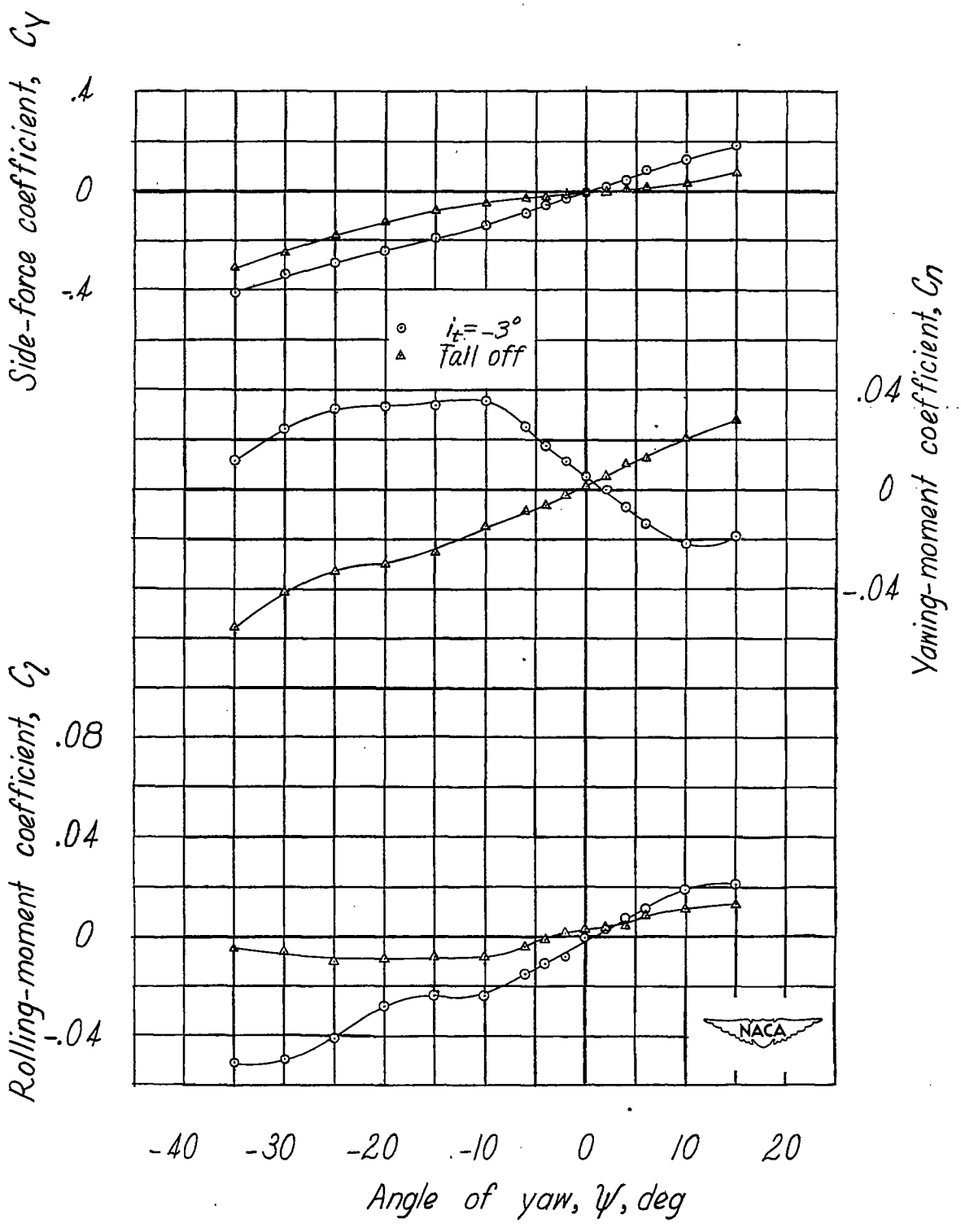

(c) $\delta_f = 50°$; $\alpha = 11.2°$.

Figure 28.- Continued.

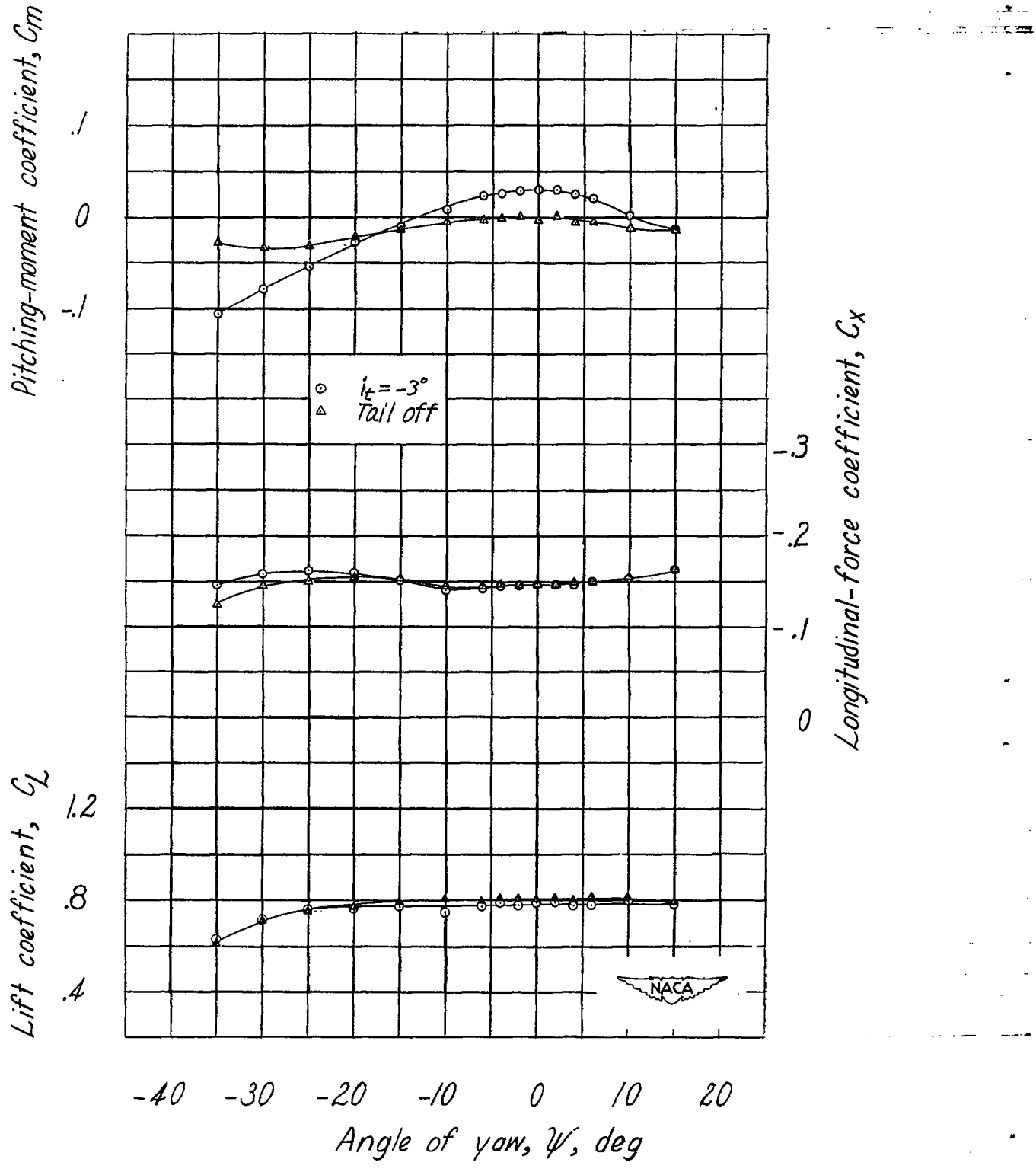

(c) Concluded.

Figure 28.- Concluded.

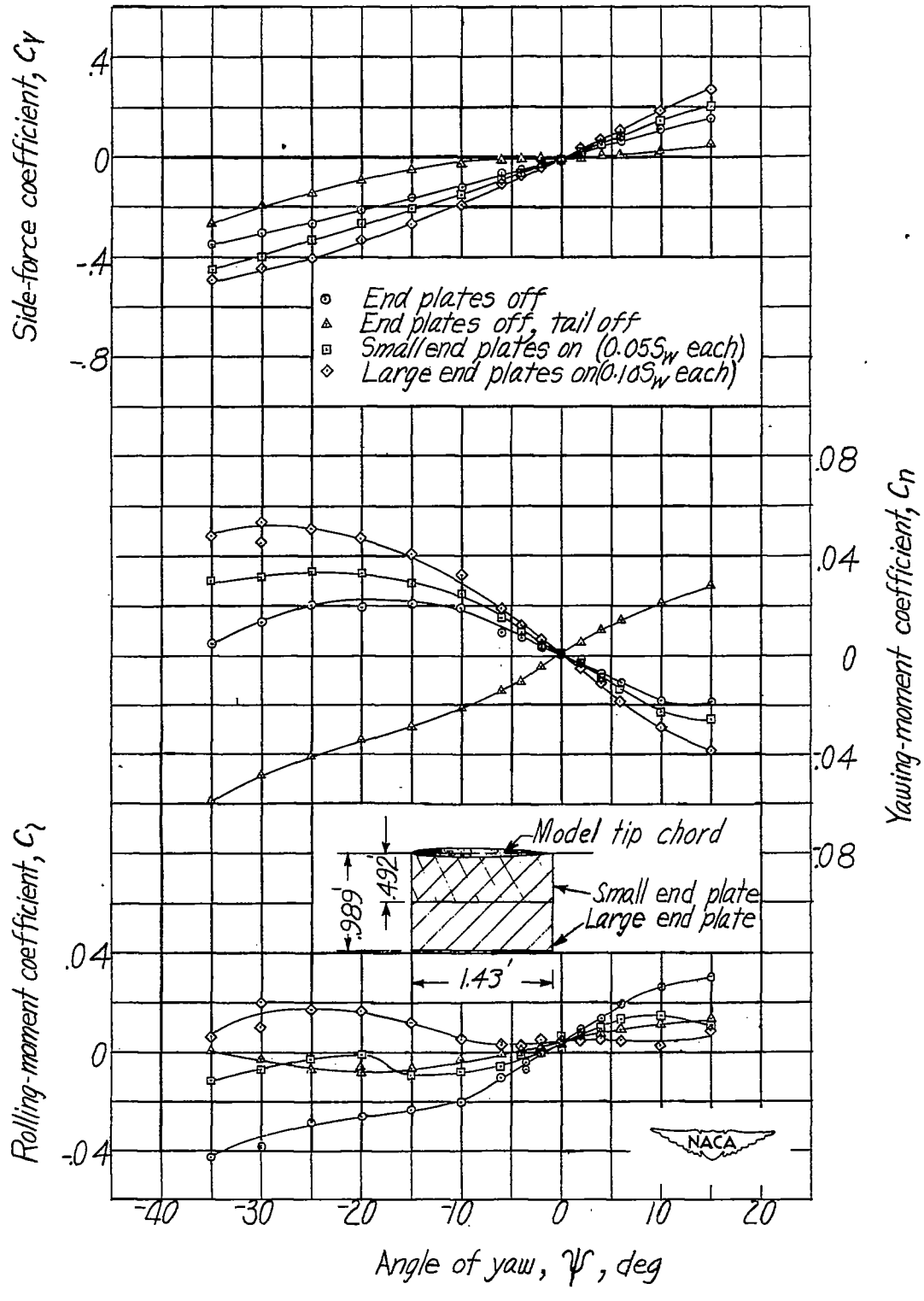

(a) $\alpha = 5.4^\circ$; $\delta_f = 0^\circ$.

Figure 29.- Effect of end plates on the aerodynamic characteristics in yaw of test model. $\Gamma = 0^\circ$.

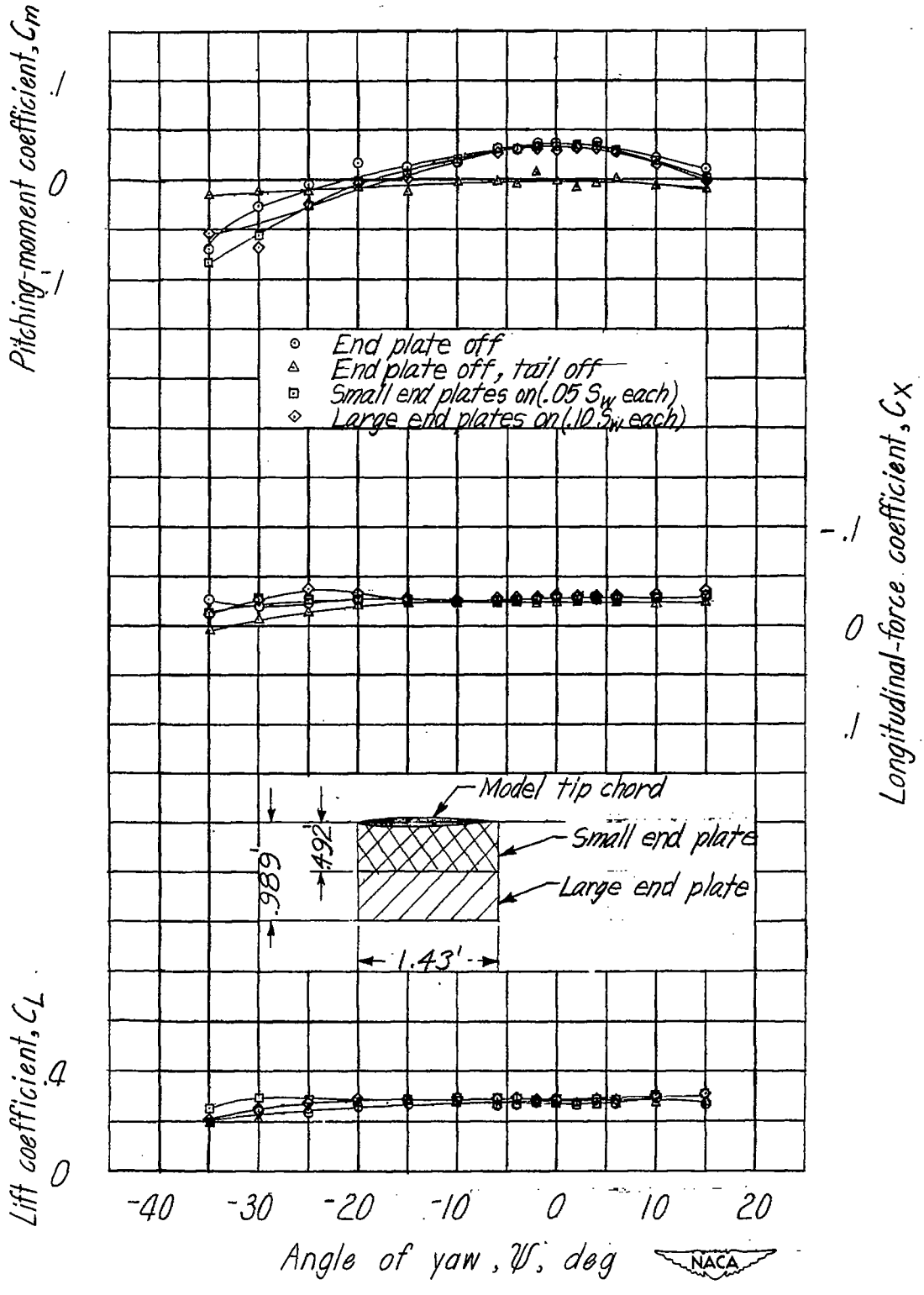

(a) Concluded.

Figure 29.- Continued.

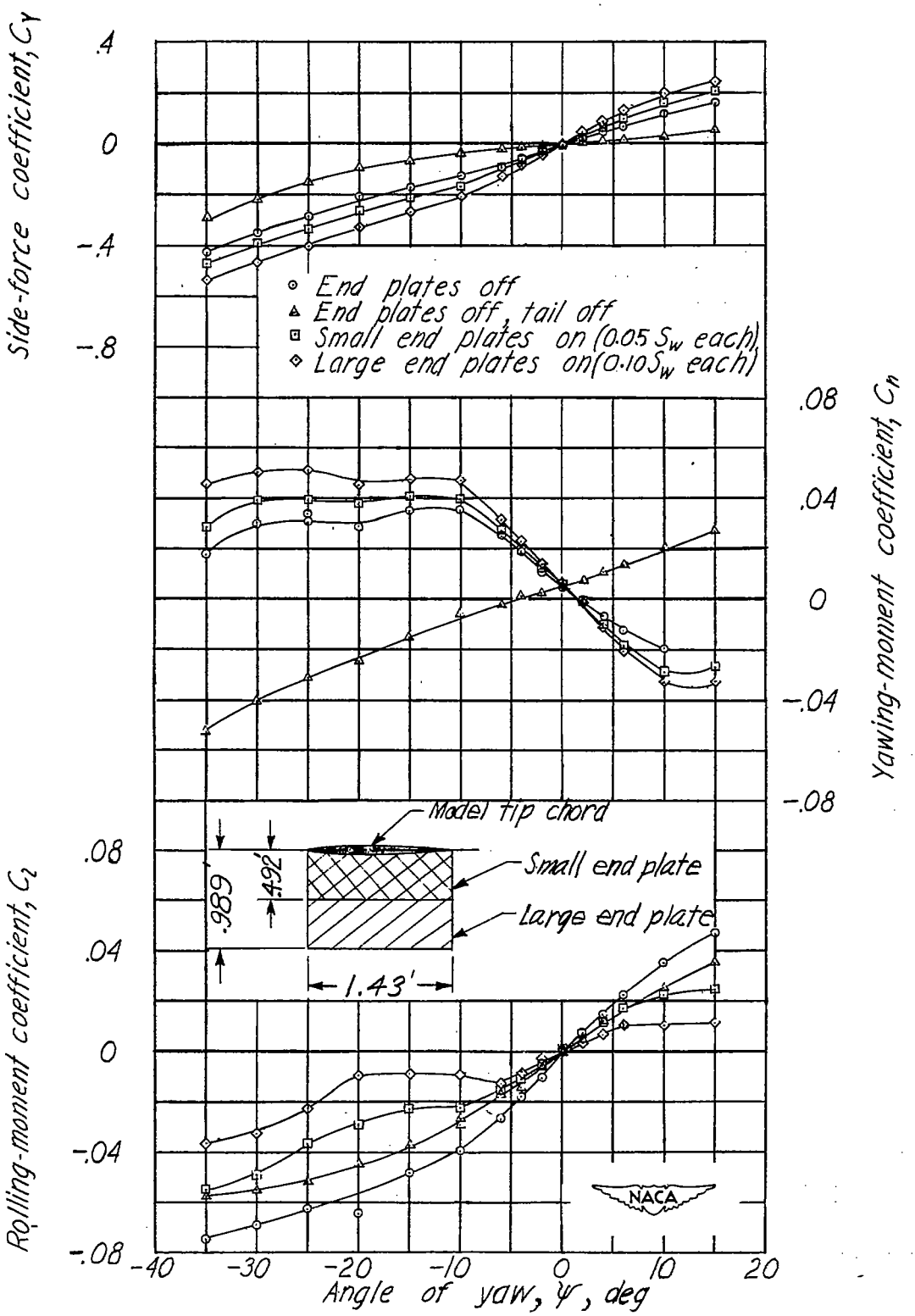

(b) $\alpha = 11.2^\circ$; $\delta_f = 50^\circ$.

Figure 29.- Continued.

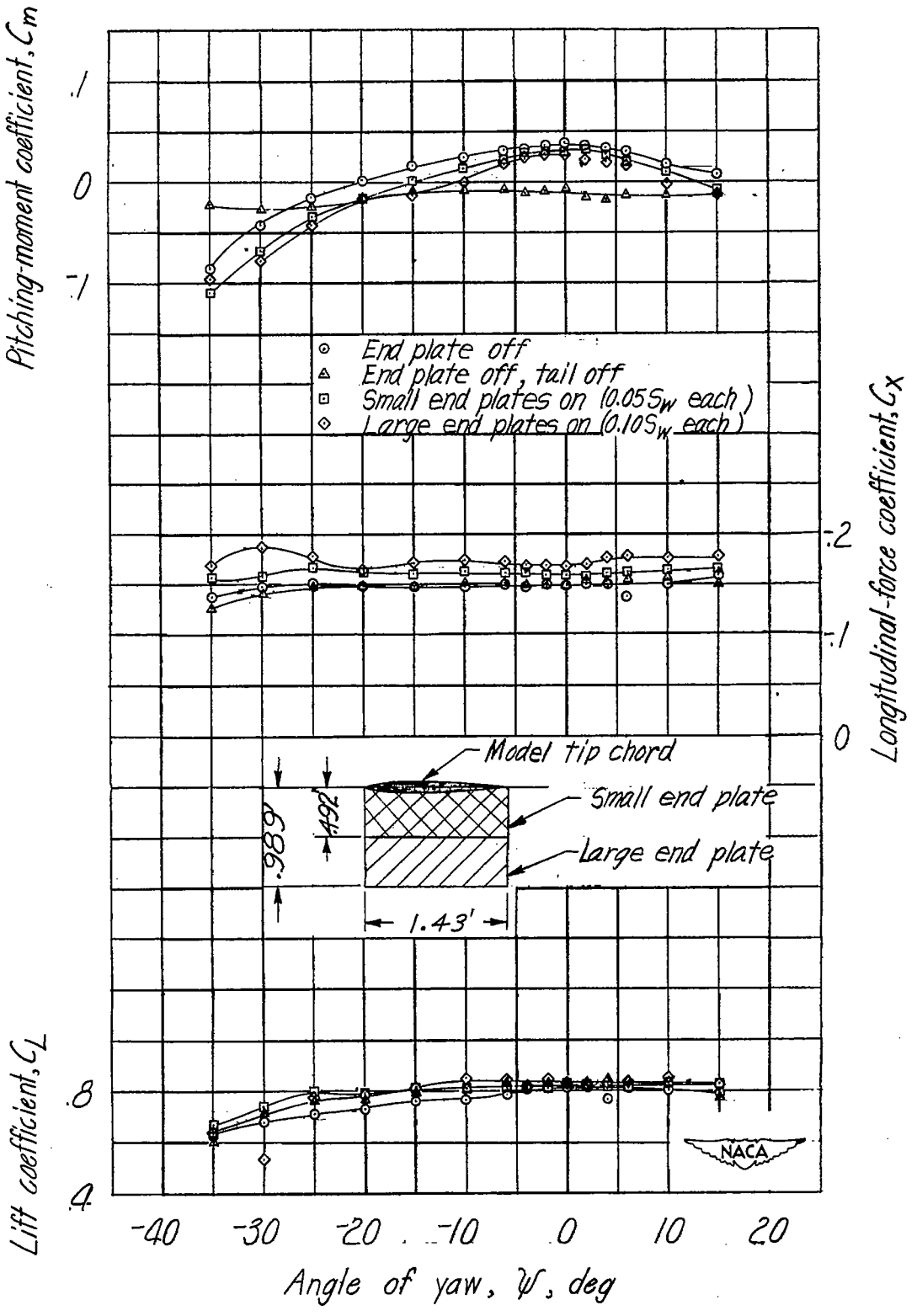

(b) Concluded.

Figure 29.- Concluded.

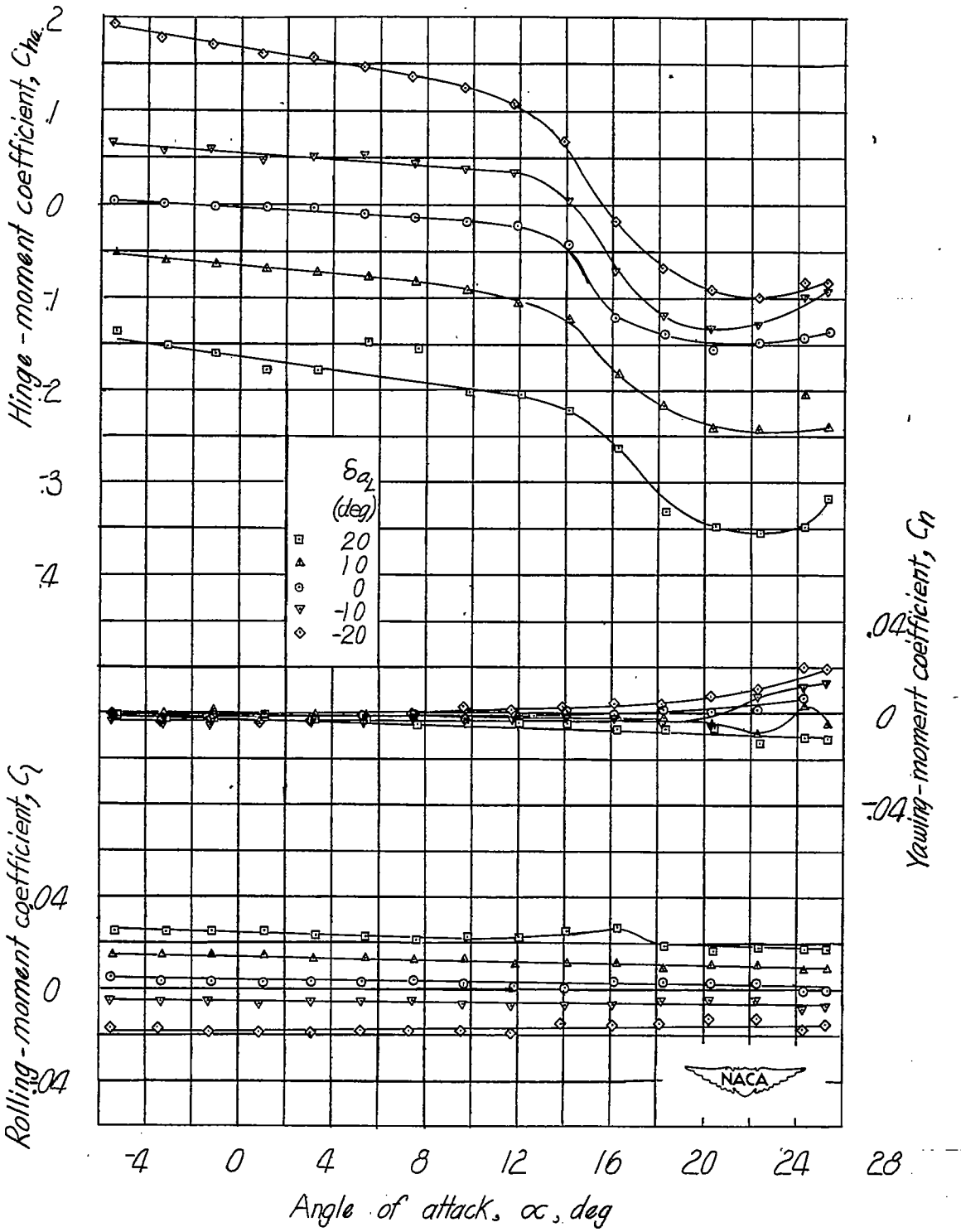

(a) $\delta_f = 0^\circ$; $\psi = 0^\circ$.

Figure 30.- Effect of aileron deflection on the aerodynamic characteristics in pitch at various angles of attack of test model. $\Gamma = 0^\circ$.

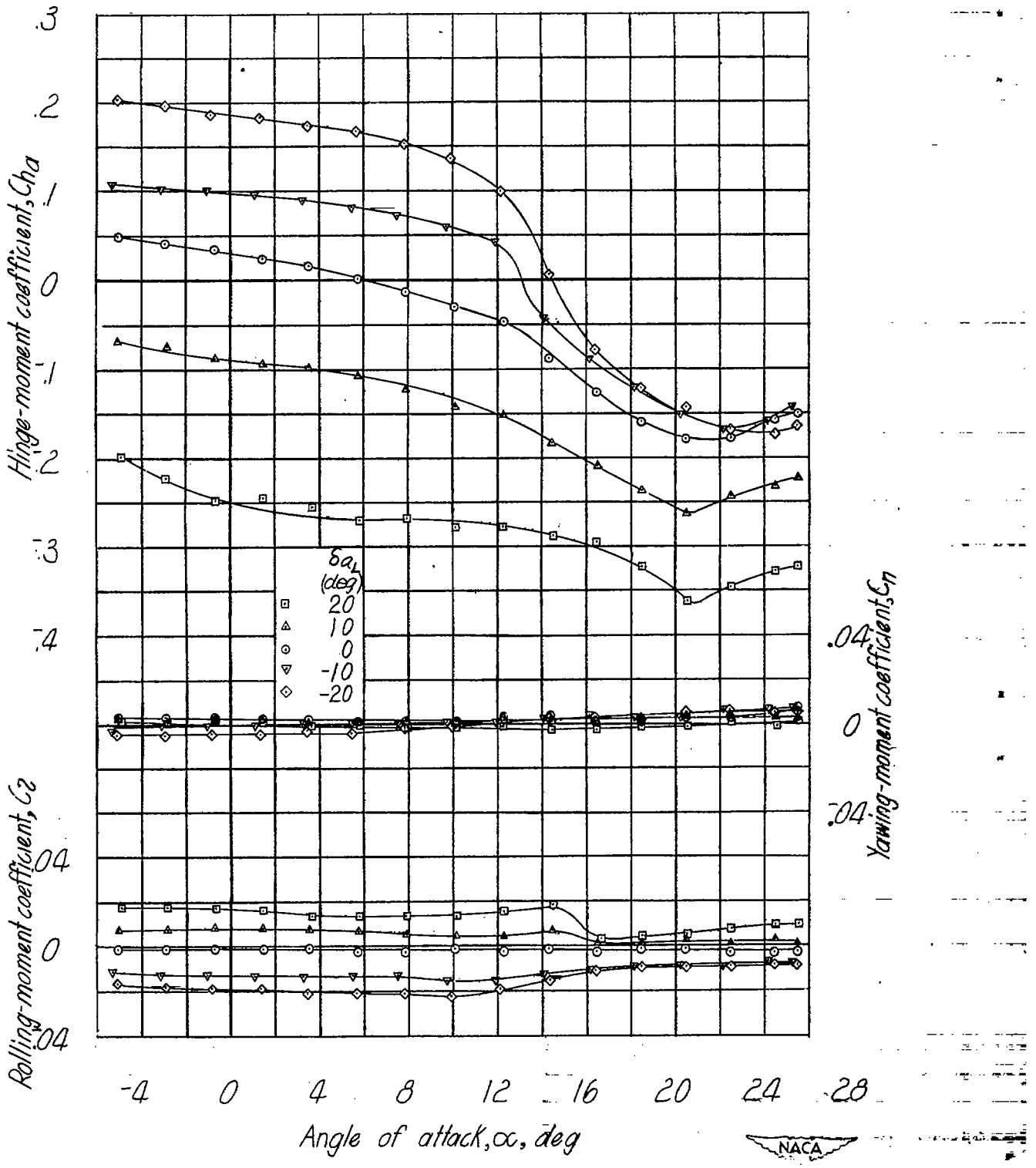

(b) $\delta_f = 50^\circ$; $\psi = 0^\circ$.

Figure 30.- Concluded.

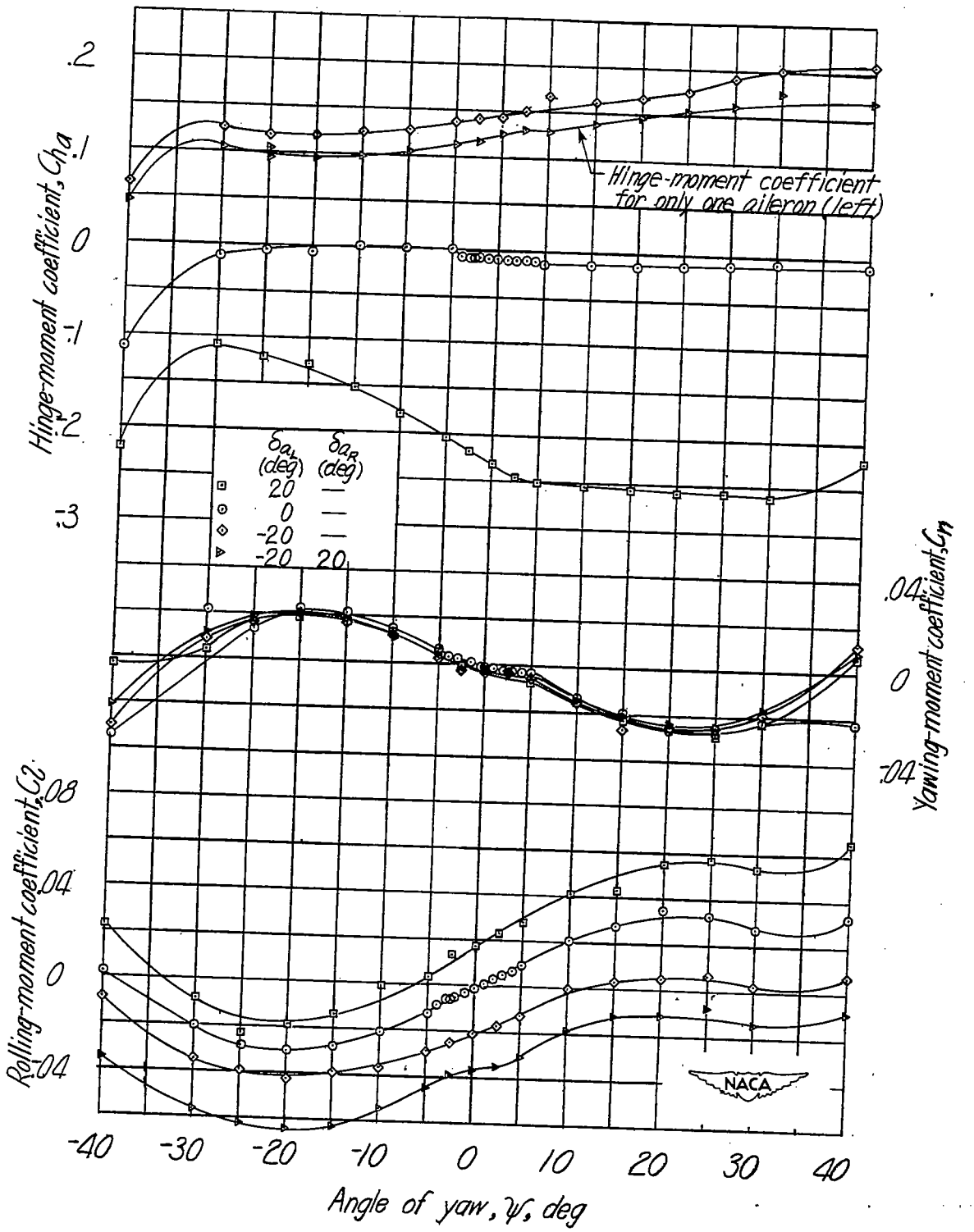

(a) $\delta_f = 0^\circ$; $\alpha = 5.4^\circ$.

Figure 31.- Effect of aileron deflection on the aerodynamic characteristics in yaw of test model. $\Gamma = 0^\circ$.

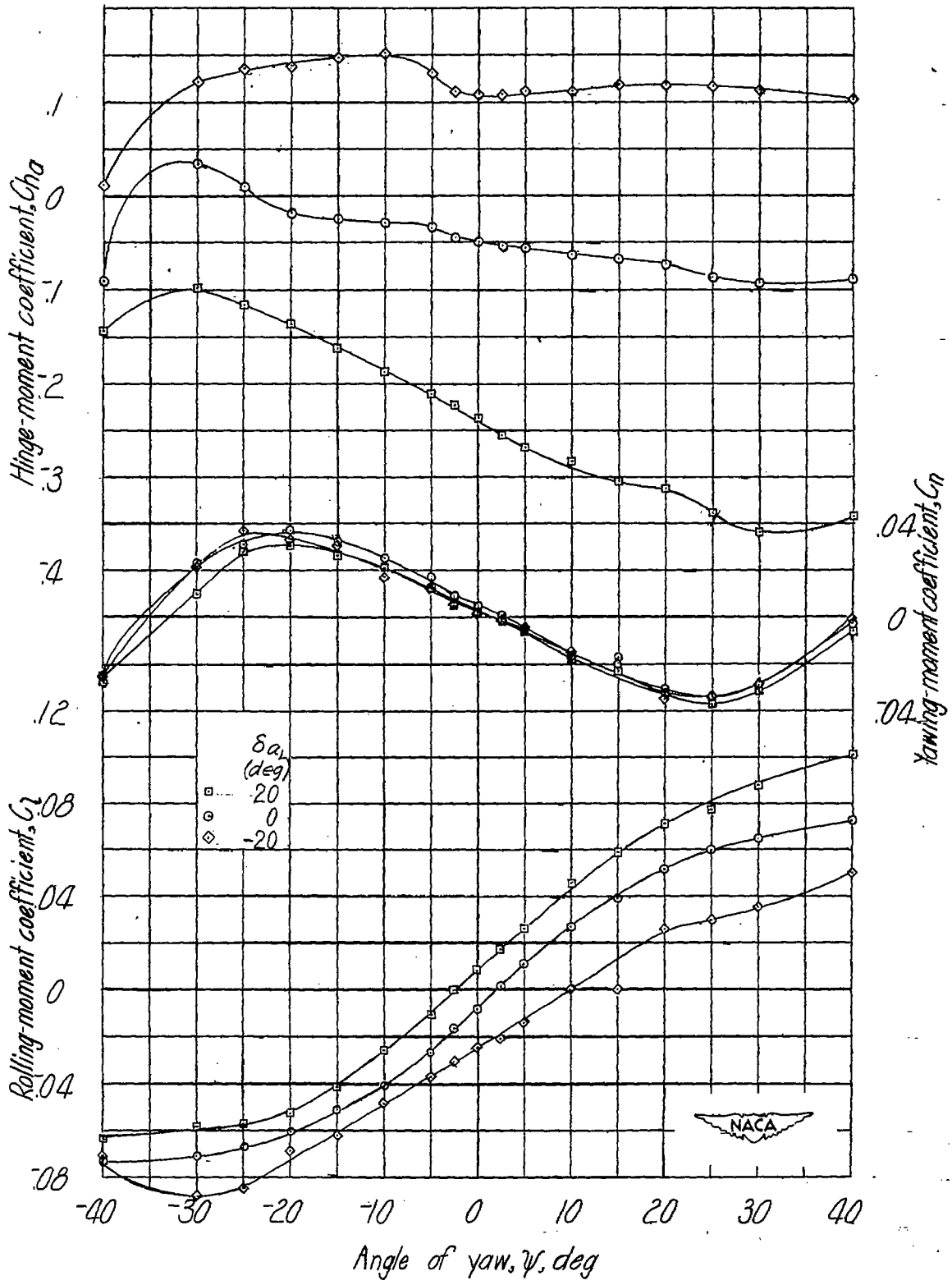

(b) $\delta_f = 50^\circ$; $\alpha = 11.2^\circ$.

Figure 31.- Concluded.

NACA-Langley - 12-4-51 - 1000